ECSS-E-HB-31-01 Part 15A
5 December 2011

Space engineering

Thermal design handbook - Part 15: Existing Satellites

ECSS Secretariat
ESA-ESTEC
Requirements & Standards Division
Noordwijk, The Netherlands

Foreword

This Handbook is one document of the series of ECSS Documents intended to be used as supporting material for ECSS Standards in space projects and applications. ECSS is a cooperative effort of the European Space Agency, national space agencies and European industry associations for the purpose of developing and maintaining common standards.

The material in this Handbook is a collection of data gathered from many projects and technical journals which provides the reader with description and recommendation on subjects to be considered when performing the work of Thermal design.

The material for the subjects has been collated from research spanning many years, therefore a subject may have been revisited or updated by science and industry.

The material is provided as good background on the subjects of thermal design, the reader is recommended to research whether a subject has been updated further, since the publication of the material contained herein.

This handbook has been prepared by TEC-MT/QR division, reviewed by the ECSS Executive Secretariat and approved by the ECSS Technical Authority.

Disclaimer

Published by: ESA Requirements and Standards Division
ESTEC, P.O. Box 299,
2200 AG Noordwijk
The Netherlands

Table of contents

Figures

Tables

1
Scope

In this Part 15, existing satellites are described and examined from a thermal control and design view. The thermal control requirements are given and an assessment is made of the thermal control systems used against performance for each satellite.

The Thermal design handbook is published in 16 Parts

ECSS-E-HB-31-01 Part 1	Thermal design handbook – Part 1: View factors
ECSS-E-HB-31-01 Part 2	Thermal design handbook – Part 2: Holes, Grooves and Cavities
ECSS-E-HB-31-01 Part 3	Thermal design handbook – Part 3: Spacecraft Surface Temperature
ECSS-E-HB-31-01 Part 4	Thermal design handbook – Part 4: Conductive Heat Transfer
ECSS-E-HB-31-01 Part 5	Thermal design handbook – Part 5: Structural Materials: Metallic and Composite
ECSS-E-HB-31-01 Part 6	Thermal design handbook – Part 6: Thermal Control Surfaces
ECSS-E-HB-31-01 Part 7	Thermal design handbook – Part 7: Insulations
ECSS-E-HB-31-01 Part 8	Thermal design handbook – Part 8: Heat Pipes
ECSS-E-HB-31-01 Part 9	Thermal design handbook – Part 9: Radiators
ECSS-E-HB-31-01 Part 10	Thermal design handbook – Part 10: Phase – Change Capacitors
ECSS-E-HB-31-01 Part 11	Thermal design handbook – Part 11: Electrical Heating
ECSS-E-HB-31-01 Part 12	Thermal design handbook – Part 12: Louvers
ECSS-E-HB-31-01 Part 13	Thermal design handbook – Part 13: Fluid Loops
ECSS-E-HB-31-01 Part 14	Thermal design handbook – Part 14: Cryogenic Cooling
ECSS-E-HB-31-01 Part 15	Thermal design handbook – Part 15: Existing Satellites
ECSS-E-HB-31-01 Part 16	Thermal design handbook – Part 16: Thermal Protection System

2 References

ECSS-S-ST-00-01	ECSS System - Glossary of terms
ECSS-E-HB-31-01 Part 3	Thermal design handbook – Part 3: Spacecraft Surface Temperature
ECSS-E-HB-31-01 Part 5	Thermal design handbook – Part 5: Structural Materials: Metallic and Composite
ECSS-E-HB-31-01 Part 6	Thermal design handbook – Part 6: Thermal Control Surfaces
ECSS-E-HB-31-01 Part 7	Thermal design handbook – Part 7: Insulations
ECSS-E-HB-31-01 Part 8	Thermal design handbook – Part 8: Heat Pipes
ECSS-E-HB-31-01 Part 9	Thermal design handbook – Part 9: Radiators
ECSS-E-HB-31-01 Part 11	Thermal design handbook – Part 11: Electrical Heating
ECSS-E-HB-31-01 Part 12	Thermal design handbook – Part 12: Louvers
ECSS-E-HB-31-01 Part 13	Thermal design handbook – Part 13: Fluid Loops
ECSS-E-HB-31-01 Part 14	Thermal design handbook – Part 14: Cryogenic Cooling

All other references made to publications in this Part are listed, alphabetically, in the **Bibliography**.

3
Terms, definitions and symbols

3.1 Terms and definitions

For the purpose of this Standard, the terms and definitions given in ECSS-S-ST-00-01 apply.

3.2 Abbreviated terms

The following abbreviated terms are defined and used within this Standard.

ABM	apogee boost motor
ACM	acquisition camera module
ACS	attitude control system Clause 8: attitude control sensors
AFNOR	(association Francaise de normalisation), French standards association.
AIT	assembly, integration and testing
AMI	active microwave instrument
AOCS	attitude and orbit control system
AOP	advanced on-board processor
ATSR	along track scanning radiometer
BAPTA	bearing and power transfer assembly
BASD	ball aerospace system division
BCU	bus coupling unit
BD	Clause 8: burst disc Clause 9: (boitier de détection), detector housing
BOL	beginning of life
BSR	back side reflection cell

CCD	coupled charge device
CCHP	constant conductance heat pipe
CEU	control electronic unit
CM	communication module
CNES	(centre national d'etudes spatiales), French space agency
CRU	command relay unit
CSS	coarse sun sensor
CU	(charge utile) payload
d.o.d.	depth of discharge
DAX	Dutch additional experiment
DBS	direct broadcast service
DC	direct current
DET	direct energy transfer
E	equinox
EAIM	attitude measurement and control electronics
ECS	European communication satellite
EGSE	electrical ground support equipment
EIRP	equivalent isotropic radiated power
EM	engineering model
EMA	(electronique de messure d'attitude), gyro electronics
EOL	end of life
EPC	electronic power conditioner
ERS	European remote sensing satellite
ETU	engineering test unit
FCV	fuel control valve
FDMA	frequency-division multiple access
FES	fine error sensor

FMW	fixed momentum wheel
FPA	focal plane assembly
FSSS	fine sun sensor
GEO	geostationary
GPS	global positioning system
GRM	global reference mission
GSE	ground support equipment.
GSFC	goddard space flight center
GYRS	gyro sensor
HAPS	hydrazine auxiliary propulsion system.
HP	heat pipe
HPA	high power amplifier
HRV	high resolution visible
HV	high voltage
IDTH	instrument data handling and transmission system
IM	instrument module
IR	infrared
IRA	inertial reference assembly
IRAS	infrared astronomical satellite
IRES	infrared earth sensor
IRX	infrared experiment
IUE	international ultraviolet explorer
LRR	laser retro-reflector
LSS	largest space simulation
LTV	low thrust vents
LV	low voltage
MAM	mission adapter module
MCL	magnetic coil

MCS	maritime communication satellite
MCT	main cryogenic tank
MEGS	(mécanisme d'entrainement du générateur solaire) solar array driver system
MLI	multilayer insulation.
MMS	multimission modular spacecraft
MP	(module de propulsion) propulsion module
MS	(module de servitude) service module
MSS	multispectral scanner
MSTH	(modèle structural et thermique), structural and thermal model
OBC	on board computer
OCOE	overall check-out equipment
OSR	optical solar reflector
OTS	orbital test satellite
Pan	panchromatic
PCU	power control unit
PDU	power distribution unit
PEM	payload electronics module
PF	platform
PFM	plateforme multimission
PL	payload
PP	porous plug
PPE	(plateau porte equipements), equipment base plate
PRARE	precision range and range rate equipment
PROPOS	programmable power supply
PSE	power supply electronics
RA	radar altimeter
RCS	reaction control system

RDU	repeater drive unit
RF	radio frequency
RIG	rate integrating gyro
RIU/EU	remote interface unit/expander unit
S	solstice
SAR	synthetic aperture radiation
SCOT	spacecraft component on telescope
SES	solar environment simulator
SHF	super high frequency
SM	service module
SPOT	(satellite probatoire d'observation de la Terre), trial Earth observation satellite (in the beginning) (satellite Pour l'observation de la Terre), Earth observation satellite (current usage) (Dyson (1986) [18])
SS	summer solstice
SSM	second surface mirror
SS-TDMA	satellite-switched time-division multiple access
STD	(senseur terrestre digital), digital Earth sensor
TCA	thrust chamber assembly
TCS	thermal control subsystem
TDH	test data handling
TDRS	tracking and data relay satellite
TIMM	thermal interface mathematical model
TM	thematic mapper
TMCU	(télémesure de la charge utile), payload telemetry system
TT&C	telemetry, tracking and command
TU	tape unit
TVBS	television broadcast system

TWT	travelling wave tube
TWTA	travelling wave tube amplifier
UV	ultra-violet
VCS	vapor cooled shield
VHF	very high frequency
WBM	wide band module
XS	multispectral

3.3 Symbols

Q	heat transfer rate, [W]
T	temperature, [K]
T_m	characteristic temperature, [K]
l_{eff}	effective heat pipe length, [m]
m	mass, [kg]
q	louver heat rejection capability, [$W.m^{-2}$]
t	time, [d]
t_0	reference time, [d]
α_s	solar absorptance
β	attitude angle of the satellite with respect to Sun line, [angular degrees] it is not defined in a unified way Clauses 9 and 12: angle between the line to the Sun and the longitudinal axis of the satellite Clause 10: angle between the lie to the Sun and the normal to orbit plane Clause 11: 90° minus the angle between the line to the Sun and the normal to orbit plane
ε	hemispherical total emittance
σ	standard deviation
τ	characteristic time

4
International ultraviolet explorer (IUE)

4.1 Mission

Observation of the ultraviolet spectra of astronomical sources in the spectral region between 1,15x10^{-7} m and 3,2x10^{-7} m.

Launching date: Jan. 26, 1978.

Mission life: 3 years design life with a 5 years design goal. After six year in orbit, a detailed study by NASA shown that the solar panels would support the operation till 1988.

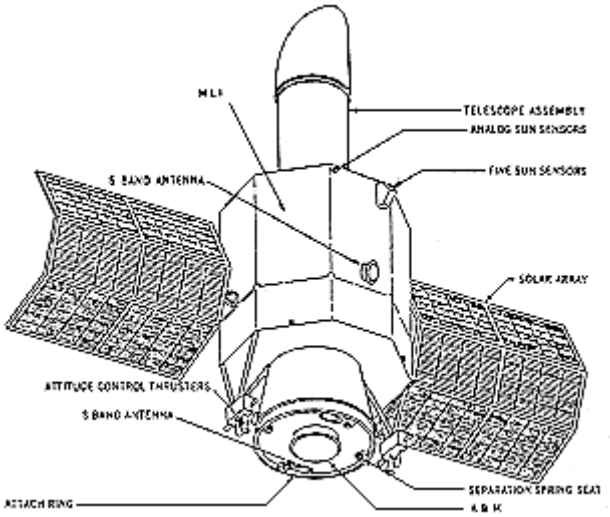

Figure 4-1: IUE spacecraft in orbital flight.

4.2 Main subsystems

IUE carries a 0,45 m diameter Casegrain telescope, which uses an echelle spectrograph for UV astronomy in the spectral region between 1,15x10^{-7} m and 3,2x10^{-7} m. Aimed resolution was 10^{-11} m in the mentioned region of the spectrum for stars and planets brighter than 7th visual magnitude, and lower resolution (6x10^{-11} m) for stellar and extended objects as faint as 12th magnitude. Spectroscopy on stars as faint as 18th magnitude has been performed with this instrument.

Relevant characteristics of the different subsystems are summarized in Table 4-1.

Table 4-1: Characteristics of the IUE Main Subsystems

Subsystem	Purpose	Components
Power Direct Energy transfer (DET)	Providing regulated (28 V DC ± 2%) power which is transferred from the solar array to the spacecraft bus.	• Two deployable solar panels furnished by ESA. Manufactured by Aérospatiale (France) and AEG-Telefunken (Germany), see Bulloch (1978) [11]. • Power supply electronics (PSE) composed of redundant power modules. A power module consists of battery charger, shunt driver, boost regulator, control unit and 12 dump resistors. • Mission Adapter Module (MAM) interfacing modules to one another, to solar arrays and to batteries. • Two $21{,}6 \times 10^3$ C (3,6 A.h) Ni-Cd batteries.
Communication	Transmitting data to ground. Receiving ground-generated commands. Providing range and range rate signals for metric tracking.	• VHF System used during transfer orbit and for tracking during mission orbit. It consists of two redundant transponders, antenna distribution and a turnstile antenna system. • S band downlink system for mission orbit. Two redundant transmitters and four S-band antennae. Active antenna is selectable on ground.
Commend & Data Handling	Accepting and decoding commands from ground or from onboard computer. Encoding spacecraft and scientific instrument telemetry. Performing attitude control computations. Monitoring critical subsystems and controlling exposure times of spectral images.	• Two redundant command decoders processing messages either from VHF receiver analog signal or from digital information generated by the onboard computer. • A Command Relay Unit (CRU). • Two data multiplex units. Each one consists of dataplexer, analog subplexer and digital subplexer. • Advanced On-board Processor (AOP) computer.
Stabilization & Control	Precessing the spacecraft spin axis 180° in preparation for the apogee engine burn. Attaining the correct orbit. Despinning once the orbit has been achieved.	• Earth and Sun sensors for ground computer attitude determination. • Rate gyros and analog Sun sensors for initial spacecraft acquisition. • Inertial Reference Assembly (IRA). Six gas-bearing, pulse rebalanced, rate-

Subsystem	Purpose	Components
	Controlled pointing and slew of the telescope according to specifications.	integrating gyros. • Redundant two-axis digital Sun sensor system. • Redundant set of star trackers within the scientific instruments and utilizing the telescope optics. • Redundant reacting wheel. • Nutation reaction accelerometers. • Apogee Boost Motor (ABM) and Hydrazine Auxiliary Propulsion System (HAPS)

4.3 Main characteristics of the satellite

The main body is octogonal in shape. The telescope extends from the upper end of the main body. It is attached to the spacecraft structure by means of s strong ring resting on three columns which carry the load to the lower spacecraft structure. The columns are supported laterally by truss members of the main body.

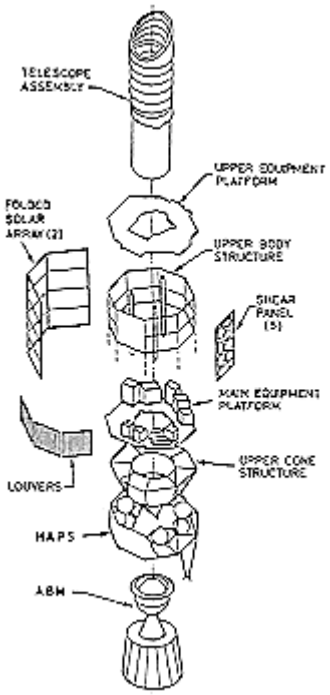

Figure 4-2: Exploded view of the IUE spacecraft.

Two fixed solar arrays extend from opposite sides. Spacecraft orientation is kept in mission orbit such that the front of the solar arrays always faces toward the Sun whereas the thermal control Louvers (see ECSS-E-HB-31-01 Part 12) face away from the Sun. Spacecraft subsystems are located as follows:

Most of the higher power electronic equipment is located on the main equipment platform, within the main spacecraft body and adjacent to the louvers.

Experiment electronics, attitude control reaction wheels, gyro electronics and Sun sensor electronics are located on the upper equipment platform.

Hydrazine auxiliary propulsion system is located below the main equipment platform.

Apogee boost motor, in the lower cone assembly.

Spacecraft length (in the roll axis direction) is 4,1 m.

IUE was launched on January 26, 1978, by a Delta 2914 booster.

The mass of the IUE Flight Segment is given in Table 4-2.

Table 4-2: IUE Flight Segment Mass Summary

Component	Mass [kg]
Spacecraft	312
Scientific Instruments	122
Apogee motor (218 kg of propellant)	237
Launch Vehicle Adapter	29
Launch Mass	700

Mass reduction was a major problem. More than 50 items were analyzed for possible mass saving during the course of the study, and 21 changes were adopted. Among them:

Orbit redesigned from initially circular synchronous to a lower energy elliptical. 59 kg savings.

Two Acquisition Camera Modules (ACM) plus a Fine Error Sensor (FES) were replaced by two FESs. 7,6 kg savings.

Battery capacity halved.

Electronics of the Inertial Reference Assembly (IRA) lightened through used of hybrids.

4.4 Orbit

Elliptical Geosynchronous (eccentricity: 0,21).

Inclination: 28,6°

Longitude: 71° W

Apogee: 44000 km

Perigee: 27000 km

These data shift with time and are daily issued by the Goddard Space Flight Center (GSFC).

Spacecraft in within continuous view of Goddard and within direct view, for at least 10 h per day, of the European Ground Observatory near Madrid (Spain).

The attitude of the spacecraft is such that

β : between 0° and 135° (Mission orbit)

between 45° and 135° (Transfer orbit)

Here β is the angle between the line from the Sun and the spacecraft roll or telescope axes, with $\beta = 0°$ when the Sun looks up to the bottom of the spacecraft, Figure 4-3.

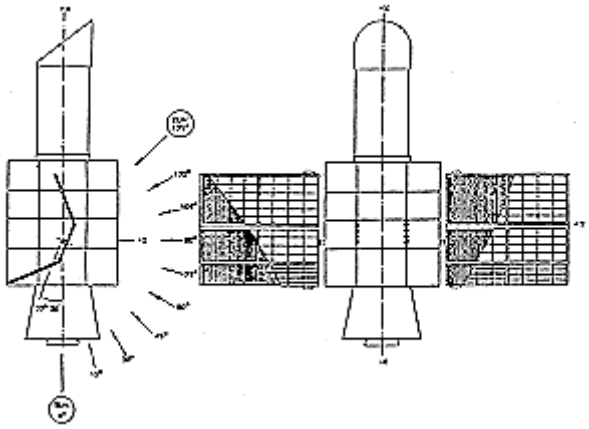

Figure 4-3: IUE orientation to the Sun and reference axes.

4.5 Thermal design requirements

The spacecraft will operate over 135° β angle range and can survive an 85 min zero power eclipse. Total power dissipation is around 186 W of which 130 W are dissipated in the main spacecraft compartment.
Thermal design requirements of the various component and subsystems are summarized in Table 4-3.

Table 4-3: Thermal Design Requirements

Component (Location in Figure 4-4)	Operating Temperature Range [K]	
Auxiliary Propulsion Area (Sta 0-45,5) ABM HAPS	 258-311 278-338	Before ignition (50 h after launch). Throughout mission.
Main Spacecraft Compartment (Sta 45,5-87,5) Batteries Gyros	 273-313 < 293 330,5 ± 1	 Contain own thermal control system.
Spectrograph	273-293	Thermal transients and thermal gradients minimized.
Telescope (Sta 87,5-164,5) Secondary mirror/focus mechanism Primary mirror	273-303 273	
Solar array		No specific requirement.

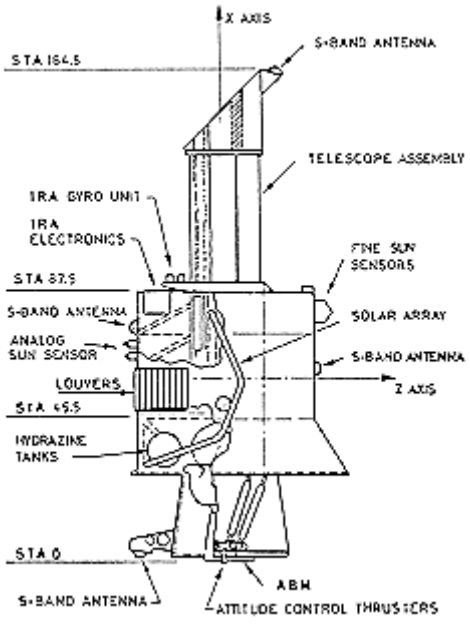

Figure 4-4: Assembled IUE Spacecraft. From Skladany & Seivold (1976) [42]. Notice that this figure, which corresponds to an earlier development, differs from Figure 4-1 in minor details.

4.6 Design tradeoffs

- Modular vs. Integrated: Modular design was selected because of the following reasons:

  The five major components listed in Table 4-3 are thermally decoupled, each with its own specific thermal problems, and may use separate thermal control.

  Majority of electronics can be controlled by a common radiator through a high thermal conductance support.

  Since there is not heat transfer among modules, significant in orbit thermal distortions should not result.

- Passive vs. Semi Active. All components are passively controlled. Nevertheless, since the power dissipation is not constant and the spacecraft can operate over a wide range of Sun angles, the heat rejection capability does change and, thence, thermal louvers are used for thermal control of the Main Spacecraft Compartment.

4.7 Thermal control of various components

The Main Spacecraft Compartment encloses the spectrograph and the electronic equipment. The spectrograph is thermally decoupled from the compartment. The majority of the electronic equipment is mounted on a honeycomb platform (Figure 4-5) and the remainder on an upper platform.

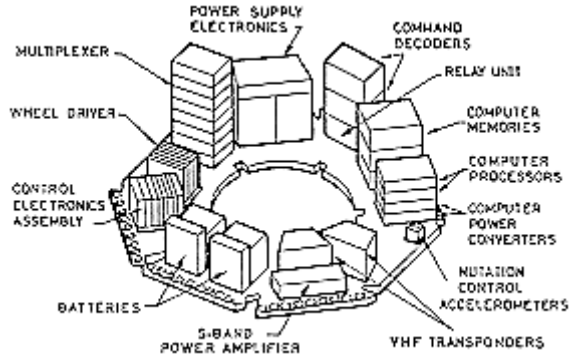

Figure 4-5: IUE main equipment platform. From Skladany & Seivold (1976) [42].

The compartment is covered with an MLI (see ECSS-E-HB-31-01 Part 7, clause 6) with a silvered Teflon outer layer.

Radiation to outer space is achieved through three sets of nine-bladed louvers located in the Anti-Sun side. Each blade is individually controlled by its own bimetallic spring located within the honeycomb platform as indicate din Figure 4-5 by three groups of nine holes each. When fully open the louvers provide 0,6 m² of radiating area, q ~ 220 W.m² Heat Rejection Capability (see ECSS-E-HB-31-01 Part 12, clause 6.1.2). The corresponding baseplate temperature is not given (although a rough estimate can be based on data in) Table 4-4). The actuators are calibrated to move from fully closed at 273K to fully open at 283 K. Similar louvers were flown on the SAS-C satellite (Explorer 53, launched on May, 7, 1975).

Two circular, ammonia-filled, grooved Heat Pipes (see ECSS-E-HB-31-01 Part 8) are attached to the underside of the main equipment platform. The integral Heat Transport Factor of each Heat Pipe is $[Q.le_{ff}]_{max}$ = 75 W.m. Temperature differences in the platform are kept below 5 K. These heat pipes are of the type flown on the ATS-6 spacecraft (see Kirckpatrick & Brennan (1975) [32]).

The telescope external surface is covered with an MLI, the outer layer of which is silvered Teflon. The primary mirror is conductively decoupled from the telescope structure and held at 273 K with 3 to 8 W Heaters (see ECSS-E-HB-31-01 Part 11). Another heater (1,5 W) is used to maintain the secondary mirror at 273 K. The secondary mirror support is not insulated although it is conductively decoupled from the Sun shade.

Radiative decoupling of the spectrograph from the main compartment is achieved by utilizing low emittance surfaces. The spectrograph temperatures are maintained within satisfactory limits by controlling the primary mirror temperature.

The thermal control of the HAPS is achieved by radiation only. The canted side of HAPS bay is covered by an SSM consisting of vapor-deposited aluminium on a Kapton layer with SiO-SiO_x overcoating. This surface (α_s = 0,25, ε = 0,23) provides a solar input of 20 W at β = 135°. The sides of the HAPS bay are covered with an MLI with a vapor-deposited aluminium outer layer. The remainder of the propulsion area is covered with MLI with a black outer layer. Radiative decoupling from the Main Spacecraft Compartment is achieved by an MLI.

ABM is covered with an MLI to prevent heat transfer to the Main Spacecraft Compartment during firing, and to the outer space during orbital flight. A heat shield covers the nozzle exit before firing.

4.8 Estimated on orbit performance

Three different thermal models were used to predict on orbit performance. One of them (165 nodes) for the scientific instruments, other (186 nodes) for the remainder of the spacecraft, and a third more detailed model (250 nodes) for the Propulsion Area.

Nominal values of α_s were taken for all β angles except in the case β = 67,5° were a degraded, conservative, value was used. Reflections and shadowing were taken into account.

An Engineering Test Unit (ETU) was constructed for a thermal balance test in the Solar Environment Simulator, (SES) located at Goddard Space Flight Center.

ETU was thermally similar to the flight unit except for the following, nor correctly modelled, items:

Sensors and antennas penetrations through MLIs, except for the S-band antenna bracket on the telescope Sun shade.

HAPS, not truly modelled, and HAPS thrusters, not included.

Burned-out apogee motor, discarded because it was a source of contamination.

Solar radiation was simulated by electric heaters supported on $1{,}27 \times 10^{-6}$ m thick Kapton sheets (see ECSS-E-HB-31-01 Part 11, clause 4.2) which were attached to the irradiated surfaces. Solararrays, apogee motor nozzle and electronic equipment were simulated in a similar way. The exception was a live VHF transponder assembly on the) main platform.

Heat loss to the mounting fixture was minimized by use of an insulated zero heat transfer unit automatically monitored to maintain less than 1 K temperature between the spacecraft interface and the adapter ring.

Outer space conditions were simulated with an LN_2 cold wall sink and a vacuum of less than $1{,}33 \times 10^{-3}$ Pa.

350 thermocouples and auxiliary equipment were used.

Several operating cases at each β angle were run. In addition, 85 min shadow runs were accomplished after reaching equilibrium at β = 0° and β = 135°.

A summary of the results are given in Table 4-4. A more complete set of data can be found in Skladany & Seivold (1976) [42].

Table 4-4: Estimated and Measured Performance of Spacecraft Components and Scientific Instrument Components with Nominal Power Dissipation.

COMPONENT	$\beta = 0°$		$\beta = 90°$		$\beta = 135°$		$\beta = 67{,}5°$	
	Estimated Temp [K]	Measured Temp [K]	Estimated Temp [K]	Measured Temp [K]	Estimated Temp [K]	Measured Temp [K]	Estimated Temp [K]	Measured Temp [K]
Command Subsystem	288,3	286,6	291,3	290,7	289,6	289,8	295,8	293,1
Multiplexer Subsystem	288,8	286,2	291,2	289,8	289,4	288,3	295,5	292,0
Computer (Processor)	294,8	296,3	300,3	300,0	299,5	299,3	304,5	302,3
Computer (Memories)	290,1	285,7	292,4	289,7	291,4	288,8	296,8	292,0
S-band Power Amp. (Base)	301,6	301,2	303,6	301,8	301,2	302,2	307,3	303,3
Batteries	285,2	285,9	287,4	287,4	281,6	286,8	291,3	289,0
Control Electronics	283,5	283,2	285,6	285,1	280,6	284,3	289,6	286,5
Power Supply Electronics	290,6	288,6	293,3	292,5	292,1	291,3	297,6	294,8
Camera Electronics	289,1	285,0	291,7	288,7	289,8	288,4	295,7	290,4
Sun Sensor Electronics	283,8	281,2	286,7	284,5	284,3	284,2	290,8	286,3

COMPONENT	$\beta = 0°$		$\beta = 90°$		$\beta = 135°$		$\beta = 67{,}5°$	
	Estimated Temp [K]	Measured Temp [K]	Estimated Temp [K]	Measured Temp [K]	Estimated Temp [K]	Measured Temp [K]	Estimated Temp [K]	Measured Temp [K]
Experiment Electronics	291,9	290,2	294,9	295,3	293,0	295,3	299,2	297,6
Pitch Reaction Wheel	285,2	284,5	288,0	289,2	284,0	288,7	292,2	290,8
Roll Reaction Wheel	285,4	282,6	288,4	287,6	284,3	287,2	292,9	289,4
Yaw Reaction Wheel	285,4	284,8	288,4	288,9	286,0	288,5	292,8	290,6
Redundant Wheel	285,2	278,9	288,3	284,5	284,0	283,9	292,7	286,6
Upper Platform	283,2	~ 280,0	287,2	285,2	283,2	285,2	293,2	288,2
Main Platform	288,2	~ 285,7	292,2	289,2	287,2	288,2	295,2	291,2
HAPS Tank (Facet D)	284,8	289,6	276,6	275,4	268,8	273,5	288,9	286,9
HAPS Tank (Facet B)	289,9	289,0	286,4	286,7	279,3	285,7	297,7	296,5
Telescope Tube (+z STA 133)	202,2	209,6	206,2	216,3	(a)	215,8	(a)	216,7
Telescope Tube (–z STA 133)	205,2	212,3	209,2	218,6	(a)	218,3	(a)	218,6
Primary Mirror	274,2	276,8	277,2	277,3	(a)	275,7	(a)	274,3

COMPONENT	$\beta = 0°$		$\beta = 90°$		$\beta = 135°$		$\beta = 67{,}5°$	
	Estimated Temp [K]	Measured Temp [K]	Estimated Temp [K]	Measured Temp [K]	Estimated Temp [K]	Measured Temp [K]	Estimated Temp [K]	Measured Temp [K]
Secondary Mirror	(b)	292,9	(b)	294,7	(a)	296,7	(a)	296,9
L.W. Camera 1	281,2 (c)	281,2	283,2 (c)	284,5	(a)	285,4	(a)	284,4
S.W. Camera 1	279,2 (c)	280,6	281,2 (c)	283,9	(a)	284,4	(a)	283,7

[a] Test conditions were not analyzed.

[b] Test conditions differed from analyzed design.

[c] Analytical Model gives component average temperature. thermocouples located to give specific information.

References: Kirckpatrick & Brennan (1975) [32], Skladany & Seivold (1976) [42], Bulloch (1978) [11], Freeman & Longanecker (1979) [22]. All the figures, unless otherwise stated, are from Freeman & Longanecker (1979) [22].

5
Orbital test satellite (OTS)

5.1 Mission

Validating the telecommunication technologies and spacecraft hardware to be used in the European Communication Satellite (ECS) program.

Launching date: May 11, 1978.

Mission life: 3 yr, expandable to 7 for operational variants. End of Service tests were conducted early in 1984, followed by an operation in "hibernation" mode for 18 mo.

First experimental telecommunication spacecraft of ESA.

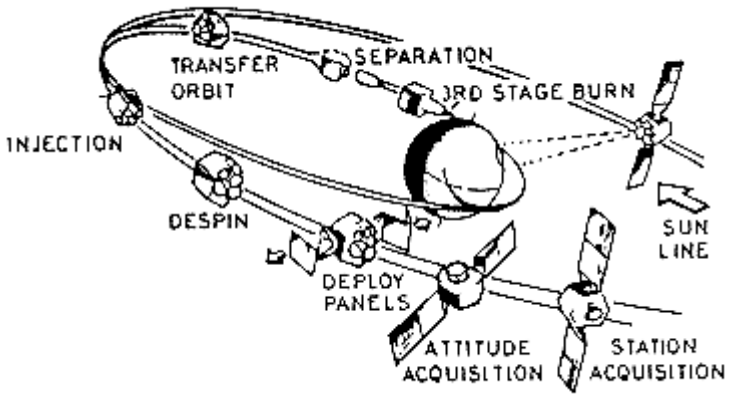

Figure 5-1: OTS mission event sequence. From Collette & Stockwell (1976) [14].

5.2 Main subsystems

OTS consists of a service module (SM) providing all the basic service functions and a communication module (CM) carrying mainly the payload.

Relevant characteristics of the different subsystems are summarized in Table 5-1.

Table 5-1: Characteristics of the OTS main Subsystems

Subsystem	Purpose	Components
Structure	To provide the means of support for the payload and service equipment. To provide the mechanical interface with the launch vehicle.	It forms a hexagonal shaped body with adequate volume on North and South faces to stow the solar arrays in the launch configuration. It consists of two separable Modules. • The CM, with antennae and repeater units. • The SM, with the subsystem equipments, providing functional services to the payload.
Power Generation and Electrical Distribution	To provide for power requirements and electrical interconnection of the various equipment and for protection of the main power bus against failures.	• Two independently steerable rigid solar arrays. They provide 105 W at transfer orbit. 750 W at Beginning of life (BOL) on station. 600 W at 5 years on station. • Two Bearing and Power Transfer Assemblies (BAPTA's) to align continuously the solar arrays to the Sun. • A digital shunt regulator system to regulate the main power bus voltage (50 V DC ± 1%). • A 28 cell 21 Ah Ni-Cd battery, that provides 122 W at end of life of the OTS. It is charged via redundant series charges.
Telemetry, Tracking and Telecommands (TT & C)	To receive incoming signals from a circular polarized antenna array used during transfer orbit and on station.	• It operates at VHF prior to normal mode operation and in back-up modes. • It operates at SHF, 14,125 GHz for the uplink and 11,575 GHz for the downlink, in normal-mode operation. • It is divided into • the SM part with • VHF antenna and branching unit. • VHF transponder. • priority select and interface unit. • SM decoder and encoder. • the CM part with • VHF receiver • SHF transmitter • payload decoder and encoder.
Attitude and	To maintain the electrical	• Attitude sensors

Subsystem	Purpose	Components
Orbit Control System (AOCS)	bore-sight of the antennae within a half-cone angle of 0,2° (3σ) and the satellite yaw error within ± 5° (3σ) under all orbital conditions. To provide the means of controlling the spacecraft attitude during transfer orbit, drift orbit and synchronous orbit phases.	• V-beam Sun sensor. • Infrared pencil-beam Earth Sensors (IRES). • Two-axis infrared sensors. • Measurement and signal processing electronics • Passive nutation damper. • Control electronics. • Rate Integrating Gyro (RIG). • Actuators • Fixed Momentum Wheel (FMW). • Hydrazine thrusters.
Reaction Control System (RCS)	To provide thrust required for: • Transfer orbit. • Spin axis orientation. • Drift Orbit. • Earth and spin acquisition, initial stabilization in three axis mode, balance torque during wheel spin up, drift orbit and initial station localization. • Operations on station. • Momentum wheel unloading, disturbance torque removal.	• Storage system 4 spherical pressure vessels. • Distribution Via launching valves, in a fully redundant manner. • Thruster Two groups of thrusters containing eight high level and two low level thrusters, each.
Apogee Boost Motor (ABM)	To impact sufficient velocity increment to the satellite at the apogee of the transfer orbit to inject it into a near-synchronous circular orbit with approximately zero inclination.	Solid-propellant motor is mounted within the central tube of the spacecraft structure.

The communication payload is split into Module A, Module B and the antennae.

Module A contains two chains of 40 MHz nominal bandwidth and two of 120 MHz, the telecommand receivers and the telemetry transmitters. There are two basic sections in this module: the wide-band section and the channelized section. Both utilize linear polarization.

The uplink and downlink frequencies planned for this module are, respectively:

Uplink

Telecommand receiver: 14 125 MHz

40 MHz chains: 14 125 MHz to 14 192,5 MHz

120 MHz chains: 14 242,5 MHz to 14 362,5 MHz

Downlink

40 MHz chains: 11 490 MHz to 11 530 MHz

Telemetry transmitter: 11 575 MHz

120 MHz chains: 11 580 MHz to 11 700 MHz

Module B includes repeater chains of 5 MHz nominal bandwidth with a gain substantially higher than the chains of module A. This module also contains an onboard beacon transmitter. It utilizes circular polarization.

Uplink

5 MHz chains: 14 455 MHz to 14 460 MHz

Downlink

Beacon transmitter: 11 786 MHz

5 MHz chains: 11 792,5 MHz to 11 797,5 MHz

There are six circular reflector antennae with frontal feedhorn supported by four struts, namely: Three Eurobeam A antennae with 26,5 db peak gains

5.3 Main characteristics of the satellite

The power subsystem capability allows to operate a maximum of six Travelling Wave Tubes (TWT's) during Sun illumination and only two during eclipse.

The battery is located as two separate units on opposite side of the spacecraft (for mass distribution) although it is considered electrically as one.

Two platforms supported by a central tube carry the electronic components.

Shunt electronics, which control the solar array output, are mounted on a dedicated radiator area on the North face of the spacecraft.

In orbital flight, a farm of white painted antennae are on the Earth viewing panel, however, the launcher adapter, the Apogee Boost Motor (ABM), the VHF antennae and 12 hydrazine thrusters are positioned facing away from the Earth.

OTS configuration can be seen in Figure 5-2.

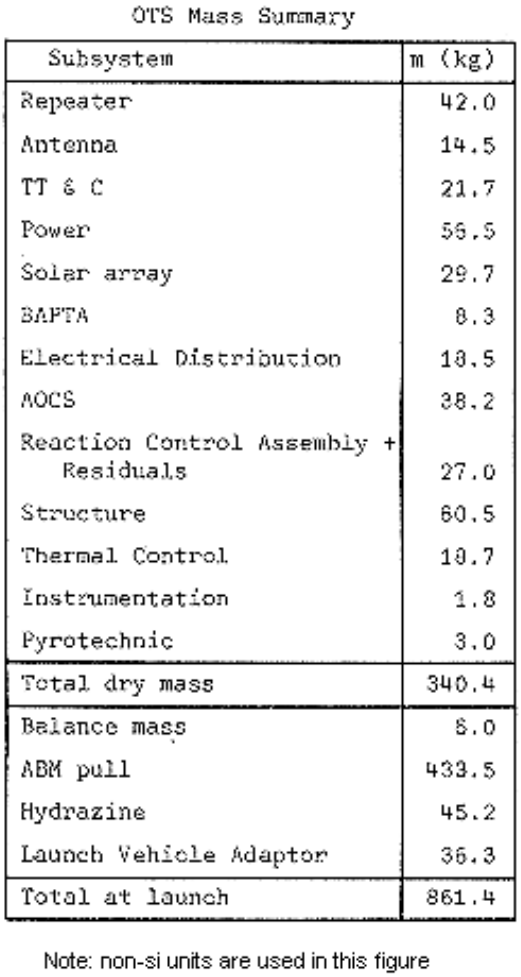

OTS Mass Summary

Subsystem	m (kg)
Repeater	42.0
Antenna	14.5
TT & C	21.7
Power	56.5
Solar array	29.7
BAPTA	8.3
Electrical Distribution	10.5
AOCS	38.2
Reaction Control Assembly + Residuals	27.0
Structure	60.5
Thermal Control	10.7
Instrumentation	1.8
Pyrotechnic	3.0
Total dry mass	340.4
Balance mass	8.0
ABM pull	433.5
Hydrazine	45.2
Launch Vehicle Adaptor	36.3
Total at launch	861.4

Note: non-si units are used in this figure

Figure 5-2: Exploded view of the OTS spacecraft. From Bouchez, Howle & Stümpel (1978) [9].

Typical dimensions are:

2,18 m diametral envelope,

2,10 m height,

8,62 m deployed arrays.

OTS was launched on May 11, 1978 by a Delta 3914 booster. The mass before launching was 865 kg, and mass in orbit 444 kg. Mass distribution, before launching, is given in Table 5-2.

Table 5-2: OTS Mass Summary

Subsystem	m [kg]
Repeater	42,0
Antenna	14,5
TT & C	21,7
Power	56,5
Solar array	29,7
BAPTA	8,3

Subsystem	m [kg]
Electrical Distribution AOCS Reaction Control Assembly + Residuals Structure Thermal Control Instrumentation Pyrotechnic	18,5 38,2 27,0 60,5 18,7 1,8 3,0
Total dry mass	340,4
Balance mass ABM pull Hydrazine Launch Vehicle Adaptor	6,0 433,5 45,2 36,3
Total at launch	861,4

NOTE From Wearmouth & McLaurin (1977) [57].

OTS was developed and manufactured by an industrial organization of firms grouped within the MESH consortium (Figure 5-3).

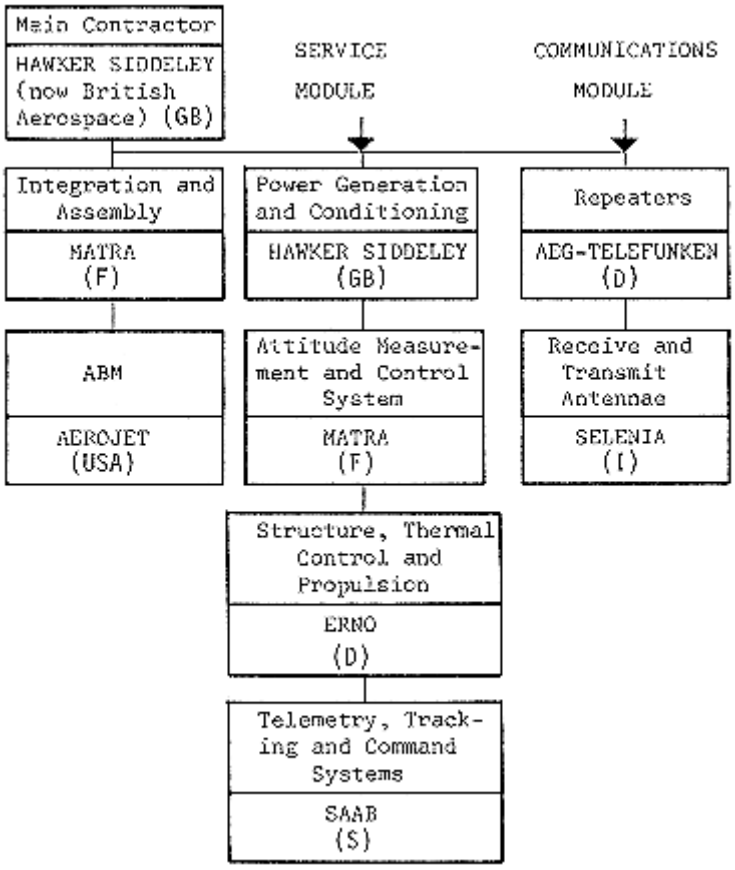

Figure 5-3: OTS main organic diagram. From Collette & Stockwell (1976) [14].

5.4 Orbit

Geostationary (over Gabon). Equatorial.
At first positioned at 10° E longitude. In April 1982 was moved to 5° E to make room for the ECS satellites.
Apogee: 35779 km.
Perigee: 35072 km.
β: the solar angle for the first 14 h after cut-off was about 20° from below (-z side of spacecraft).
During the second half of the transfer orbit, β was close to zero (x-y plane).
On station β varied between 0° and 23,5°.

5.5 Thermal design requirements

The temperature requirements of each unit area are represented in Figure 5-4.

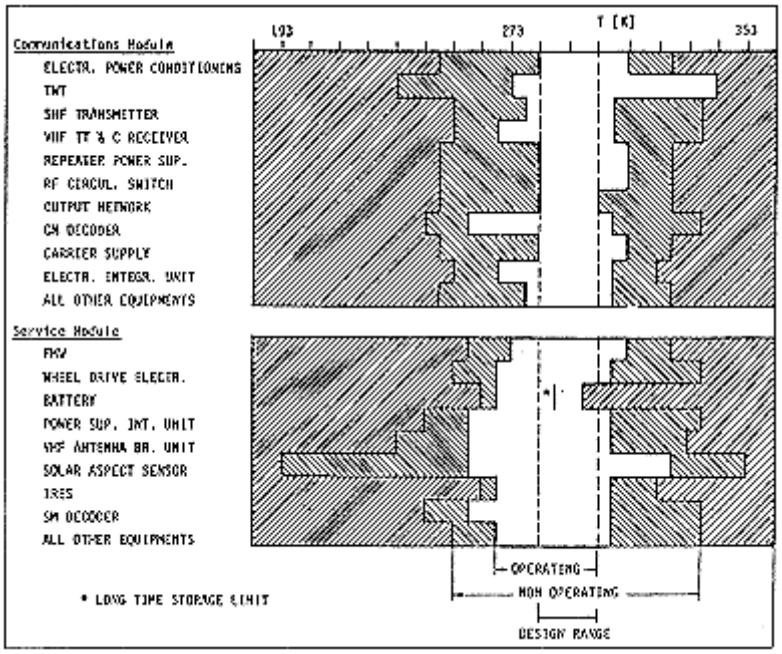

Figure 5-4: OTS Thermal Control Subsystem temperature limits. From Stümpel (1978)a [45].

The major constraints besides those generated by the temperature limits were:

- No active thermal control elements except for RCS heaters of very limited total heating power (≤ 25 W), controlled by telemetry command switches.
- No heating admitted in transfer orbit and on station eclipses.
- Large range between maximum and minimum total unit dissipation (approx. 100 W shunt power variation possible).
- Three-axis stabilization causing extreme sensitivity to polar input.
- Maximum eclipse of 72 minutes.

The RCS configuration imposed severe requirements on the thermal control, for example:

- The lowest temperature of any part in contact with hydrazine should be above 277 K.

— The highest temperature of the Fuel Control Valve (FCV) under all operational conditions of the thruster (preheated, firing, stand by) and under daily and seasonal extremes should be below 328 K (and 348 K for short time peaks).

— The Thrust Chamber Assembly (TCA) should be preheated for firing to ≥ 463 K, for the 0,5 N thrusters, and to 363 K, for the 2,0 N thrusters.

— FCV heater power minimized.

— Thermostats to automatically operate heaters were not permitted.

— Telecommand switches minimized (initially 4, finally 9).

— Operation of telecommand switches restricted to seasonal variations and operation of boost heaters prior to eclipses.

— FVC & TCA had to penetrate the insulation of the spacecraft and had to be located in remote corners, poorly coupled to the thermal mass of the spacecraft.

5.6 Design tradeoffs

— Modular vs. integrated. The thermal design of OTS was conceived to achieve the modularity of the spacecraft to the greatest extent. It was, however, constrained by the desire to embark previously developed European units, payload and electronic units (antennae, TWT's, FMW, etc.).

— Passive vs. active: ESA requested a passive thermal design. ESA didn't allow for this spacecraft the use of heat pipes, automatically controlled heaters, or other active or semiactive elements, to ease the thermal design task.

5.7 Thermal control of various components

The main characteristics of the OTS thermal control are summarized in Figure 5-5.

1. TWT RADIATORS

- Located on North-South panels of the CM conductively decoupled from the structure.
- Profiled honeycomb construction.
- Front surface coated with rigid Second Surface Mirrors (SSMs) (see ECSS-E-HB-31-01 Part 6, clause 5.2.6) and flexible Optical Solar Reflectors (OSRs), rear painted black. Power output of each TWT variable within a few W per tube. Two extra redundant TWT carried on the central radiator of each North and South panel, but only one energized) at any time.

2. CONTROL RADIATOR

- North-South panels of the SM.
- Front Surface coated ad TWT radiator.

3. SHUNT RADIATOR

- Located on South face of SM, conductively decoupled from the structure.
- Solid aluminium plate, profiled with respect to attachment points and heat distribution capability.
- Front surface coated as TWT radiator, rear painted black.

Shunt electronic power dissipation in the range 40 W to 145 W.

4. MULTILAYER INSULATION (MLI)

(see ECSS-E-HB-31-01 Part 7, clause 6).

4.1. High temperature resistant type to shield spacecraft against heat generated by the ABM and hydrazine thruster.

- Located at upper and lower dome of ABM, inner thrust cone and cylinder, -z plane of the spacecraft, in the vicinity of hydrazine thruster.
- Kapton insulation: 18 crinkled sheets of 0,5 mil ($12x10^{-6}$ m) aluminized Kapton, sandwiched between two 3 mil ($76,2x10^{-6}$ m) aluminized Kapton foils. Launcher adapter, ABM, VHF antennae and 12 hydrazine thrusters pierce the MLIs on the -z plane.

4.2. Mylar insulation.

- Located at ± x sides, antenna platform, antennae.
- 10 crinkled Mylar sheets of 0,25 mil ($6,35x10^{-6}$ m) aluminized on one side, sandwiched between 2 mil ($50,8x10^{-6}$ m) and 1 mil ($25,4x10^{-6}$ m) Mylar foils, rear side aluminized.
- Where no VHF shield is applied (antennae, antenna platform), an outer layer of 3 mil ($76,2x10^{-6}$ m) Kapton, aluminized rear side, is applied.

4.3. VHF shield.

- Covering all blanketed areas except inner thrust cone, cylinder, ABM rear dome, antennae, antenna platform.
- $30x10^{-6}$ m aluminium foil, 0,25 mil ($6,25x10^{-6}$ m) clear Kapton foil and 3 mil ($76,2x10^{-6}$ m) Kapton foil, aluminized rear side.
- Grounded to structure by equally spaced straps of $70x10^{-3}$ m length and 10^{-2} m width.

4.4. Blow-off insulation at ABM.

(see ECSS-E-HB-31-01 Part 7, Clause 4).

- Closing the exit plane.

Same type as used on antennae.

4.5. Insulation Supporting Grid.

- Pretensioned wires to support the -z insulation at the free areas of the -z framework.

5. HEATERS (see ECSS-E-HB-31-01 Part 11).

5.1. Travelling Wave Tube Amplifier (TWTA) Simulation Heaters.

- Operated to simulate dissipation of switch off TWT Electronic Power Conditioner (EPC) during on-station sunlight to keep constant the spacecraft internal temperature.
- Bonded onto the radiator or structure of CM adjacent to the TWTA units.

5.2. Line Heater (see Figure 5-7).

- Wrapped on spirals onto the lines.
- Fixed by aluminium tape.
- Prevent hydrazine from freezing.
- Operated by ground command.

5.3. Tank Heater (see Figure 5-8).

- Bonded onto tanks.
- Prevent hydrazine from freezing.
- Operated by ground command.

5.4. Valve Heaters.

- Bonded onto FCV.
- Prevent hydrazine from freezing within the valve.
- Operated by ground command.

5.5. Batteries Heaters.

- Bonded onto batteries.
- Operated by ground command.

6. BRACKETS OR FLANGES OF LIMITED CONDUCTANCE

- Fiber-glass polyimid prepreg stand-offs, brackets, etc., to provide minimum conductive heat exchange between:
  - Antenna dishes - platform.
  - Radiators - structure.
  - BAPTA. - yoke, structure.
  - Batteries - structure.
  - Tanks - structure.
  - Lines - structure.
  - RCA thrusters (see Figure 5-9) - thrusters brackets.
  - ABM - structure.
  - Antenna Platform - support structure.

7. THERMAL CONTROL PAINT- Black paint for spacecraft interior and units

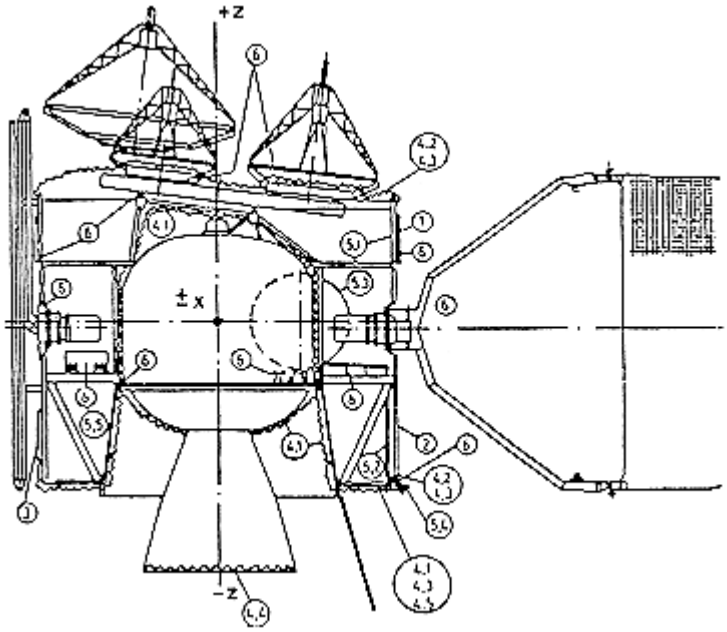

Figure 5-5: OTS thermal control layout summary. From Stümpel (1978)a [45].

The AOCS presents its own thermal control problems which are not dealt with in Figure 5-5.

Figure 5-6 shows the insulation of the hydrazine line system. Heating to avoid freezing of hydrazine in tanks, lines and valves under widely varying environmental conditions demands for a complex electric circuitry operated by ground command, Figure 5-7. Figure 5-8 shows the heaters of the hydrazine tank and Figure 5-9 the thermal decoupling between the TCA and FCV.

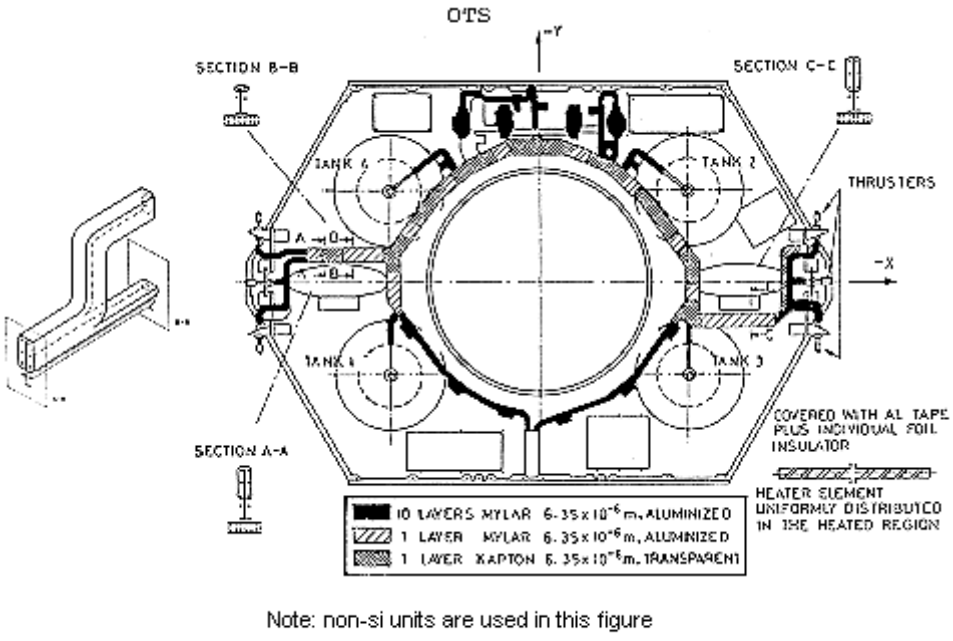

Note: non-si units are used in this figure

Figure 5-6: Insulation in the OTS hydrazine line system. From Stümpel (1978)a [45].

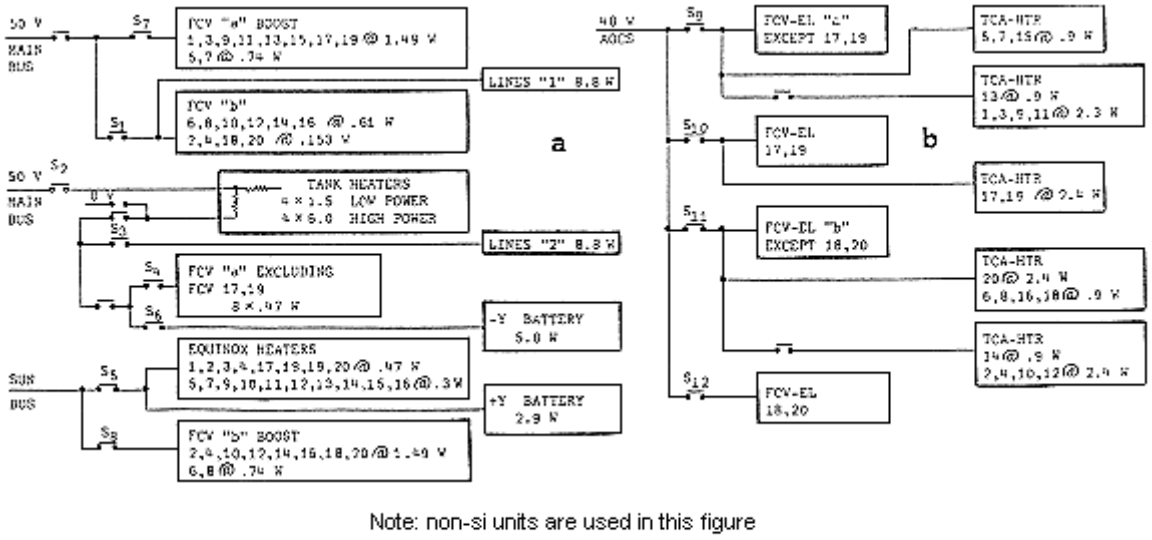

Note: non-si units are used in this figure

Figure 5-7: OTS heater switching diagram.

a) Heating of lines tanks, valves and batteries.

The different heaters are grouped in 8 circuits. Five circuits (corresponding to telecommand switches S1 to S5) are implemented for seasonal operation, one of them (S5) also activates the heater of one battery half. The other battery half has its own separate heater (through switch S6) to limit the temperature differences between the two halves. Two heater circuits (S7 and S8) are reserved for boost heating of the hydrazine components prior to solar eclipse periods which have to be survived without heating.

The telecommand switch in the tank heater circuit (not labelled) allows either the normal heating or the boost heating of the tank.

b) Heating of valves and thrusters of the AOCS (telecommand switches S9 to S12) is also shown.

From Stümpel (1978)b [46] and Bouchez & Gülpen (1980) [5].

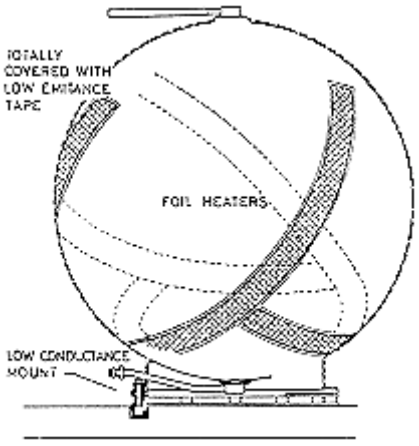

Figure 5-8: Thermal insulation of the hydrazine tank. The tank is totally covered with low emittance tape. Heaters are of the foil type (see ECSS-E-HB-31-01 Part 11, clause 4.2). The tank contacts the platform via a low conductance amount. From Stümpel (1978)b [46].

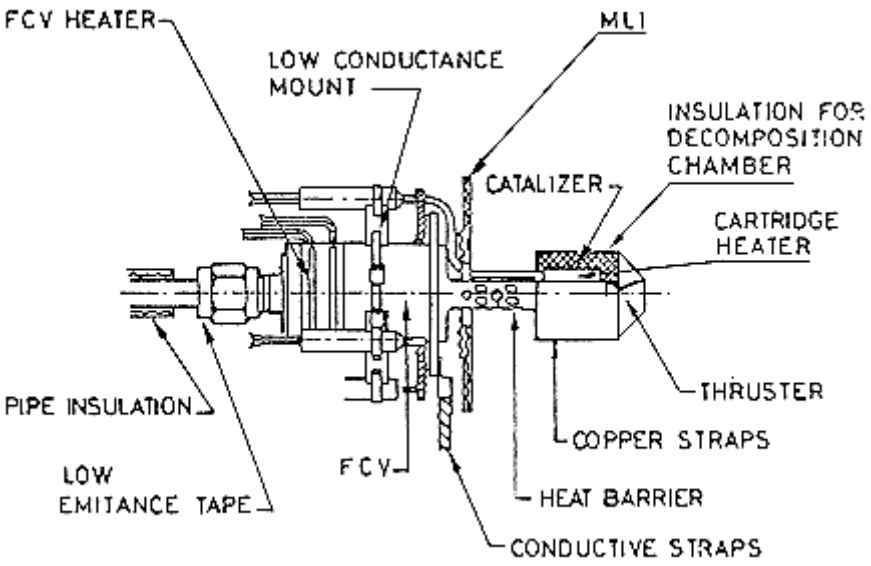

Figure 5-9: Thermal decoupling of FCV from TCA onboard OTS. The heat barrier maintains temperature differences up to 800 K via a length of 0,03 m.

A radiation fixture of three copper straps spot-welded to the heat barrier close to its junction into the thrust chamber head plate was used to avoid the flashback problem. Flashback results in a reduction of the refrigerating effect of hydrazine and heating of the feed tube to the hydrazine decomposition temperature, and in a strong reduction in thrust. From Stümpel (1978)b [46].

Possible improvements in thermal control of future spacecraft, based on OTS experience:

— Introduction of an equinox heater system. A reduction of the seasonal temperature sing to less than 5 K would be achievable by more complex heater system applying certain heating also under solstice conditions. This would require a thermostatic heater control, desirably with an electronic control unit (Proposed by ERNO for implementation in ECS/MCS).

— Direct coupling of the battery to space through 3 circular view ports in the adjacent side walls.

— Thermostatic control for RCS. Two approaches are conceived for future projects: An "on-off" electronic thermo-switch which operates each heater individually and the optimization of proper heater power.

— Isolation of external units. Equipment causing leaks in the insulation may contribute considerably to the spacecraft diurnal temperature variation without being directly controllable by the thermal control system. It is necessary to provide individual component level thermal control for such units which allow their total isolation from the spacecraft interior.

5.8 Estimated on orbit performance

The investigation of the long term stability of the employed thermal control technologies in geostationary orbit was one of the main aims of the OTS (see also ECSS-E-HB-31-01 Part 6, clause 5.2.6).

Thermal tests were performed on the ground and in orbit. The purpose of ground tests was to verify that the spacecraft performance was within acceptable limits and that the mathematical model used was capable of predicting) the test results. In order to achieve this two-fold aim, tests were performed simulating space temperatures and solar irradiation at extreme equinox and solstice conditions under selected fixed solar input angles (steady-state tests).

The spacecraft was instrumented with 152 thermistors, thermocouples and platinum wire resistances. Their distribution is given in Table 5-3. The total number of thermal sensors was constrained by the available telemetry channels in orbit.

All sensors were calibrated. The error sources associated with temperature readings were partially due to the mathematical function introduced to represent the calibration curve (which was very small an error), and partially due to the quantization associated with a one bit of the telemetry channel (between 0,3 K and 0,8 K).

Table 5-3: Sensor Distribution

Subsystem	Sensors
RCS	38
Power	13
ABM	2
AOCS	14
TT & C	9
Antenna	24
Repeater	40
Structure	12
Total	152

NOTE From Bouchez & Howle (1982) [7].

Mathematical models were used to predict both the steady state thermal conditions and the transient temperature response to the daily cycle of the spacecraft relative to the Sun and to variations in on-board power dissipation.

The accuracy of the mathematical model could be verified by comparison of the actual orbit temperatures with those predicted with identical operating and environmental conditions. This comparison will be introduced in the following clause.

5.9 Measured in orbit performance

The objectives of the orbit tests were to assess the adequacy of the thermal control subsystems, to validate the analytical predictions, to provide the possibility of assessing the thermal distortion of a large antenna dish, and to detect and quantify degradations of the thermal control coatings.

All tests were well defined beforehand in order to model accurately the dissipation of the individual equipment. The estimation of the dissipations that had to be introduced in the mathematical prediction model was a major problem in the thermal analysis. During tests the activity of the repeater was kept to a minimum and as few channels as possible were operated. Nevertheless, identical operating conditions at all comparable orbit test was not fully achieved because of operational constraints.

Each test lasted two days, and readings of sensors were telemetered at 25,6 s intervals during test time.

The first in orbit thermal test was conducted on May 25-26, 1978 after the spacecraft had reached its final position and was set into normal operation mode. Histograms of the deviation between measured and predicted temperatures are shown in Figure 5-10. Tests were performed with 48 thermal sensors internally placed on the radiators of the spacecraft. The accuracy of each sensor was around 0,3 K to 0,5 K, although, due to the number and situation of the 48 selected sensors, the mean spacecraft temperature had an accuracy better than 0,1 K in some cases.

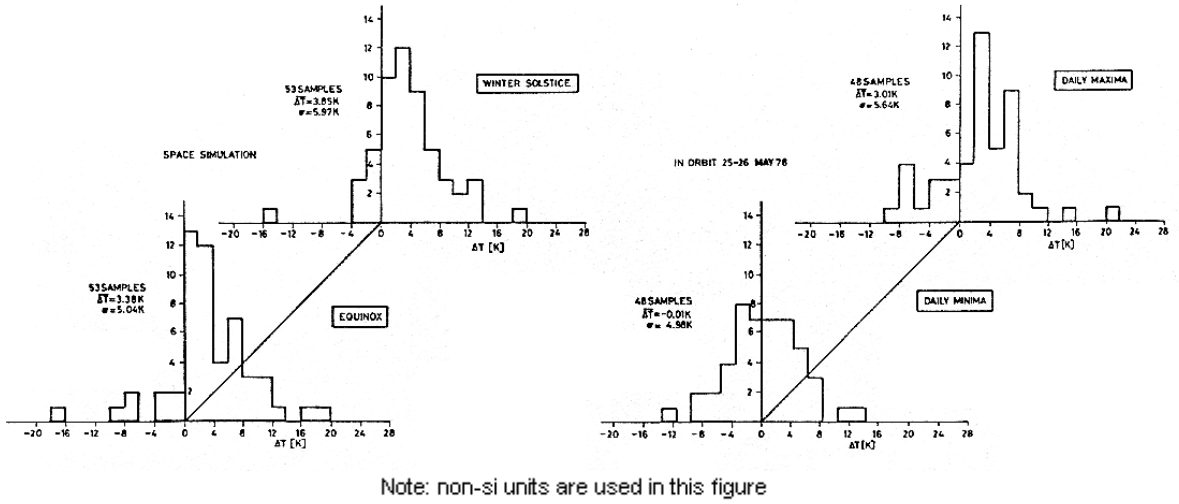

Note: non-si units are used in this figure

Figure 5-10: Histograms for ground and first orbit test. From Bouchez & Gülpen (1980) [5]. The ordinates show the number of samples the temperature deviation of which stays within the limits shown in abscissae.
($\Delta T = T_{measured} - T_{predicted}$).

The main differences found between measured and predicted temperatures were that mean diurnal temperature was about 1,5 K above predictions, with a standard deviation of 5 K, and diurnal temperature variation was about 3 K larger than predicted. The reason was an underestimated solar input into the spacecraft adapter and the cavity of the ABM never properly simulated during ground tests. Once this effect was accounted for, the mean diurnal temperature was reduced to 0,7 K, the standard deviation to 4,5 K and the diurnal temperature variation to 1,8 K.

In Figure 5-11, three typical histograms for daily maximum and minimum temperature of test performed during Summer Solstices (SS) of 1978, 1980 and 1981 are shown. Here the predicted temperature corresponds to BOL.

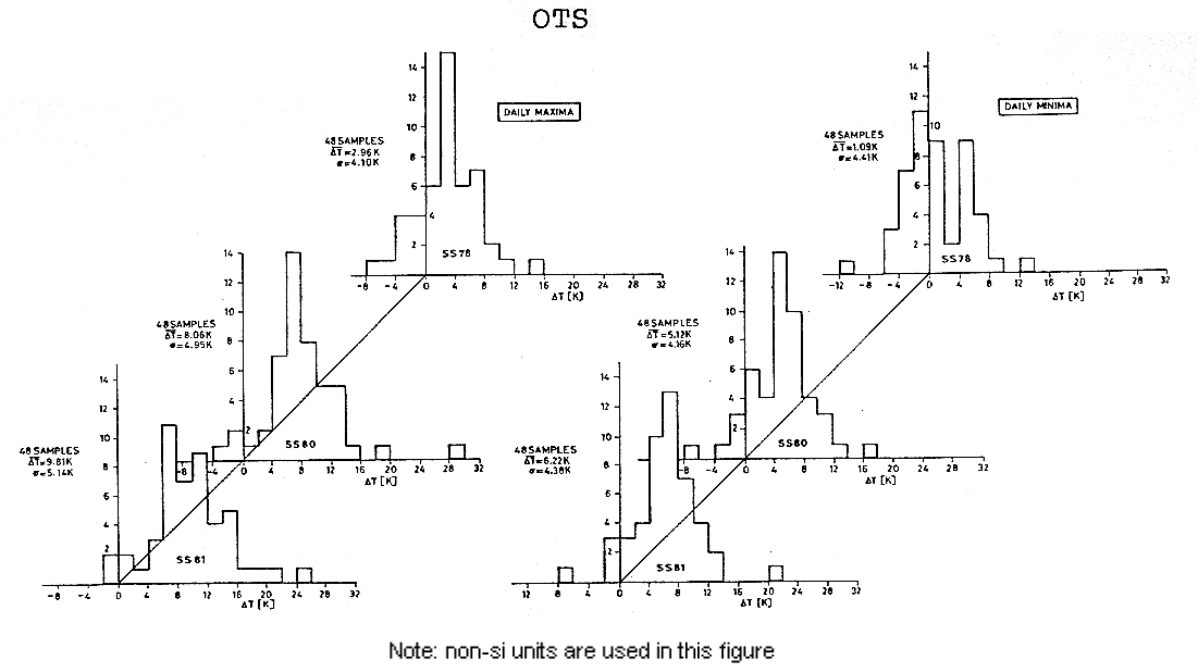

Note: non-si units are used in this figure

Figure 5-11: Histograms for orbit tests during different summer solstices. Data for 1978 and 1980 are from Bouchez & Gülpen (1981) [5] and those for 1981 from Bouchez & Howle (1982) [7].

During solstice the inaccuracy associated to power dissipation can be approximately 0,8 K, this is so since solstice involves few spacecraft switching activities and the operating mode is more or less constant. During the equinox there are operational RF mode changes, extra switching of heaters in pre-eclipse periods, battery recharging and a drastic change of external input after eclipse. The inaccuracy is estimated to be round 1,4 K.

Daily maximum temperature increases respect BOL predictions are given in Table 5-4 and Figure 5-12. Exponential time function have been fitted to measured data.

Table 5-4: In Orbit Measured Values and Curve Fitting Values

Date	Daily Max.		Daily Min.		Differences		Fitting Exponential Function			
Solstice (S) Equinox (E)	Test ΔT [K]	Curve Fitting ΔT [K]	Test ΔT [K]	Curve Fitting ΔT [K]	Daily Max $\Delta\Delta T$ [K]	Daily Min $\Delta\Delta T$ [K]	$\Delta T = \Delta T_m\ (1-e^{-(t-to)/\tau})$			
Summer S 1978	2,96	3,05	1,09	1,09	– 0,09	0	Summer Daily Max.	ΔT_m [K]	t_o [d]	τ [d]
Winter S 1978	3,84	4,02	1,52	1,72	– 0,18	– 0,20				
Summer S 1979	6,39	6,04	3,61	3,55	0,35	0,06		15,5	–122	1333
Winter S 1979	7,63	7,42	4,68	4,36	0,21	0,32				
Summer S 1980	8,06	8,29	5,12	5,22	– 0,23	– 0,10	Daily Min.	9,1	42	1003
Winter S 1980	9,93	9,69	6,60	6,13	0,24	0,47				
Summer S 1981	9,81	10,00	6,22	6,39	– 0,19	– 0,17	Winter Daily Max.	14,4	42	933
Winter S 1981	11,13	11,21	6,87	7,33	– 0,08	– 0,46				
Summer S 1982	11,68	11,30	7,64	7,20	0,38	0,44				
Winter S 1982	11,12	12,23	7,15	8,14	– 1,11	– 0,99				
Summer S 1983	12,20	12,30	7,54	7,77	– 0,10	– 0,23	Daily Min.	9,9	164	942
Winter S 1983	13,73	12,92	9,56	8,70	0,81	0,86				
Autum. E 1978	2,47	2,63			– 0,16		Daily Max. (Outside eclipse)	7,9	–212	1181
Vernal E 1979	3,90	3,38			0,52					
Autum. E 1979	3,98	4,04			– 0,06					
Vernal E	4,53	4,59			– 0,06					

Date	Daily Max.		Daily Min.		Differences		Fitting Exponential Function			
Solstice (S) Equinox (E)	Test ΔT [K]	Curve Fitting ΔT [K]	Test ΔT [K]	Curve Fitting ΔT [K]	Daily Max $\Delta\Delta T$ [K]	Daily Min $\Delta\Delta T$ [K]	$\Delta T = \Delta T_m\ (1-e^{-(t-to)/\tau})$			
1980 Autum. E 1980	4,21	5,07			– 0,86					
Vernal E 1981 Autum. E 1981	5,19 6,25	5,47 5,82			– 0,28 0,43		Beginning of eclipse	4,7	7	798
Vernal E 1982 Autum. E 1982	6,76 6,88	6,12 6,38			0,64 0,50					
Vernal E 1983 Autum. E 1983	6,52 6,20	6,60 6,79			– 0,08 – 0,59		End of eclipse	5,3	–126	830

NOTE From Bouchez & Howle (1984) [7].

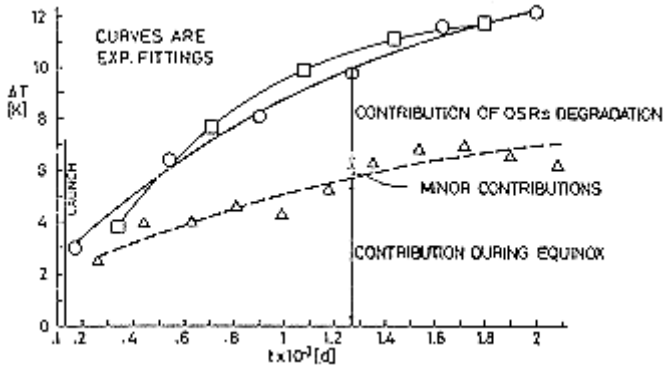

Figure 5-12: Temperature increases ΔT as a function of time, t elapsed since Jan 1, 1978. From Chalmers, Konzok, Bouchez & Howlw (1983) [13].
Circle: Summer Solstice test points.
Square: Winter Solstice test points.
Triangle: Equinox test points.

The temperature increases can be traced back to surface degradation which results in an increase of absorptance. This effect can be assessed through orbit thermal test data via a duplication of the orbit measurements by a mathematical model which takes into account the actual operational configuration of each test.

The surfaces which degradate during equinox were MLIs, S-13 G/LO white paint on the antenna dishes, spacecraft adapter and some small Earth and Sun sensor apertures. The estimated increase in absorptance of the MLI and white paint would give a temperature increase of 3,3 K. Since according to Figure 5-12 the increase since the first equinox is of the order of 4 K, some degradation of the spacecraft adapter should be taken into account.

In solstice, the effect on the radiation of OSRs degradation should add to the mentioned effects. Causes of OSR degradation are discussed in ECSS-E-HB-31-01 Part6, clause 5.2.6. Results from solstice data are summarized in Table 5-5. Compare these data with similar results in ECSS-E-HB-31-01 Part6, clause 5.2.6.

Table 5-5: Change in Solar Absorptance, $\Delta\alpha_s$, of OSR vs. Exposure Time as Deduced from OTS Solstice Data

Time from Launch [d]		40	214	400	582	773	949	1137	1312	1501	1676	1865
Summer Solstice	$\Delta\alpha_s$	0,016		0,050		0,080		0,099		0,113		0,131
Winter Solstice	$\Delta\alpha_s$		0,016		0,074		0,100		0,112		0,113	

NOTE From Chalmers, Konzok, Bouchez & Howle (1983) [13]

In order to estimate the solar absorptance degradation of the S-13 G/LO white paint the spotbeam antenna dish was instrumented with a total of 14 temperature sensors (3 platinum resistance and 11 thermistors). Due to deterioration in performance of some sensors with time, a group of 10 of the original 14 sensors has been used to calculate the points which appear in Figure 5-13. The BOL absorptance (α_s = 0,18) and a predicted band of absorptance values are also shown in the figure.

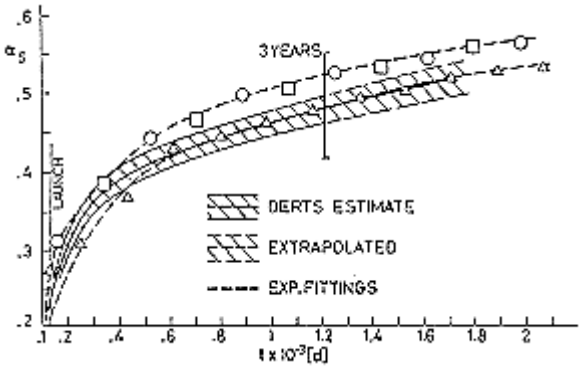

Note: non-si units are used in this figure

Figure 5-13: Mean solar absorptance, α_s, on antenna dish white S-13 G/LO paint. From Chalmers, Konzok, Bouchez & Howle (1983) [13]. Circle: Summer Solstice test points. Square: Winter Solstice test points. Triangle: Equinox test points.

It can be seen that while the first two values after launch are significantly greater than expected, subsequent values are generally only a little above the prediction band. Good lines can be drawn through the winter and the summer solstice points and through the autumn and vernal equinox points although, in the first case, the angles that the Sun vector made with the planes of the sensors were quite different in the two seasons.

A re-evaluation of the properties of S-13 G/LO white paint has been made recently by Cull et al. (1984) [17].

References: Collette & Stockwell (1976) [14]; Wearmouth & McLaurin (1977) [57]; Bouchez, Howle & Stümpel (1978) [9]; Bulloch (1978) [11]; Stümpel (1978)a [45]; Stümpel (1978)b [46]; Bouchez & Gülpen (1980) [5]: Bouchez & Howle (1981) [6]; McLaurin & Gregory (1981) [35]; Bouchez & Howle (1982) [7]; Chalmers, Konzok, Bouchez & Howle (1983) [13]; Bouchez & Howle (1984) [8].

6
Landsat D

6.1 Mission

Imaging the same 185 km belt of the Earth surface each 20 days.

Launching date: July 16, 1982.

Mission life: 3 years.

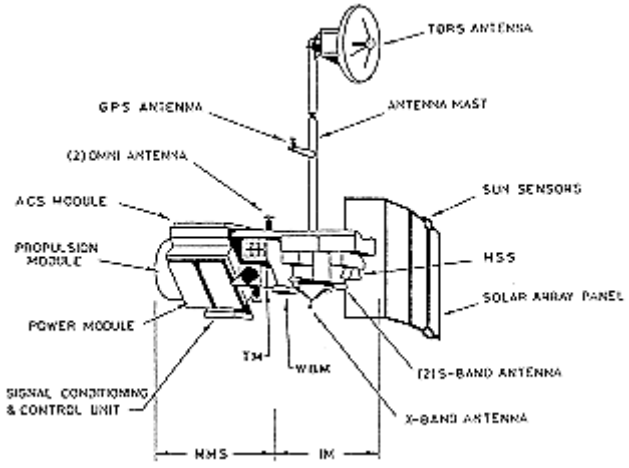

Figure 6-1: Landsat spacecraft in orbital flight.

6.2 Main subsystems

Landsat D (now, that is in orbit, known as Landsat 4) incorporates the Thematic Mapper (TM), a seven spectral band mechanically scanned radiometer with 30 m spatial resolution, and the MultiSpectral Scanner (MSS), 80 m resolution and four spectral bands, similar to that flown on Landsat 1 and 2 (see ECSS-E-HB-31-01 Part 9 clause 6.6). TM was not flown before. Both instruments were built for NASA by Santa Barbara Research Center, Goleta, Calif., a subsidiary of Hughes Aircraft.

Data from TM and MSS are transmitted through the wideband communication system to the Tracking and Data Relay Satellite (TDRS) and to ground based stations.

Landsat D is the first NASA Satellite to utilize the Global Positioning System (GPS) which receives navigation messages from a constellation of Navigation Data Satellites and computes position, velocity and time for the host satellite.

6.3 Main characteristics of the satellite:

The main body of the spacecraft consists of NASA's standard Multimission Modular Spacecraft (MMS), and the Landsat Instrument Module (IM), Figure 6-2. MMS provides: power, attitude control, communications and data handling, and propulsion. The same module was used in the future with different payload (Caruso & Stipandic (1980) [12]).

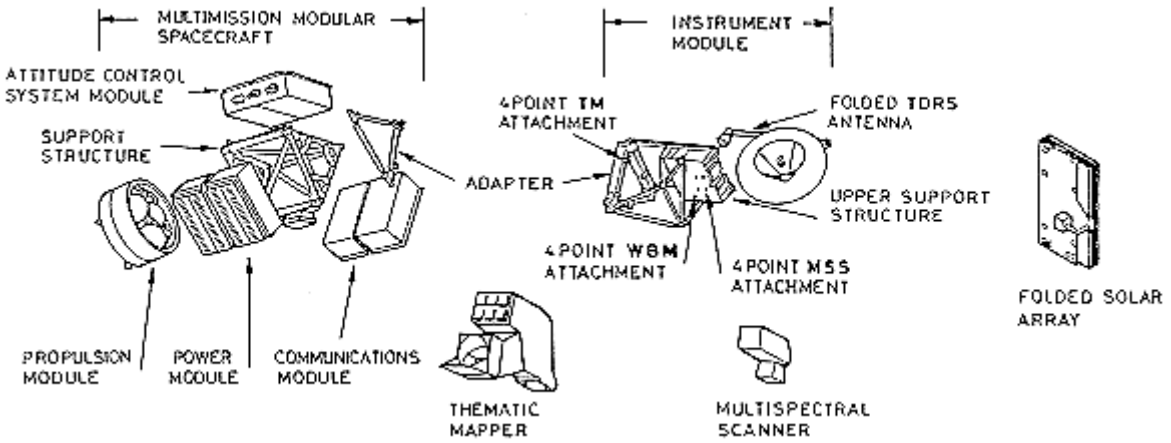

Figure 6-2: Exploded view of the Landsat D spacecraft before deployment.

The long dimension of the spacecraft body (the roll axis) lies in the plane of the orbit, the yaw axis is oriented to the local vertical (parallel to the antenna mast), and the pitch axis is normal to the orbit plane and parallel to the axis of rotation of the solar array.

Landsat D was launched on July 16, 1982, by a Delta 3910 booster. Subsequent launches of Landsat satellites are planned for the Shuttle, commencing in late 1984. The already launched satellite were recovered by the Shuttle before the second launch.

The mass of the Landsat D Flight Segment (as of May 1979) is given in Table 6-1.

Table 6-1: Landsat D Flight Segment Mass Summary

Component	Mass [kg]
Multimission Modular Spacecraft	
Spacecraft Dry	754
Payload Attachment Fitting	63
Payload Instruments	
Thematic Mapper	234
MultiSpectral Scanner	65
Instrument Module	
Global Positioning System	21
WideBand Module	73
RF Module and Antenna	72
Tracking and Data Relay System Antenna Boom	55
Solar Array & Drive	71
Structure	92
Thermal Subsystem	14
Electrical Integration	50
Total Dry Mass	1564
Fuel & Pressurant	77
Launch Mass	1641

6.4 Orbit

Circular Sunsynchronous.

Altitude: 709 km.

Inclination: 98,2°.

Descending node: between 9 h 30 min and 10 h a.m.

β: between 23,4° and 41,8°.

6.5 Thermal design requirements

The thermal control subsystem maintains all components within the required operating temperature limits (Table 6-2) during launch, ascent to orbit and deployments, on orbit mission modes, Safe Hold, and Shuttle storage and retrieval operations. Safe Hold mode of operation aims at recovering after a computer malfunction.

Temperature control for Earth ambient can be accomplished with the assistance of suitable Ground Support Equipment.

Table 6-2 itemizes the thermal design requirements of the various components and subsystems.

Table 6-2: Thermal Design Requirements

Component	Operating Temp. Range [K]
Instrument Module Structure	283-303
S-Band Transmitters	278-308
Sensors	283-303
WideBand Module	283-303
RF Module/Boom	261-303
GPS Preamplifier	253-303
Multimission Modular Spacecraft	283-303

6.6 Design tradeoffs

- Modular vs. Integrated. Modular design was selected because of the following reasons:

  Hardware for major subsystems is modularized and use separate thermal control.

  WideBand system can be packaged into self-contained units with minimal interfaces with the other subsystems.

  Majority of remaining electronics can be controlled by a common radiator.

  Since there is no heat transfer among modules, the temperature of the structure remains very stable. Thence, significant in-orbit thermal distortions should not result.

- Passive vs. Active. All components were passively controlled with the exception of MMS which, being designed for a wide range of missions, is controlled by means of Louvers (see ECSS-E-HB-31-01 Part 12, and also, Karam (1979) [30], Hwangbo & Kelly (1980) [27]).

  Passively controlled components are mounted within a thermal enclosure covered with MLIs (see ECSS-E-HB-31-01 Part 9 clause 6). Heat is rejected to space through openings in the insulation (Radiators, see ECSS-E-HB-31-01 Part 9). The components are mounted as close as practical to the radiators to minimize heat paths. Structural interfaces will provide maximum heat transfer.

6.7 Thermal control of various components

The Instrument Module radiator is placed in the anti-earth face of the spacecraft, removed from the payload instrument interfaces.

The S-band transmitters are mounted on the anti-Sun face of the spacecraft to allow for maximum fin efficiency. When the transmitters do not operate at all, or when the duty is low, electrical heating is used to keep temperatures above minimum.

The Thematic Mapper uses a two-stage passive radian cooler (see ECSS-E-HB-31-01 Part 9 clause 6), oriented to the anti-Sun side of the spacecraft, for temperature control of the thermal band detectors. The detector heat load is 85 mW, whereas Sherman (1982) [41] quotes values of the order of 30 mW.

The MultiSpectral Scanner incorporates a cone cooler (see ECSS-E-HB-31-01 Part 9, clause 6.6), the axis of which is oriented toward the Earth.

The Travelling Wave Tube Amplifiers (TWTA) of the WideBand Module (WBM) are placed in the partially Sun illuminated face of the spacecraft because) of their high operating temperatures (Table 6-2). MLIs are used with the aim of diminishing heat transfer from these amplifiers to the RF and gimbal drive components, which are placed in the Sun-shadowed face of the spacecraft. Figure 6-3.

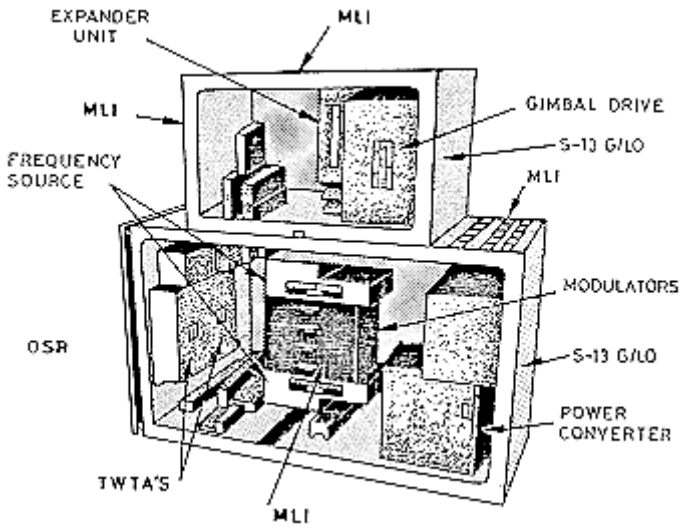

Figure 6-3: Assembled Wide Band Module.

Thermostatically controlled heaters are used to compensate for variables and uncertainties such as:

Internal heat generation.

Heat leaks in the MLIs.

Coating degradation.

Solar heat load effects.

Sensor interface performance.

Heater requirements for the Instrument Module include: six electrical circuits for nominal operation modes, two for Safe Hold and seven for operating during storage and retrieval within the Shuttle.

All subsystems have individual heaters for thermal control when the particular subsystem is turned off.

Coating used are shown in the Figure 6-4.

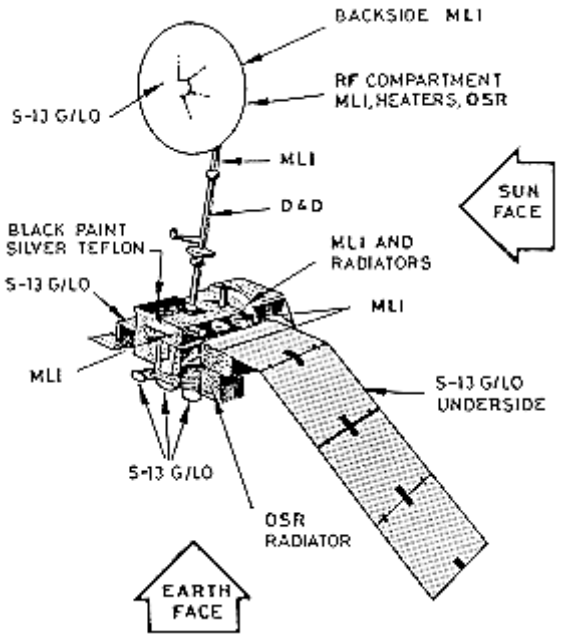

Figure 6-4: Thermal Control coatings used on Landsat D.

D4D is a leafing Aluminium coating manufactured by GEC.

S-13 G/LO is a Zinc Oxide-Methyl Silicone white paint manufactured by IITRI.

OSR see

6.8 Estimated on orbit performance

Model incorporates an automatic heater routine which senses structural temperature and applies heat at a given heater-setting until the temperature rises to a predetermined cut-off value.

Table 6-3 gives average temperatures and day-night temperature variations for all components in the Instrument Module and for hot and old case conditions corresponding to extreme β values. All temperature values are within the extremes given in Table 6-2.

Table 6-3: Estimated on Orbit Performance of the Instrument Module Components

COMPONENT	Mounting Structure Temperature [K]		Day-night Temperature Variation [K]		COMMENTS
	Hot Case $\beta = 26°$	Cold Case $\beta = 41{,}8°$ [a]	Hot Case $\beta = 26°$	Cold Case $\beta = 41{,}8°$ [a]	
Global Positioning System Receiver Processor	302,5	285,3	2,0	0,6	
Bus Coupling Unit BCU No. 1	301,8	284,1	5,5	4,2	
BCU No. 2	302,7	285,2	4,3	3,6	
Remote Interface Unit/Expander Unit RIU/EU No. 1	300,4	284,2	7,8	5,4	Mounted adjacent to MSS multiplexer.
MultiSpectral Scanner Multiplexer	302,8	288,7	10,7	9,1	Large heat dissipation and partial duty cycle.
Solar Array Drive	303,0	286,6	0,6	0,5	
RIU/EU No. 2	300,3	284,9	1,6	0,8	
Global Positioning System Local Oscillator	300,3	283,9	9,0	5,8	Large heat dissipation. Change in solar flux absorbed over orbit.
S-Band Transmitter A	293,7	278,7	5,5	2,8	Large heat dissipation and partial duty cycle.
S-Band Transmitter B	302,4	279,7	24,0	6,2	
Digital Processor Unit	301,7	286,0	7,1	0,5	
BCU No. 3	300,9	284,5	6,1	3,9	
Power Distribution Unit	300,5	296,5	0,1	0	
RF Combiner	292,6	288,3	0	0	
RIU/EU No. 3	295,0	289,3	0,2	0,1	

COMPONENT	Mounting Structure Temperature [K]		Day-night Temperature Variation [K]		COMMENTS
	Hot Case $\beta = 26°$	Cold Case $\beta = 41{,}8°$ [a]	Hot Case $\beta = 26°$	Cold Case $\beta = 41{,}8°$ [a]	
MMS Intermediate Frequency	292,6	288,1	0,1	0,1	
TM Intermediate Frequency	293,0	288,6	0,4	0,2	
MSS Intermediate Frequency	302,4	284,1	0,8	0,4	
Wide Band Intermediate Frequency	301,0	284,6	1,7	1,9	

[a] Average heater power $Q = 20{,}3$ W.

6.9 Verification

Accomplished by a combination of testing, analysis and inspection.

At Component level

Equipments were acceptance and qualification tested according with NASA approved standards and specifications.

Optical properties of the coating were measured.

Each honeycomb panel was checked for thermal compliance.

Heaters and thermostats were tested at the manufacturing facilities and acceptance tested.

At System level

A thermal analysis was performed to check the basic thermal design and performance.

Thermal balance tests of the protoflight Instrument Module were made in a solar simulation facility. The IM was positioned in the chamber and rotated to simulate worse case transient orbit environmental conditions.

Earth and albedo radiations were simulated by IR lamps attached to the test support structure.

Interfaces were simulated as follows:

The solar array panels by a fixed heater dummy model.

The TDRS antenna boom by a partial boom length with appropriate thermal coating and thermal properties.

MMS and the MSS sensor by means of models which duplicate the heat capacity and blockage effects of the prime hardware provided with an attachment point heater to simulate the interface heat transfer.

A separate thermal test was performed to verify the thermal design of the TDRS antenna -RF Module and gimbal drive assembly.

6.10 Measured on orbit performance

No data have been found.

On 20 February 1983 the X-band radio transmitter, that beams TM, did not recover proper functioning after a Safe Hold (Waldrop (1983)a [55]).

Other breakdown since February 1983 were (Waldrop (1983)b [56]):

Failure of communications and data handling module. Commands from ground are being sorted and routed by a backup.

Progressive deterioration of the electrical cables from the solar panel. Two of the panels are inoperable (as of August 1983). This leaves just enough power to run MSS.

TDRS was still undergoing checkout in orbit during August 1983, and will be used mainly for Space Shuttle operations when fully operational.

References: All the data in this item, unless otherwise stated, are from Bachofer (1979) [2].

7
Infrared astronomical satellite (IRAS)

7.1 Mission

To make a first time all-sky survey of infrared sources in the universe in the wavelength region $8x10^{-6}$ m to $119x10^{-6}$ m and auxiliary observations from $8x10^{-6}$ m to $300x10^{-6}$ m.

Launching date: January 25, 1983.

Mission life: 300 d. Mission life is controlled by the venting rate of superfluid helium in the cryocooling system of the Telescope.

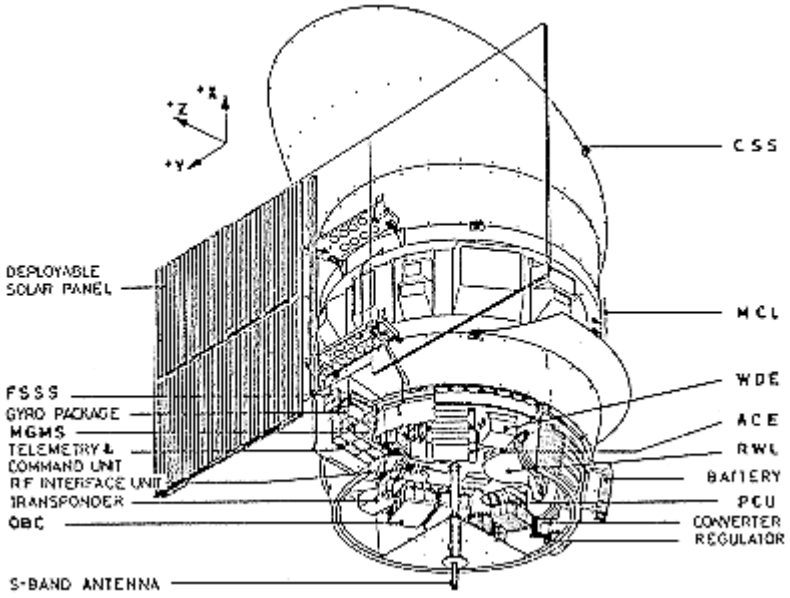

Figure 7-1: IRAS spacecraft in orbital flight. See also Table 7-1. From Van Leeuwen (1983) [53].

7.2 Main subsystems

IRAS satellite consists of two parts, the Spacecraft providing the housekeeping systems, and the cryogenic system and Telescope.

The spacecraft system provides the support functions, such as attitude control, power, communications and data storage.

The cryogenic system is required to maintain the telescope optics below 10 K, and the focal plane below 3,5 K.

Table 7-1 presents the subsystems and components which require thermal control (see Figure 7-1).

Table 7-1: IRAS Main Subsystems

Subsystem	Components	Localization in the Satellite
Power	Solar Panel Assembly	
	Fixed Panel	Attached to the dewar (SCOT)*.
	Deployable Arrays	Attached to the fixed panel
	Power Control Unit (PCU)	
	Converter	Inner surface on the cone, –*z* side.
	Regulator	Inner surface on the cone, –*z* side.
	Battery	Cone rearside.
Command & Data Handling	Transponder	Equipment platform, +*y* side.
	Telemetry & Command Unit	Equipment platform, +*z* side.
	On-Board Computer (OBC)	Equipment platform, +*y*/+*z* quadrant.
	Antenna	-x side of the spacecraft.
Stabilization & Control	Attitude Control Sensors (ACS) Package containing	Outer +*z* side of the cone.
	Fine Sun Sensor (FSSS)	+*z* viewing.
	Gyro Sensor (GYRS)	Inside.
	Gyro Electronics (GYRS)	Inside.
	Magnetometer (MGMS) + Electronics (MGME)	Inside. Inside.
	Coarse Sun Sensors (CSSS)	ACS package ±*y* ±*y* side of the sunshade. On HSE.
	Horizon Sensor (HSE)	–*z* side of the cone outside.
	Reaction Wheels (RWL) + Electronics (WDE)	Equipment platform. (RWL –*x*, –*y*, –*z*).

Subsystem	Components	Localization in the Satellite
	Magnetic Coils (MCL)	Rearside of the dewar. Outer shell (MCL +*y*/−*z* and −*y*/−*z*). Equipment platform +*x* side.
	Attitude Control Electronics (ACE)	Equipment platform.
Payload	Telescope	Surrounded by the dewar.

NOTE (*) SCOT: Spacecraft Component On the Telescope.
From Van Leeuwen (1985) [54].

7.3 Spacecraft main characteristics

The structure of the Spacecraft consists of an aluminium truncated cone supporting a honeycomb platform at the Telescope side. The cone serves on one side as the interface of the satellite with the Delta launcher, on the other side the cone supports the Infrared Experiment (IRX). The cone is also the main radiator for internal Spacecraft dissipations.

Most of the housekeeping units are mounted on the Spacecraft platform. Some of them are mounted on the outer-side of the cone. The SCOT units are mounted on the telescope for reasons of dimensions or required field of view.

Figure 7-2 presents a view of the IRAS telescope subsystem. Two cryogenic systems are used: 1) The main cryogenic tank (MCT) with superfluid helium to surround the telescope, and 2) a cover containing supercritical helium to seal the aperture of the dewar. The cover is ejected in space once the satellite outgassing rate has reached an acceptable level.

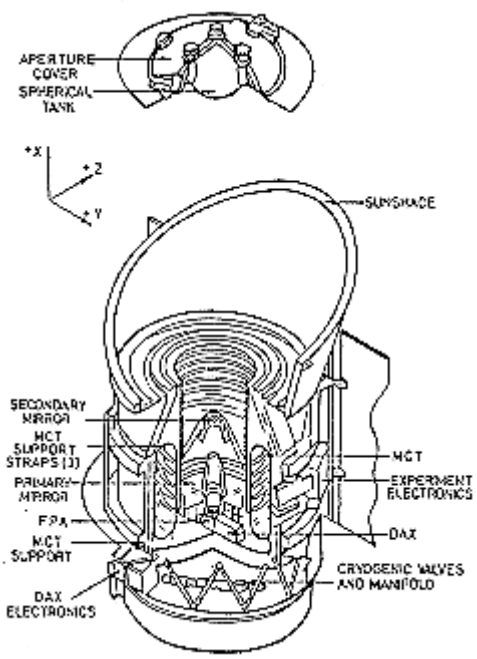

Figure 7-2: IRAS telescope subsystem. From Urbach et al. (1982) [52]

MCT (which is annular in shape) contains 70 kg of superfluid helium with 120llage at a temperature of 1,8 K. The telescope mounting ring is welded to the surface of the 0,75 m cavity and the entire cavity is surrounded by a thin aluminium thermal shroud. MCT and insulation system are supported by three supports at the top and by six at the bottom. Anchored to one of the upper support brackets is a getter cup containing 0,5 kg of charcoal. A main shell provides the primary structural integrity of the system.

The aperture cover subassembly is the vacuum seal for the main shell during ground operation. It is also a gas condensation trap prior to and during cooldown of the MCT and it minimizes heat leak to the MCT during launch hold. It contains 6 kg of supercritical helium, which allows fourteen days in orbit with a 48 h launch pad hold. After a minimum of four days the cover is ejected into space and the all-sky survey starts.

IRAS was launched on January 25, 1983 from Western Test Range, California, by a two-stage Delta 3910 launch vehicle. Total mass of the satellite was 1077 kg.

IRAS is a joint project by the Netherlands, United States and United Kingdom. Dutch contribution (Fokker BV with Signaal Co., and NLR) consisted of the design and manufacture of the Spacecraft, integration, testing, launch preparation and a significant part of the ground operations. USA developed and manufactured the IRX, launched the satellite and processed the scientific data. The cryogenic system and Telescope were supplied by Ball Aerospace System Division (BASD), whereas the Jet Propulsion Laboratory (JPL) had USA project management responsibility and supplied the detector focal plane assembly (FPA). The Space Research Laboratory of the University of Groningen developed the Dutch Additional Experiment (DAX), an infrared experiment package in the telescope. The UK contribution, mainly conducted at the Rutherford-Appleton Laboratories, provided the ground station and operations.

7.4 Orbit

Near polar sunsynchronous circular twilight:

Inclination: 99°

Altitude: 900 km

β: between 60° and 120°. These are upper and lower bounds. β depends on the mission day. Here, as in clause 4.4, β is the angle between the line to the Sun and the telescope axis.

7.5 Thermal design requirements

The Spacecraft Thermal Control Subsystem provides three main functions:

1st. Maintain the prescribed temperature requirements for all subsystems, including SCOT but excluding IRX, for all mission phases.

2nd. Minimize the heat flow from the Spacecraft to the telescope.

3rd. Minimize the thermal contribution to structural distortions.

The cryogenic system will maintain the telescope optics and focal plane at the prescribed temperature.

Table 7-2 summarizes the thermal design requirements of the various components and subsystems that were used. The temperature requirements for the electronic equipment are, in general, the acceptance temperature as defined by the unit suppliers.

Table 7-2: Thermal Design Requirements

<table>
<tr><th colspan="3">Spacecraft</th><th colspan="2">Telescope</th></tr>
<tr><th colspan="2">Components</th><th>Operating Temp. Range [K]</th><th>Components</th><th>Operating Temp. Range [K]</th></tr>
<tr><td colspan="2">Electronic Equipment</td><td>263-313</td><td>Optics</td><td>< 10</td></tr>
<tr><td colspan="2">Battery</td><td>273-293</td><td>Focal Plane Assembly (FPA)</td><td>< 3,5</td></tr>
<tr><td colspan="2">Transponders</td><td>263-328</td><td>Baffle</td><td>95</td></tr>
<tr><td rowspan="2">FSSS</td><td>Preferred Range</td><td>278-298</td><td>Main Shell</td><td>170</td></tr>
<tr><td>Acceptance Range</td><td>263-313</td><td colspan="2" rowspan="4">From Urbach et al. (1982) [52].</td></tr>
<tr><td rowspan="2">GYRS</td><td>Sensor</td><td>343</td></tr>
<tr><td>Sensor Environment</td><td>263-313</td></tr>
<tr><td colspan="2">CSS</td><td>93-333</td></tr>
<tr><td colspan="2">MCL</td><td>118-338</td><td colspan="2"></td></tr>
<tr><td colspan="5">CSS and MCL are mounted on the Telescope. Minimizing heat flow to the Telescope results in an extremely wide temperature range for the mentioned units.</td></tr>
</table>

NOTE From Van Leeuwen (1983) [53].

Interface requirements that were applied in the IRAS project:

1st. The heat flow from Spacecraft structure to telescope shall not exceed 15 W conductively plus 10 W radiatively.

2nd. The heat flow through the Solar Array Mounting to the telescope shall not exceed 6 W.

3rd. The CSS and MCL, mounted on the telescope, shall not contribute more than 1 W each.

7.6 Design constraints

IRAS mission includes the following phases:

(a) Launch and ascent.

(b) Sun/Earth acquisition.

(c) Normal operation in orbit. During orbital flight a number of attitude restrictions apply to keep Sun and Earth from the innerside of the telescope baffle. These limits the β angle as indicated above (see clause 7.4). A rotation around the +z axis of at most 30° is allowed. During observation both this angle and β can change continuously (Figure 7-3).

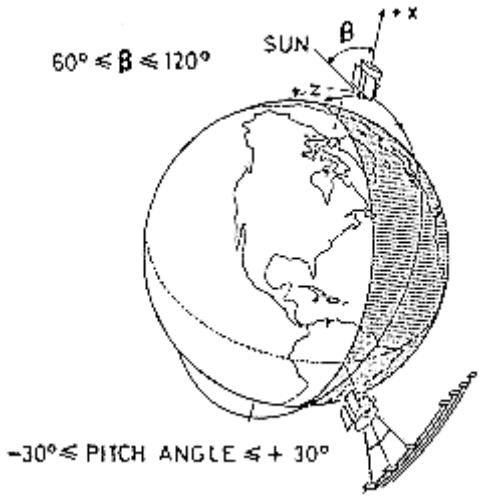

Figure 7-3: IRAS attitude constraints during mission. From Van Leeuwen (1983) [53].

The following constrains have been taken into account:

1st. The spacecraft power dissipation can vary between 160 W and 195 W, depending on the observation programme and attitude maneuvers (orbit averaged).

2nd. Seasonal variation of the solar intensity is:

$S_0 = 1353 \pm 46$ W.m^{-2}.

This was the best estimate when the IRAS thermal control project was undertaken. A more precise value, $S_0 = 1371 \pm 5$ W.m^{-2}, is given in Smith & West (1983).

3rd. Maximum eclipse duration of 16 min.

4th. Earth radiation, 237 ± 7 $W.m^{-2}$.

Earth albedo, F = 0,30 ± 0,05 (see ECSS-E-HB-31-01 Part 3 clause 5.1)

The above requirements and constraints are fulfilled with a passive thermal design with properly controlled heater.

The battery is provided with heaters and thermistors controlled by the OBC. The GYRS is provided with internally controlled heaters.

7.7 Thermal control of various components

The main characteristics of the IRAS thermal control are summarized in Figure 7-4, concerning the spacecraft, and Figure 7-5 the telescope.

1. EQUIPMENT PLATFORM

- Attached to the +x side of the spacecraft cone.
- Supports most of the electronic units.
- Platform attached to the cone by 48 thermally isolated washers.
- Cubertin 306 black paint on all units and structural parts inside the compartment.
- MLI on the +x side of the platform.

1.1. 0,5 mil ($1{,}27 \times 10^{-6}$ m) silvered Teflon and outside-aluminized Kapton tape on the cone outside.

1.2. Bottom panel as received aluminium covered on the outer side (−x face) with MLI, the outer layer of which is 2 mil inside-aluminized Kapton.

1.3. The horizon sensor is attached to the −z outer side of the cone through 4 isolation washers and covered with outside-aluminized Kapton.

- Launch adapter, integrated on the cone, polished and treated with an Alodine 1000 anticorrosion finish. Polished part kept small relative to the main control surface area.

2. ACS PACKAGE

- Attached to the +z side of the cone.
- MLIs on the top, front and bottom side. The outer layer of the MLI is 2 mil inside-aluminized Kapton.
- Radiator areas on +y and −y side covered by silvered Teflon and outside-aluminized Kapton tape.
- Internal units on isolation washers. Black paint on all units.

2.1. FSSS is mounted on a sub-bracket which consists on a 3 points mounting with one of mounting pins flexible, made of titanium, so as to allow a longitudinal translation if a thermal gradient occurs along the brackets. Outer face silvered Teflon on FSSS.

3. BATTERY

- Mounted on the cone rearside by 8 mounting foot each provided with isolating washers.
- The top surface and part of the sides are radiating areas (silvered Teflon, aluminized Kapton), the rest is covered by MLI, the outer layer of which is 2 mil inside-aluminized Kapton.

— Redundant heater system provides up to 9,8 W. The heater is controlled by the OBC which switches it around a set points of 283 K with a minimum interval time of 512 s. A back-up is implemented by hardwired circuit in the PCU, switching-on the heater at 277 K and off at 289 K (± 2 K), and overriding the OBC control-loop in case of OBC failure.

4. SOLAR PANEL ASSEMBLY

4,1.Central panel attached to the dewar through fiber-glass mounting lugs.

— Both sides covered with 1,27x10^{-6} m thick silvered Teflon tape.

4.2. Two solar arrays attached to the central panel.

— Each panel provided with 8 modules of 2408 solar cells to obtain 420 W in total.

— Low α/ε silvered Teflon tape is applied between the cell modules to minimize the operating temperature.

— Panel rearside is fully covered with 1,27x10^{-6} m thick silvered Teflon tape.

— Attitude maneuvers have been carried out by the Delta launcher to avoid perpendicular solar illumination of the undeployed solar array during launch temperatures exceeding 363 K.

5. SCOT

5.1. CSSS is enclosed in low α, low ε titanium casing and hard mounted to the telescope sunshade.

5.2. Two MCLs mounted on the rearside of the dewar outer shell.

— Covered with a strip pattern of aluminized Kapton and silvered Kapton tape.

— Very low temperature reduce the heat transfer to the dewar but result in high electrical currents if the MCLs are designed for just-after-launch operating temperature (close to 293 K). During mission the minimum operating temperature is 141 K. A special switched circuit is available in the ACE to cope with the difference between these temperatures.

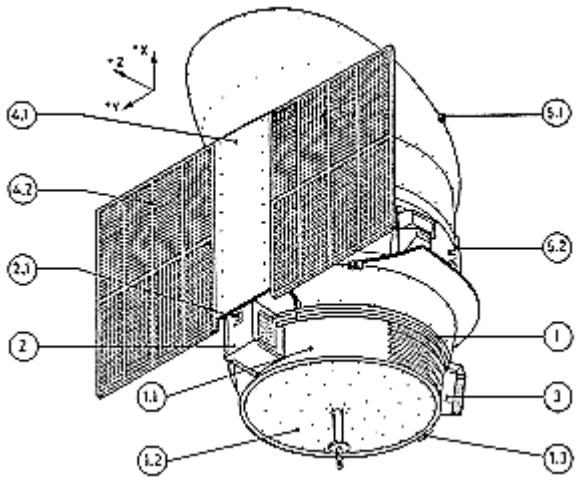

Figure 7-4: IRAS spacecraft thermal control layout summary. From Van Leewen (1983, 1985) [53] & [54].

1. MAIN CRYOGENIC TANK (MCT)

— Annular in shape, constructed of 5083 Al alloy with internal stiffening rings.

— The inner cavity is surrounded by a thin aluminium thermal shroud.

— Surrounded by four MLIs spaced by three VCSs. (See ECSS-E-HB-31-01 Part 6 clause 5).

— The MLI is $6{,}4 \times 10^{-6}$ m double aluminized Mylar with polyester net spacers. (See ECSS-E-HB-31-01 Part 6 clause 5).

— A black radiator ring is thermally attached to the outer VCS.

2. MAIN SHELL

— It serves both as vacuum vessel of the insulation and as a rigidizer of the support system.

— Covered by MLI on the side facing the Earth and the Sun, and with ZOT white paint (see ECSS-E-HB-31-01 Part 6, clause 5.2.3) in the face radiating to space.

3. APERTURE COVER SUBASSEMBLY)

It consists of:

— spherical tank

— two MLIs and one VCS

— three fiber-glass supports

— Valves, back pressure regulator, instrumentation

4. FLUID MANAGEMENT SYSTEM

— Three internal valves:

— V2 internal fill valve. Avoids superfluid helium creeping into plumbing.

— V3 crossover valve to permit venting through either the fill or the vent line.

— V4 porous plug bypass valve used during tank fill operations. Avoids superfluid helium creeping into plumbing.

— Two external valves, V1 and V5, to close of the fill and vent lines.

— Burst Discs (BD) to protect the tank and plumbing against rupture.

— Low Thrust Vents (LTV) to eliminate a disturbing torque during venting.

— Normal operating pressure of the MCT is below $3{,}2 \times 10^{3}$ Pa. BD pressure differential is $7{,}5 \times 10^{3}$ Pa.

4.1. Porous Plug (PP)

— Pore size: $3{,}9 \times 10^{-6}$ m.

— Surface area: $0{,}35 \times 10^{-3}$ m^2.

— Thickness: $6{,}4 \times 10^{-3}$ m.

— Heat transfer rate: $Q = 22 \times 10^{-3}$ W to 0,350 W.

Compare with ECSS-E-HB-31-01 Part 14 clause 7.4.2.6.

5. THERMAL INTERFACE CONTACT JOINTS

— FPA is supported by a copper strap with a $25{,}4 \times 10^{-3}$m square block on each end. The joint at one end is $0{,}127 \times 10^{-3}$ m thick annealed gold foil and indium $0{,}076 \times 10^{-3}$ m at the other.

— Electrical isolation is achieved by coating one block with Parylene (Parylene is a polymer film manufactured by Union Carbide Corporation. Its main features are: very low outgassing, even film thickness, and various thicknesses (Urbach (1986) [49]) bonding the gold foil to it.

— The optics/FPA assembly contacts the dewar mounting ring through twelve $25{,}4 \times 10^{-3}$ m square pieces of $0{,}127 \times 10^{-3}$ m annealed gold foil mounted between the two aluminium rings. Loading is applied by torquing a bolt at each joint to approximately $0{,}7 \times 10^{6}$ Pa.

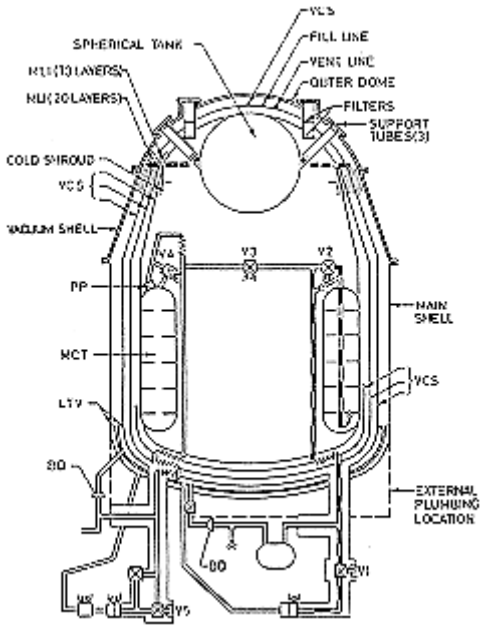

Figure 7-5: IRAS Telescope thermal control layout summary. From Urbach et al. (1982) [52] and Sherman (1982) [41].

7.8 Test of the spacecraft system

A thermal model of the Spacecraft (i.e. excluding the IRX) was built and tested in ESTEC HBF 3 solar simulation facility. The thermal model consisted of the complete Spacecraft with dummy units to provide the correct distribution. The truss, on which will be mounted the Telescope, served as a part of the support to the facility. To this end the ESA GEOS test adapter provided the interface with the gimbal system of the facility, Figure 7-6a

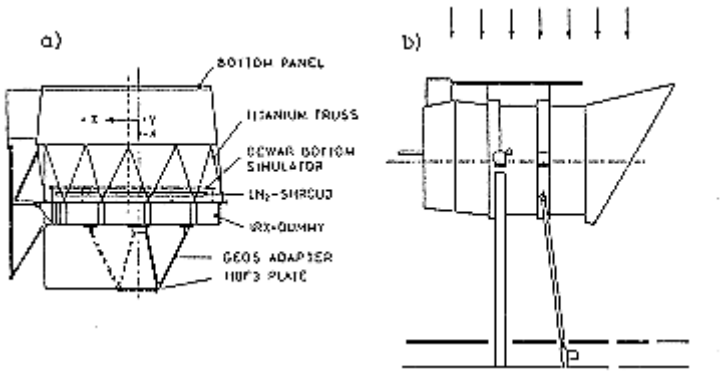

Figure 7-6: IRAS Test Configuration. a. Thermal model. b. Complete satellite in JPL facility. From Van Leeuwen (1983) [53].

The expected Telescope temperature were applied at the adapter side of the truss on the IRX dummy, whereas Earth shine and albedo were simulated by electrical heaters on the cone inside. One special steady state test phase was carried out to check the simulation of the Earth radiation on the bottom panel. Earth radiation was simulated this way using the TM bottom panel in the flight model test.

The solar array was simulated by stiffened plates representing the relevant dimensions. Real size solar array could not be present due to the physical limitations of the ESTEC facility. Five steady state plus a number of transient phases were carried out to check the thermal design and validate thermal modelling.

The complete flight Spacecraft was subjected to a thermal vacuum test at ESTEC in 1980-1981. In May 1981 the IRAS Telescope was assembled with the Spacecraft and, after a number of tests at ESTEC (vibration, electrical), it was flow to JPL for the final modifications and test activities.

At JPL the satellite was mounted horizontally to the floor by a support structure attached to the telescope girth rings. A special mechanism made it possible to change the solar aspect angle without opening the chamber, Figure 7-6b.

7.9 Test of the superfluid Helium Dewar

7.9.1 General

Prior to MCT tests several slightly different computer models were developed over several years. All were of the lumped parameter thermal network type, sharing in common the following important assumptions:

The vacuum shell, the VCSs and the helium tanks are each isothermal.

The temperature of effluent in the vent line reaches that of a given VCS before the vent line leaves that shield.

There is no gaseous conduction.

The support straps are perfectly attached (thermally) to the VCS.

The thermal conductivity of the multilayer insulation was finally given by

$k_{eff} = 1{,}69\text{x}10^{-12}(T_1^2+T_2^2)(T_1+T_2)+0{,}15\text{x}10^{-6}\ \text{W.m}^{-1}\text{.K}^{-1}$

See ECSS-E-HB-31-01 Part 7 clause 6.

The major paths of heat flow into the MCT are through the VCS. Conduction through the center conductors of the 400 stainless steal coaxial cables is assumed to pass straightway into the tank. Wires inside the fill lines are also not vapor-cooled. The rest of the electrical cabling is vapor cooled by spot bonding to the support straps at the locations where they are attached to the VCS.

The ground test results indicated that the model was underestimating the radiative heat loads at the front-end of the MCT (i.e. the interface with the cover). After this area at the interface was carefully inspected and a computer model of that area prepared to evaluate more rigorously the radiation exchange factors for input to the model. Also, the conductances representing the support strap end fittings were adjusted on the basis of temperature measured during MCT testing. When values based on the observed temperature drop were added to the model between the cabling and each VCS, only a slight degradation in predicted superfluid flow rate resulted.

After four months of testing, the VCS and line attachment were redesigned and the aperture cover rebuilt. After adding several radiation barriers at the interface between the main dewar and the cover, the cover was installed and the system evacuated for testing.

The superfluid flow rate measured was 20 percent greater than predicted, and shield temperatures agreed fairly well. Two new radiation paths were added to the model, one from the vacuum shell to the outer VCS and one from the outer VCS to the helium tank. These paths were adjusted so that predicted shield temperatures and boil-off rate exactly matched the test data. The model then matched the Flow Swap test results (tests in which the MCT was vented through the fill line, which was attached only to the inner VCS).

Figure 7-7 shows the sensitivity of cryogen boil-off rate to changes in important design parameters as computed through the final mathematical model. Vacuum shell temperature is by far the greatest uncertainty in the prediction of dewar performance.

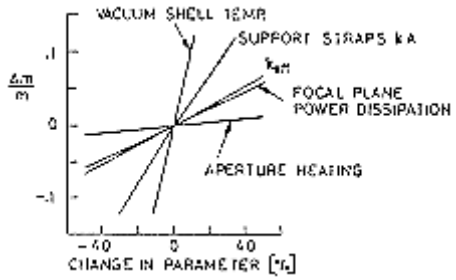

Note: non-si units are used in this figure

Figure 7-7: Effect of Critical parameters on heat load to cryogen. From Urbach, Hopkins & Mason (1983) [50].

The cryogenic system was subjected to sine wave, random, and acoustic vibration tests. No degradation of the system performance was detected. On the other hand, helium slosh effects were also absent; the tank ring stiffeners, acting as baffles, would dampen the small mass of helium during potential slosh modes.

7.9.2 Test of the plug

The IRAS flight porous plug was tested in the laboratory before installation in 1979. These tests furnished the mass flow rate versus tank temperature and the temperature drop through the plug, indicating that the plug fulfilled the requirements for the range of mass flow expected under both flight and ground operations.

In situ tests were performed with the fully assembled system in order to verify that the performance was the same as in the laboratory. Three tests were performed:

1. Flight conditions were simulated by tilting the MCT in increments up to a maximum of 55° from vertical position. (Figure 7-8). Plug temperature before tilting, with bypass valve V4 open, was higher than MCT temperature. Once tilted the MCT with V4 closed, the plug temperature dropped to the liquid temperature indicating hat the plug was submerged. In situ data were in reasonable agreement with laboratory data except temperature down-stream of the plug which was slightly higher in situ.

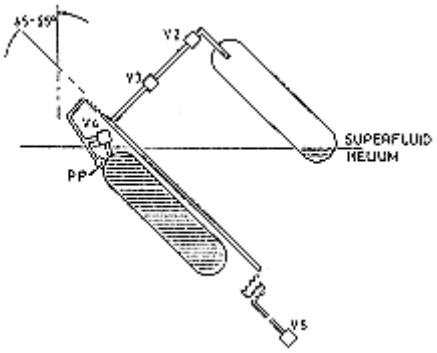

Figure 7-8: Tilting of the MCT for porous plug submersion. From Petrac & Mason (1984) [39].

2. Restarting after flooding the plug was demonstrated in the so called restart test. The plug was submerged by tilting the MCT. Initially, the vent valve V5 was open, and temperature readings showed that the plug was performing rightly. V5 was then closed and in one minute the temperature difference across the plug reduced to 0,1 K (the best resolution of the data system). After 15 minutes, venting was re-established by opening V5. Within two minutes the temperature jump across the plug indicated that phase separation restarted, and with the same flow rate as before closing V5.

3. Cleanliness of the plug was checked in the cold vapor flow tests. First the vapors from the heated MCT were vented with bypass valve V4 open. When V4 was closed the flow rate through the plug was almost the same as that in the laboratory tests (Figure 7-9).

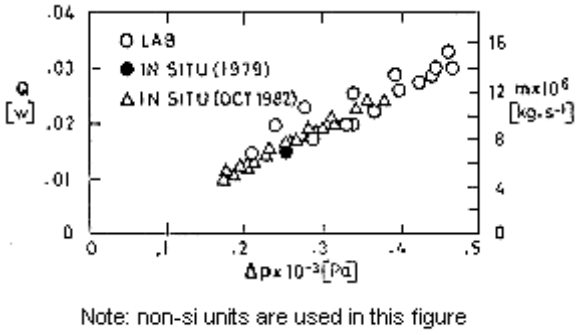

Note: non-si units are used in this figure

Figure 7-9: Vapor mass flow rate, *m*, and heat transfer rate, *Q*, through the plug vs. pressure drop, *Δp*. From Petrac & Mason (1984) [39].

7.9.3 Prelaunch preparations

Filling the MCT with superfluid helium was performed more or less in the lines of ECSS-E-HB-31-01 Part 14, clause 7.5.

First filling with near-superfluid helium took place 8 days before launch. Afterwards the liquid in the tank was maintained superfluid at 1,6 K by pumping until launch minus 42 h, when the tank was 85% full.

Final filling, achieving a 93% fill of superfluid helium at 1,6 K was performed at launch minus 42 h and the tank was valved off in preparation for launch at launch time minus 26 h.

During satellite development tests, problems arose while transferring because of the occurrence of large transient pressure pulses in the transfer line. In order to avoid these pressure pulses the transfer system was modified. See Tward & Mason (1982) [48].

The aperture cover was filled with 6 kg of normal helium at launch minus 23 h and was immediately valved off and allowed to become supercritical. At launch minus 15 h it reaches the 255×10^3 Pa and maintained this pressure through cover ejection.

7.10 On orbit performance of the spacecraft

30 temperature sensors were mounted for on orbit temperature measurements in the Spacecraft. 7 among them were required by the thermal control subsystem and the other 23 were mounted, by the suppliers, on the electronic units.

A problem occurred during the first day of the mission in the ACS. This could be traced to a randomly occurring spiking of the FSSS which was intercepted by the ACS as an anomalous attitude, placing frequently the satellite into a "safe mode". Three decisions were taken:

1. To keep the satellite with the solar array normal to the Sun without performing attitude maneuvers.
2. To re-program the OBC to obtain more information on the nature of the failure, and
3. To adapt the safety algorithm in the OBC. After 27 h the satellite continued the normal in-orbit checkout phase and, subsequently, the observation programme.

The fact that the satellite remained during 27 h with a β angle of 90° allowed comparing flight temperature with one of the design cases.

Measured temperatures of the electronic units were compared with the average unit temperatures as recorded during ESTEC and JPL tests. The agreement was fair for units with a rather constant power dissipation. Results of this comparison directly after launch are shown in Figure 7-10. Differences are well within the claimed uncertainty wit some exception concerning units with different power profile than those assumed in the pre-flight predictions.

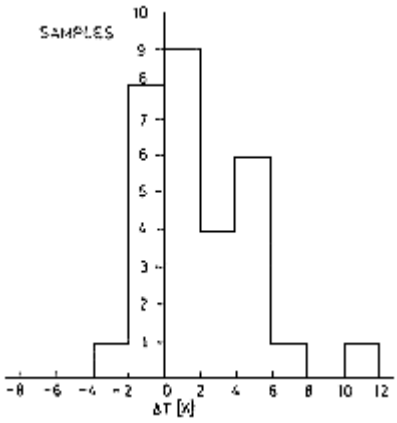

Figure 7-10: Histogram for ground and orbit test just after launching. The temperature deviation is $\Delta T = T_{measured} - T_{predicted}$. From Van Leeuwen (1983) [53].

The average temperature of several components of the Spacecraft increased at a rate higher than predicted. The analysis showed that this can be attributed to degradation of a silvered Teflon coating.

In the pre-flight analysis a $\Delta\alpha_s$ of 0,02/yr was assumed whereas a higher value of 0,011/mo fits better experimental data. Typical results with this adjusted value of $\Delta\alpha_s$ are shown in Figure 7-11.

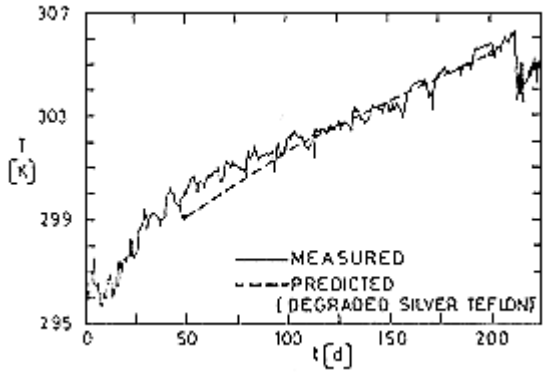

Figure 7-11: FSSS temperature, *T*, as a function of time, *t*, elapsed after launch. From Van Leeuwen (1983) [53].

A thermal misalignment phenomenon, occurred during the experimental phase of the mission, has been reported by Karsten & Teule (1984) [31]. This phenomenon, which was adequately modelled and partially overcome, was responsible for the development of cross-scan attitude errors of up to 100 arcsec. The origins of the misalignment changes could be traced to both spacecraft structure and FSSS brackets.

7.11 On orbit performance of the cryogenic system

Figure 7-3 summarizes the flight performance of the IRAS cryogenic system regarding initial transient and long term steady state performance. See also Figure 7-12 with steady state temperatures.

Table 7-3: Cryogenic System performance Summary

	Design Req.	Prelaunch	Initial Orbital	Peak	Flight Actual
Boil-off rate, mx10^3 [kg.s^{-1}]	2,29	N/A	2,77	4,20	2,39
MCT Pressure, px10^3 [Pa]	N/A	N/A	1,14	1,55	1,12
Liquid Helium Temp. [K]	1,8	1,60 [a]	1,80	1,95	1,80
Porous Plug, Upstream [K]	N/A	1,57 [a]	1,72	1,81	1,72
Porous Plug, Downstream [K]	N/A	1,52 [a]	1,68	1,77	1,68

	Design Req.	Prelaunch	Initial Orbital	Peak	Flight Actual
Barrel Baffle, Heat Exch. [K]	N/A	3,20 [a]	4,03	No	2,13
Middle VCS [K]	N/A	36,0 [a]	82,1	83,9	47,9
Outer VCS [K]	N/A	87,3 [a]	143,4	No	87,9
FPA Main Frame [K]	< 3,0				2,39
Dewar Mounting Ring [K]	N/A	1,62 [a]	1,88	1,90	1,82
Optics Interface Ring [K]	N/A	1,69 [a]	2,14	No	1,91
Optics Baseplate [K]	N/A	2,05 [a]	2,56	No	2,10
Barrel Baffle [K]	< 8	5,28 [a]	7,04	No	3,67
Barrel Baffle Fin [K]	< 8	6,00 [a]	9,17	9,17	4,12
Flowmeter [K]	300	294	292	292	268
Mainshell (average) [K]	170	294	286	286	197
Sunshade (average) [K]	90	294			97

[a] launch minus 48 h.

NOTE From Urbach & Mason (1984) [51].

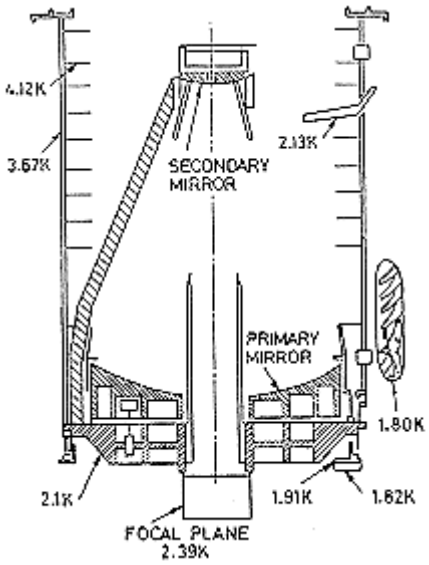

Figure 7-12: Cryogenic System Equilibrium Temperatures. From Urbach & Mason (1984) [51].

There are no focal plane temperature data for the first day of orbit because the aperture cover temperature sensor shared the telemetry channel with the focal plane sensor.

The transient performance of the MCT was influenced by the 26 h of no vapor cooling before launching (see clause 7.9.3). Twenty days after launch the insulation system, and MCT temperature and pressure approached stability. The flow rate had reduced to within 7% of its ultimate value. At launch plus 80 d the flow rate was stable within ± 1%.

Immediately after cover ejection the focal plane temperature was less than the required design temperature.

The cryogen system performed on orbit better than predicted because the analysis was based on ground test data in which the cryogenic system never stabilized. Additional factors such as vacuum level, gravity effects on the insulation and thermal interactions at the MCT-aperture cover interface also contributed to the conservative lifetime predictions.

As indicated in clause 7.9, the MCT thermal model gradually evolved toward its final form.

A mathematical model was developed during the program design phase. The model was adjusted to force agreement of calculated temperatures and heat transfer rates with measurements from initial dewar testing with the vacuum shell at room temperature. correlation of that model with the test data and resulting predictions of in orbit performance were described by Hopkins and Brooks (1982).

Modifications n the dewar and thermal balance tests resulted in a refined model with two additional radiation paths. Following these tests the model was adjusted independently by BASD and by JPL. Finally, agreement with the flight performance data, including the in-orbit measured boil-off rate was achieved on a later adjustment. The influence of the several refinements of the thermal model on the cryogen boil-off rate is summarized in chronological order in Figure 7-13.

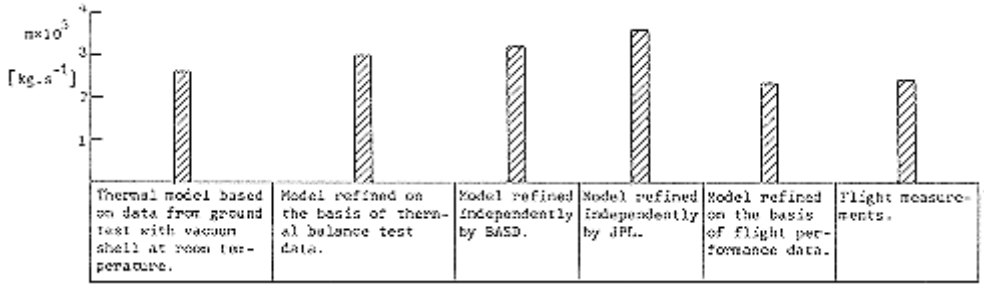

Figure 7-13: Cryogenic boil-off rate according to different models. From Urbach, Hopkings & Mason (1983) [50].

During the development of the thermal model additional heat paths were introduced to force the agreement with ground tests (see clause 7.9). Since the effects accounted for in the model refinements based on ground test data disappeared in flight, the final model was basically the same as that used before initial MCT thermal performance testing except minor refinements in the thermal conductivity of the supports and in the effective thermal conductivity of the MLI which finally was that given in.

References: Brooks (1982); Urbach, Hopkins & Mason (1983) [50]; van Leeuwen (1983, 1985) [53] & [54]; Karsten & Teule (1984) [31]; Petrac & Mason (1984) [39]; Urbach & Mason (1984) [51].

8
Satellite probatoire d'observation de la terre (SPOT)

The complete SPOT programme uses four satellites, SPOT 1 to SPOT 4. This data item corresponds to SPOT 1.

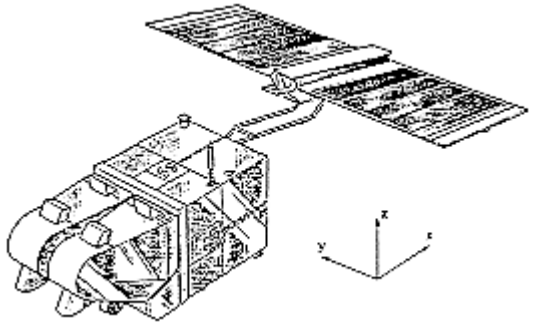

Figure 8-1: SPOT 1 spacecraft in orbital flight.

8.1 Mission

The objectives of the SPOT mission are to:

1. Contribute to remote sensing from space.
2. Research and develop applications requiring data with high resolution (10 m - 20 m), rapid visit or revisit time, frequent access, and stereo terrain perception.
3. Build up a data base of planimetric and stereo data over important areas of the world.
4. Qualify a multimission platform and linear array sensors for extended free-flying missions.

Launching date: Feb. 21, 1986.

Mission life: 3 years. The complete SPOT programme will last no less than 10 years.

8.2 Main subsystems

The SPOT 1 satellite has two parts: the multimission platform and the mission specific payload. The SPOT 1 platform is one model of a multimission bus developed within the SPOT project. The SPOT 1

payload includes two identical high-resolution visible range instrument (HRV). These instruments are pointable in the across-track direction to allow rapid access to any point in the globe and the acquisition of stereoscopic image pairs from different satellite passes. Data generated by the instruments are transmitted to the ground or stored by two onboard recorders for later recovery by the ground stations.

From Courtois & Weill (1985) [16].

8.3 Main characteristics of the satellite

The SPOT 1 platform consists of a Service Module (MS) and a Propulsion Module (MP). The latter is assembled around a central tube housing the batteries and part of the hydrazine tanks.

A description of subsystems and components requiring thermal control is given in Table 8-1.

Table 8-1: Characteristics of the SPOT 1 Main Subsystems

Subsystem	Component	Comments
Service Module (MS)	Power Supplies	• Deployable solar panel, located 2,3 m away from the satellite body. Its span is 8,12 m and its area 12 m^2.
	Batteries Compartment	• Contains 2 to 4 batteries (3 in SPOT 1 case) of 24 Ni-Cd battery cells each (SAFT type V024S), and the associated electric and electronic systems.
	Telemetry & Command Unit Attitude and Orbital Control On board Computer (OBC)	
Propulsion Module (MP)	Thrusters	• Two redundant lines of 8 thrusters each (3x1,5 N thrust + 5x15,6 N thrust). Thrusters are hydrazine-fed by flown-down pressurized helium ($22x10^5$ Pa to $5,5x10^5$ Pa).
	Tanks	• 2 to 4 tanks (in SPOT 1 case) containing respectively 150 kg and 300 kg of hydrazine.
	Ducts, Filters, Valves, Servovalves	• One monitoring pressure-gage by line. • One filter by line. • Valves for filling-empting tanks and valves for pressurization-depressurization.
Payload Interface	Structural Plate	• Interfaces the above mission-independent subsystems with the mission-specific subsystem, below.

Subsystem	Component	Comments
Payload	Two High-Resolution Visible-Range Instruments (HRV)	• HRV uses push-broom image generation based on available CCDs. It can operate in the multispectral mode-XS-(two CCDs to produce each image element (pixel), or in the panchromatic mode-Pan (one CCD per pixel). HRV performance specifications are given by Courtois & Weill (1985) [16]. See Henry, Juvigny & Serradeil (1988) [25] for on-orbit results.
	Optics and Detection System	• Folded catadioptric telescope with 1,082 m focal length and f/3,5 numerical aperture. It also includes correcting and/or focussing lenses.
	Image processing Electronic System	• It handles separately 12 XS arrays and 4 Pan arrays. The reading frequency of the XS mode is half that of the Pan mode. In the last case, high ground resolution requires parallel reading of 4 chains.
	Off-Nadir Viewing Mechanism	• A complete steerable mirror assembly driven by a 1200 step revolution stepper motor (one motor step ≅ 0,3° mirror step). Mirror position is measured by a shaft angle encoder with output connected to the OBC.
	Payload Telemetry System (TMCU)	• Each HRV delivers two bit streams corresponding to XS and Pan modes. Only two among the 4 bit streams are transmitted to the ground or recorded for later recovery by the Toulouse and Kiruna receiving stations. The Payload telemetry System consists of an $8x10^9$ Hz quadriphase modulator, two 20 W power TWTs and a set of filters.
	Antenna	• Fixed antenna (0,8 m dia.) covering the entire cone of visibility of the Earth.
	Hyperfrequency Plate	• Thermal spreading plate supporting the two TWTs.
	Two On Board Tape Recorders	

NOTE From Corsai (1983) [15], Fagnoni (1983) [20], Racaud, d'Antin, & Lelièvre (1983) [40], Courtois & Weill (1985) [16].

The SPOT programme is being coordinated by CNES.

The thermal control of the SPOT 1 platform has been studied by Aerospatiale, Cannes. The structure and solar panel assembly have been developed by MATRA, Toulouse. The thermal control of the HRV instruments has been developed by MATRA, Toulouse, and that of the TMCU by Thomson-CSF, Toulouse.

SPOT IMAGE is a venture of CNES together with 18 public and private institutions in France, Belgium and Sweden, the aim of which is to organize, promote, distribute and sale SPOT data on a worldwide basis.

SPOT 1 was launched on the evening of 21 of February 1986 from Kourou, French Guiana, aboard the ESA Ariane rocket. The launch was followed by two months of in-flight acceptance testing.

The dimensions of the satellite body are 4,7 m x 2 m x 2 m in the X, Y and Z directions, respectively.

The SPOT 1 Mass Summary, at launch, is given in Table 8-2.

Table 8-2: SPOT 1 Mass Summary

Component	Mass [kg]
Platform	
Structure	370,0
Computer System	35,0
Solar Generator & Controls	128,0
Power Package (including Batteries)	158,0
Orbit & Attitude Control	106,0
Propulsion System	194,0 BOL
Wiring	44,0 EOL
Thermal Control	43,0
Telemetry, Localization	18,0
Miscellaneous	10,0
	16,0
Total Platform	1078,0 BOL
Payload	
HRV 1	241,5
HRV 2	241,5
Recorder & Telemetry	248,0
Miscellaneous	3,0
Total Payload	734,0
Total Satellite	1812,0 BOL

NOTE From Courtois & Weill (1985) [16].

8.4 Orbit

Circular Sunsynchronous.

Altitude (45° N): 832 km.

Inclination (mean): 98,37°.

Revolutions/day: 14 + 5/26.

Nodal period: 101,46 min.

Orbital (repeat) cycle: 26 d.

Number of tracks/orbital cycle: 369.

Intertrack distance (equatorial): 108,4 km.

Accessibility pattern at 45° latitude: 1,4,1,4,1,4,1,4,1 days.

Mean local solar time at descending node: 10 h 30 min a.m.

From Courtois & Weill (1985) [16].

8.5 Thermal design requirements

The following general constraints have been taken into account.

8.5.1 Functional modes

1. Launching phase, with and without shroud envelope.

2. Acquisition phase. Between injection and normal operation.

3. Normal in-orbit operation which could consist of the following three modes:

3.1. Nominal mode. With the –Z axis in the orbital plane and pointing to Earth.

3.2. Survival mode. During a failure the satellite spins around the +Z axis, which points to the Sun.

3.3. Orbital control mode. When orbital corrections, if required, are being performed.

8.5.2 Orbital constraints

1. Solar radiation. The solar angle changes along the year. Its influence on the satellite also depends on the ascent time of the nodes (nodal time) for the chosen orbit, and on the functional mode (geocentric or spin, see 3.1 and 3.2 above). The nodal time uncertitude for the SPOT 1 orbit is ± 20 min.
2. Albedo and Earth radiation, the influence of which are important for low altitude orbits (~ 832 km).
3. In the case of SPOT 1, orbit duration is around 100 min with an eclipse duration of 30 min.

8.5.3 Limiting temperatures

The thermal design requirements can be hardly systematized. They result from different considerations regarding the performance of the electronic equipment, thermal gradients along a given battery cell, thermal balance between cells, CCDs temperature stability, thermoelastic stability of the HRV optical axis, etc. Limiting operating temperatures and heat dissipation rates of several SPOT 1 components are summarized in Table 8-3 below.

Table 8-3: Limiting Temperatures and Heat Dissipation Rates of Typical Components – SPOT 1 Satellite

Component Localization	**Component**	**Operating Temp. Range [K]**		**Heat Dissipation Rate, *Q* [W]**		**References**	
		on	**off**	**min**	**max**		
Included in the Platform Thermal Control	OBC	263-323	233-343	0	13,5	Alet & Foret (1983) [1]	
	Transponder	263-323	233-333	4,5	8,0		
	EAIM	263-323	253-333	0	30,0		
	EMA	263-318	263-333	7,0	40,0		
	Shunt	263-323		13,0	61,0		
	Inertial Wheel	263-323	233-333	0	6,0		
	Hydrazine System		283-323	0	0		
	Total Platform			160,0	380,0		
		Thermal Requirements		Heat Dissipation Rate, *Q* [W]			
				Discharge Rate [a]	d.o.d. [b]	*Q*	
Included in the Batteries Compartment Thermal	Battery Cell	268-293 Top to Bottom Single		Battery Cell Nominal Discharge	5	0,30	Fagnoni (1983) [20]
					15	1,09	
					22	1,94	

Component Localization	Component	Operating Temp. Range [K]		Heat Dissipation Rate, Q [W]		References
		on	off	min	max	
Control		Cell. $\Delta T \leq 2{,}5$. Homologous Points of Two Cells in the Same Battery. $\Delta T \leq 2$. Homologous Points of Two Cells from Different Batteries. $\Delta T \leq 5$.		Satellite Nominal Mode Discharge		268 [K] 293 [K]
					5	0,40 0,72
					15	0,45 0,80
					22	0,70 1,22
				Satellite Survival Mode Discharge		0,54 to 0,58 depending on the orbit nodal time
		Thermal Requirements [K]		Heat Dissipation Rate, Q [W]		
Included in the HRV Thermal Control	Electronics [c]	263-323				Mauduyt, Bonnet & Toulemont (1983) [34]
	Image Chain	293-318				
	CCDs [d]	293 ± 2				
	Telescope [e] Pyramid	288 ± 5. $\Delta T <$ 5 between ± Z				
	Tilted Plate	293 ± 5				
	Payload Interface	293 ± 10				
	Exposure Plane	293 ± 2				
Included in the TMCU Thermal Control	Electronics	253-333		10,0 (Average)		Racaud, d'Antin & Lelièvre (1983) [40]
	TWT	258-343		32,0 (During Direct Transmission or Reading)		
	EPC	253-328		13,0 (As above)		

Component Localization	Component	Operating Temp. Range [K]		Heat Dissipation Rate, *Q* [W]		References
		on	off	min	max	
	TU	283-313		92,9 (During Reading)		
	Total TMCU Direct Transmission			174,0		
	Writing			246,0		
	Reading			362,0		
	Standby			39,0 (In nominal orbit) 60,0 (In survival orbit)		

[a] Discharge rate is the current flow required to discharge a cell or battery to a specified end-point voltage in a specified period of time. Data in the Table correspond to different discharge histories.

[b] Depth of Discharge is the proportion (expressed in percent) of the nominal capacity removed from a cell or battery during each discharge portion of a cycle.

[c] Except Image Chain.

[d] In order to limit the fluctuation of the detectors threshold-light current.

[e] Structural deviations should be kept within specified limits. The maximum specified structural deviation around the *X* and *Y* axes, with reference to a sensor cube placed on the payload platform, is $2x10^{-4}$ radians for the whole satellite.

8.5.4 Thermal interfaces

The subsystems are thermally decoupled from each other, both radiatively (by MLIs) and conductively (by insulators).

The interfaces which have been considered are the following:

At the platform level: solar panel, payload, batteries compartment, antenna and external appendages.

At the batteries compartment level: platform (heat leaks through connecting wires cannot be completely eliminated), solar panel and its storage housing (radiative exchange and shadowing).

At the HRV level: platform, TMCU.

At the TMCU level: HRV, payload interface.

8.6 Design tradeoffs

The selection of the thermal control concept is based on the following leading principles:

1. Fulfilment of the above thermal design requirements.
2. Use of simple and reliable components based on proven technology: passive thermal control supplemented with electric heaters, many of them activated by the OBC.
3. Multimission adaptability by limited changes in the outer coatings. The main platform components should be adapted, with minimal modifications, to any orbital sunsynchronous mission ranging from 600 km to 1200 km altitude and 8 h to 16 h solar time at ascending or descending node.

8.7 Thermal control of various components

The main characteristics of the SPOT 1 thermal control are summarized in Figure 8-2, which concerns the platform, and in Figure 8-3 to Figure 8-7, which concern the batteries compartment, the HRV and the TMCU.

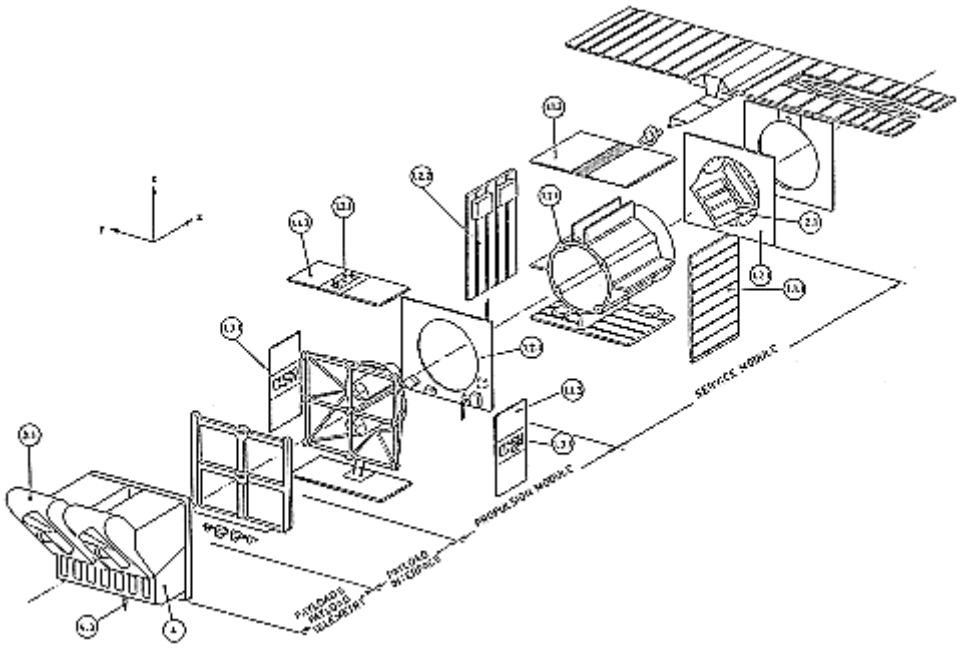

Figure 8-2: Exploded view of the SPOT 1 subsystems and components which require thermal control. Drawn by the compiler after Alet & Foret (1983) [1], Fagnoni (1983) [20], Courtois & Weill (1985) [16]. Encircled numbers in the figure are the same as those of the clauses in the text.

8.7.1 Platform

The platform thermal control is passive except regarding the propulsion (hydrazine) system. The latter is achieved by means of electrical heaters. Highly dissipating components are placed near the walls, conductively coupled to them. Heat is radiated to the outer space through SSMs (aluminized Teflon) windows.

8.7.1.1 Outer Elements

8.7.1.1.1. The overall thermal control of the platform is achieved by SSM-aluminium mosaics on the outer faces of the walls of both the MS and MP.

8.7.1.1.2. The +Z face is covered by a solar absorber (goldized Kapton) and thermally coupled to the inside of the platform. During the survival mode, when most of the electronic equipment is switched on, solar radiation is absorbed through the +Z face which points to the Sun.

8.7.1.1.3. The four faces of the MP are covered by a Kapton foil uncoated in the inner face and aluminized on the outer face so as to form an SSM-Kapton aluminized mosaic. The film thickness depends on the prevailing vibration level. Another Kapton foil closes the cavity of the Solar Array Drive System (MEGS) which is entirely covered by SSMs (not shown).

8.7.1.1.4. MLIs cover most of the sensitive outer elements (Earth and Sun Sensors), mainly those exposed to solar radiation, such as the lower plate and the external part of the central tube. Other MLIs form a closed cavity, radiatively coupled to the inner part of the MP around sensors placed an the –Z face (which points to Earth). These sensors are in contact with the payload interface. Other MLIs shield the external structural joints from the Sun. External access holes, reservoir filling opening, wiring passages, and the interface between the MEGS and the arm of the solar panel are closed by easily detachable MLIs.

8.7.1.2 Inner Elements

8.7.1.2.1. All inner structures are covered with black paint to homogenize the inner temperature of the platform.

8.7.1.2.2. The inner faces of the MS walls are covered by a mosaic of black paint and structural aluminium which provide some flexibility in the inner thermal balance.

8.7.1.2.3. The inner face of the +Z axis is completely black.

The mass allotted to the platform thermal control is 31 kg. The available electric power is 120 W for the survival mode and 50 W for any other mode. Electric heating is controlled by the OBC (through 8 different feeding lines) for any functional mode except survival. In this last case heating is controlled by thermostats, and the required heating power is only available during the sunlighted phase of the orbit.

8.7.1.3 Propulsion System

The thermal control of the hydrazine system (except the thrusters) is based on MLIs, fiber-glass supports or insulating rings, and thermostatically controlled local heaters.

8.7.1.3.1. The thermal control of the thrusters located in ± Y and +Z faces of the propulsion module is based, on one hand, on high temperature MLIs covering the whole supporting structure, and, on the other hand, on heaters bonded to the servovalves (or to their supports). These servovalves are radiatively coupled to the inside of the cavity and conductively coupled to each other and to the structure. The required heating power is about 100 W for the survival mode, and 30 W for any other mode.

8.7.2 Batteries compartment

The batteries compartment is placed on the +X base of the platform tube, radiatively and conductively decoupled from the platform. Conductive decoupling is achieved by the AMT (Architecture Mechanique et Thermique) subsystem. The batteries compartment consists of:

8.7.2.1. A structural support joined to the platform tube serving both as a thermal spreader and as a radiator.

8.7.2.2. Three batteries of 24 cells each.

8.7.2.3. Passive thermal control with an additional system of thermostatically controlled heaters.

8.7.2.4. The associated electric and electronic systems.

The thermal design constraints are based on:

1. Functional modes 3.1 and 3.2 in clause 8.5.1.
2. Orbital constraints as in clause 8.5.2.
3. Heat dissipation rates and thermal design requirements as in Table 8-3, clause 8.5.3. Thermal interfaces as in clause 8.5.4.

The solution which has been worked out in order to fulfil the thermal design requirements has the following characteristics (the description concerns the battery assembly of the SPOT multimission platform (Figure 8-3)):

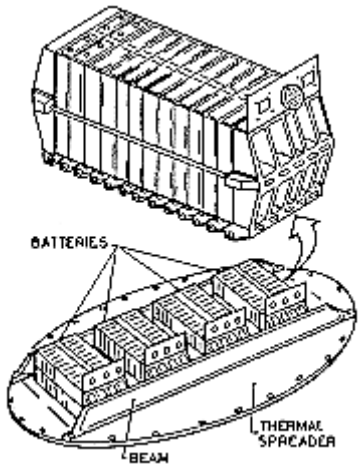

Figure 8-3: Battery assembly of the SPOT multimission platform. From Fagnoni (1983) [20].

1. A5 Al alloy (AFNOR designation, ECSS-E-HB-31-01 Part 5, clause 4.2) dividing plates, $2x10^{-3}$m thick, sandwiched between the large faces of the cells. These dividing plates are in good thermal contact with the structural support. The thermal) conductance between the battery cells and the dividing plates in enhanced by compression and by an adhesive. The conductance between the dividing plates and the support is enhanced by many attachment points and by the use of a filler.

2. The dissipated heat is evacuated to the outer space through the SSM-coated +X wall. The radiator area can be adjusted to the particular mission of the platform.

3. Thermostatically controlled heaters keep the temperature above 268 K. These heaters are bonded to the dividing plates near the cells.

The supporting structure is a compromise between mechanical and thermal requirements. It is made of A5 Al alloy, of maximum thickness $13x10^{-3}$ m.

The batteries compartment is radiatively decoupled from the rest of the satellite by MLIs. The interfaces between the base of the central tube and the compartment borders are filled with MLIs.

The estimated battery lifetime is 3 yr. For 15% d.o.d. and 2 yr. For 22% d.o.d. The allotted mass should not exceed 170 kg including batteries, structure and thermal control.

8.7.3 High-resolution visible range instruments

Two HRV instrument are enclosed in the SPOT 1 payload. An exploded view of an HRV system is shown in Figure 8-4.

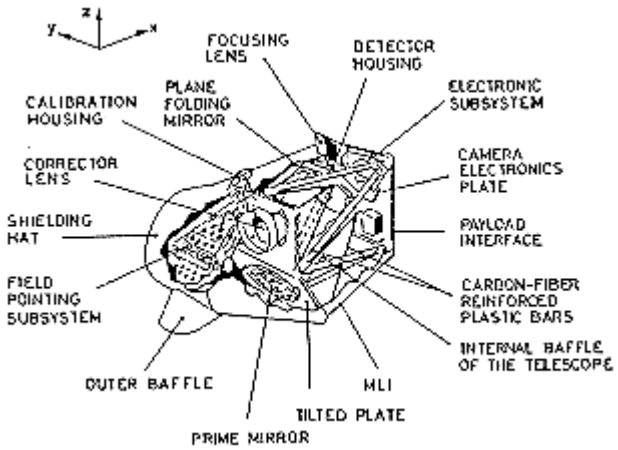

Figure 8-4: Exploded view of the HRVs. From Mauduyt, Bonnet & Toulemont (1983) [34].

The thermal design constraints are based on:

1. Functional modes 3,1 and 3,2 in clause 8.5.1.
2. Orbital constraints as in clause 8.5.2.
3. Mission constraints.

Image acquisition could last from 0 to 30 min per day. The most thermal controldemanding mission is summarized in Figure 8-5. The coldest case corresponds to permanent standby of the HRV. Limiting temperatures and heat dissipation rates were given in Table 8-3, clause 8.5.3. Note the right requirement for the CCDs. In order to fulfil it the detectorhousing is fully decoupled from the rest of the HRV, and independently controlled.

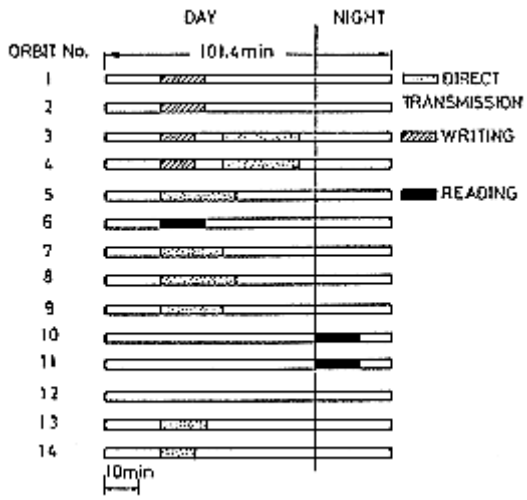

Figure 8-5: Design hot mission profile for HRV and TMCU. From Racaud, d'Antin & Lelièvret (1983) [40].

From the thermal control point of view the main components of the HVR system are:

8.7.3.1. Detectors housing. Placed within a cavity of aluminium-copper alloy A-U4G (AFNOR designation, ECSS-E-HB-31-01 Part 5, clause 4.3) internally polished to achieve high reflectance ($\rho \cong$ 0,95) and low emittance. The heat dissipated within the detector housing (BD) is transferred toward a radiative cold) plate, and the cavity is both decoupled from the HRV and from the outerspace.

The positioning accuracy of the detectors requires a rigid connection with the exposure plane which precludes the use of insulating rings. Heat transfer occurs via inner reflections within the cavity, absorption by the radiator and rejection to outer space. Coatings have been so chosen as to enhance the heat transfer within the cavity (detector housing and inner face of the radiator are both black). This improves heat rejection to space and limits the influence of the solar flux on the MLI covering the +Z face. The outer face of the radiator is painted white with an MLI framing-out the radiative surface. The thermal stability of the detectors is actively achieved at three levels:

1. Commutation-controlled compensation heaters near the CCDs.
2. Ground-controlled level heaters within the housing to achieve a 4 K temperature increase of the CCDs when the thermal control falls short.
3. OBC controlled heaters bonded to the radiator to attenuate the thermal fluctuations of the CCDs around 293 K. The estimated lifetime of the HVRs is 2 yr.

The power allocated for thermal control is 33 W during standby in the nominal orbital mode, or 50 W during the sunlighted phase of the orbit in the survival mode. No power is allocated to the payload during the first three orbit after survival.

8.7.3.2. Telescope. The telescope was adjusted on Earth in a 293 K environment and had to operate at this temperature. In order to fulfil the thermal control requirements (Table 8-3, clause 8.5.3) the whole telescope assembly has been covered by MLIs except for radiative windows, and the most sensitive components were electrically heated. Two heating circuits are placed on the +Z and –Z faces of the pyramid. These circuits are monitored by teleoperated threshold thermistors. Changing the threshold allows to minimize temperature differentials and influences the temperature level.

Temperature differentials between ± Y faces, due to the steeper motor in +Y, are reduced by heaters placed in –Y. These heaters are operated by OBC-actuated thermistors.

8.7.3.3. Equipment. The image chain, the specifications of which are given in Table 8-3, clause 8.5.3, is placed in the video housing. Radiation to outer space takes place through MLIs covering the shielding hat (see Figure 8-6). Not shown in the figure are lateral MLIs which have fewer layers than those of the shielding hat, and two MLIs which face to each other have windows opened. These windows only receive reflected external heat.

During survival (see clause 8.5.1) power for thermal control is limited to 50 W (for the sunlighted part of the orbit) and the OBC does not work. The +Z face of the detectors housing is sunlighted and compensation and level heaters are powered by a permanent bus. Equipment is heated by thermostatically-controlled heaters bonded to the shielding faces. The thermostats do not operate during the first three orbits of the survival mode.

The thermal control layout of the HRV is summarized in Figure 8-6.

1. MLIs

1.1. Outer shield: Kapton single aluminized, 1 mil (1 mil = 2,54x10^{-5}m).

Spacers: 11 layers tulle.

Intermediate shields: 10 layers Mylar double aluminized, 1/4 mil.

Inner shield: Mylar single aluminized, 2 mil.

1.2. Outer shield: Kapton single aluminized, 1 mil.

Spacers: 6 layers tulle.

Intermediate shields: 5 layers Mylar double aluminized, 1/4 mil.

Inner shield: Mylar single aluminized, 2 mil.

1.3. Outer shield: Mylar single aluminized, 2 mil.

Spacers: 11 layers tulle.

Intermediate shields: 10 layers Mylar double aluminized, 1/4 mil.

Inner shield: Mylar single aluminized, 2 mil.

1.4. Mylar double aluminized, 1/4 mil.

2. Radiators

2.1. Telescope radiant window (not shown). Single aluminized Kapton layer (1 mil) on surface obtained by pickling a black coated aluminium plate.

2.2. Radiator of the detector housing. A-U4G Al alloy. Inner face black, outer face white framed-out by an MLI.

3. Coatings

3.1. Inner face of the shielding hat and equipments, black paint.

3.2. Radiator of the detector housing, white paint.

4. Insulation

4.1. Conductive decoupling: PPE/Telescope

Cavity/Telescope

Radiator of the detector housing/Cavity

Baffle/Shielding hat

Insulating rings are used.

5. Nominal Electric Heaters

5.1. Pyramid. Heaters on the +Z and –Z sides controlled by thermistors of ground selectable threshold.

5.2. Driving rod. Heaters bonded to –Y rod opposite to stepper motor in +Y. The largest temperature differential is ground selectable.

5.3. Tilted plate. Heaters on four sides controlled by thermostors of ground selectable threshold.

5.4. Payload supporting plate. Heaters bonded to the plate and controlled by thermistors of ground selectable threshold.

5.5. Radiative plate. Heaters bonded to the plate are controlled by thermistors the threshold of which depends on CCD temperature.

5.6. Detector housing level heater bonded to the detector housing fairing, and ground operated.

6. Survival Electric Heaters

Heaters on the sides of the shielding hat controlled by two in-parallel thermostats (not shown).

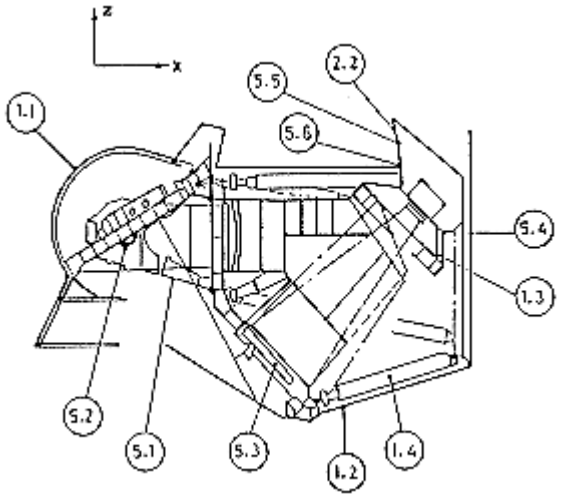

Figure 8-6: Thermal control layout summary of the HRV. From Mauduyt, Bonnet & Toulemont (1983) [34].

8.7.4 Payload telemetry system

The SPOT 1 payload platform contains, in addition to the two HRVs, the Payload Telemetry System (TMCU). It is attached to the Payload Interface (which shares with the HRVs) at six points. A view of the SPOT 1 Satellite facing the TMCU is given in Figure 8-7.

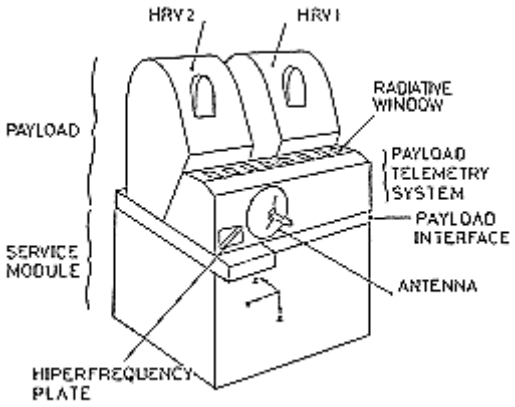

Figure 8-7: SPOT 1 Satellite as seen from the –*Z* side. From Racaud et al. (1983) [40].

The TMCU consists of:

8.7.4.1. The Payload Telemetry itself. A honeycomb sandwiched between carbon fiber plates (NIDA platform) supports a mechanical structure on one side and the electronic equipments on the other side.

8.7.4.2. The hyper frequency platform. It supports the TWTs which are characterized by high heat dissipation peaks. This platform is provided with a radiative window facing the Earth, and conductively decoupled from the TMCU.

8.7.4.3. The Payload Antenna. $8x10^9$ Hz, 0,8 m dia. It faces the Earth, and is fully decoupled from the TMCU.

The thermal design constraints of these subsystems are based on:

1. Functional modes 3,1 and 3,2 in clause 8.5.1. These functional modes of the satellite correspond to five functional modes of the TMCU itself. Four correspond to the nominal mode of the satellite and the last one to the survival mode (see Table 8-3, clause 8.5.3).
2. Operating temperatures and thermal dissipation of representative subsystems as given in Table 8-3, clause 8.5.3. The main characteristics of these constraints are: thermal transients, large heat dissipation, peaks, very strict temperature ranges for the TU (because of mechanical problems with the magnetic tape)... The accessibility of ground stations limits to 300 min per orbit the use of equipments. The controlling mission profile is that of Figure 8-5, clause 8.7.3. The cold corresponds to the survival mode.
3. Thermal interfaces as in clause 8.5.4.

The thermal control of the various components is achieved as follows:

1. TMCU itself. The radiative window mentioned in 4,2 above, is placed on the –X face of the satellite, which does not receive any solar flux and does not suffer from large albedo-radiation changes during the nominal mode operation. TMCU is shielded from the outer radiation by an MLI (outer face Kapton). Conductive decoupling from the payload interface is achieved with insulating rings and titanium bolts.

   The thermal environment around the TMCU directly depends on the size of the radiative window and to a lesser extent on the structure of the MLI. Windows devised to cope with the hot case are oversized for the cold case. Thus, electric heaters are implemented to keep the head-tape above 283 K. The problem worsens during the survival mode when the TMCU does not work and the nominal heaters cannot be used. Thus, an independent system of thermostatically controlled heaters are implemented. The equipment placed on the NIDA platform rests on protruding supports and, thence, it is not in direct contact

with the platform. Heat transfer is mainly radiative. The same occurs with the recorders on the hyperfrequency plate (see below).

2. Hyperfrequency plate. Highly dissipating equipments are mounted on a thermal spreader platform. The operating temperature range of these equipments is narrower than for other equipments. To meet these strict requirements the hyperfrequency plate and its equipment are radiatively and conductively decoupled from the TMCU. Conductive decoupling is achieved through many supports imposed by mechanical and dynamical stability requirements.

   In order to minimize the heat transfer rate towards the TMCU the following provisions were taken:

   (a) Correct sizing of the radiative window.

   (b) Implementing MLIs to radiatively decouple the TMCU from the hyperfrequency plate.

   (c) Carefully selecting materials and attachment procedures.

3. Antenna. The thermal control of the antenna is independent of that of any other system. The antenna is placed outside the satellite, radiatively and conductively decoupled from the TMCU. An MLI jacket is placed at the rear of the reflector. The conductive decoupling is achieved by a notched fiber-glass rod, the notched part of which is wrapped by an MLI to avoid axial radiative transfer between the support ends.

8.8 Estimated on-orbit performance

In this clause the efforts made for predicting the on-orbit behavior of SPOT 1 thermal control will be summarized. The subsystems are arranged here as in

8.8.1 Platform

Of the components have been used with the following aims: refining the chosen configuration, optimizing the SSM-aluminium mosaics, evaluating the required heating power, and assessing the thermal control performance under every operational and preoperational modes. A lumped model (260 nodes) represented the platform, and three different models the propulsion system: 110 nodes for the thrusters, 100 nodes for the ducting and 40 nodes for the filling-empting valves.

Thermal balance tests of the MSTH (Modèle Structural et Thermique) were made, during May 1983, at INTESPACE (Ingénierie Tests en Environnement Spatial) Toulouse, by use of the SIMLESS solar simulator. Tests on the flight model were also performed at Toulouse by the beginning of 1984. No data on the last tests have been found.

The solar simulator yielded an uniform flux over surface 3 m in diameter with shadowing for simulating eclipses. The required solar attitude angle of the satellite was obtained by rotation of the tilted platform. Transient thermal evolutions were simulated turning the platform 1 revolution every 100 min, and the steady state by rotating the platform at 10 rpm. The MSTH was furnished with mechanically representative dummies.

Albedo and Earth radiations were simulated by electrical heaters bonded to the outer faces except when highly dissipative components are placed nearby the walls. In these cases heating is provided near the dummies so that the thermo-optical characteristics of the wall remained unchanged.

The following tests were made:

1. Steady state test simulating the hot nominal mode of the SPOT 1 satellite (10 h 30 min nodal time). Mean values of the external flux were used. This test aimed at refining the thermal model of the equipment and the outer thermal balance of the platform.
2. Transient tests simulating the hot nominal and cold survival modes of the SPOT 1 orbit with corresponding eclipse. These tests aimed at estimating thermal variations (amplitude and time lags).
3. Two transient tests simulating the hot nominal modes of alternative orbits (8h and 12 h nodal time). The aimed at the evaluation of the thermal behavior of a multimission platform.

The results of transient tests are summarized in Figure 8-8.

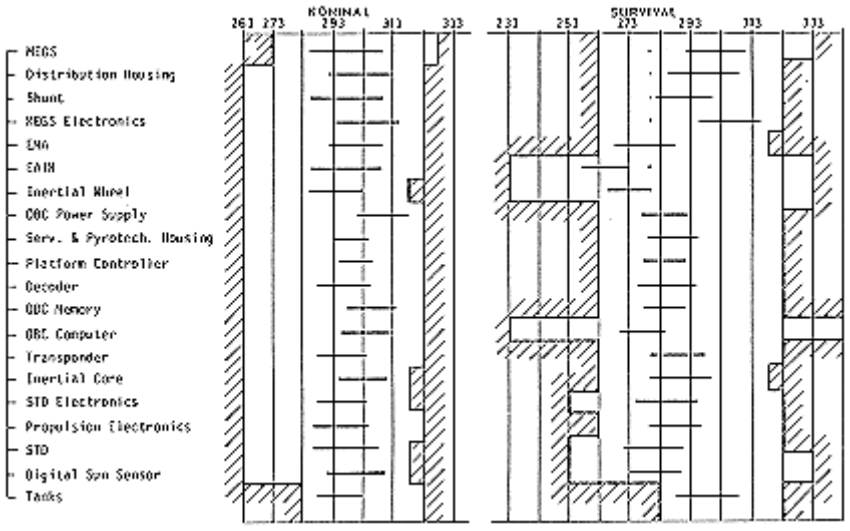

Figure 8-8: Temperature limits of the SPOT 1 platform components. From Alet & Foret (1983) [1].

Major departures from predictions (in the hot direction), which appeared in the survival mode, were associated to an incorrect estimate of goldized Kapton absorptance in the simulator wavelength range. No problems are anticipated since survival is a cold case.

8.8.2 Batteries compartment

The thermal analysis of the batteries compartment has been made on the basis of three different models:

1. An overall thermal model, with 36 nodes, of the battery compartment. It is used to estimate the mean temperature of the batteries.
2. A 105-node model of the battery cell for calculating the temperature distribution throughout the battery call and for estimating the thickness of the dividing plates (see clause 5.5).
3. A 250-node model of the structural support (see clause 5.1) to calculate the temperature differentials between the battery cells and for estimating the thickness of the support. These thermal tests aimed at assessing the chosen configuration, improving the accuracy of the inputs to the thermal model and verifying the whole batteries compartment under conditions closely simulating the in-orbit performance. The test setup in shown in Figure

8-9. It represents a 9 m^3 vacuum chamber, internally cooled with liquid nitrogen (77 K), the operating pressure of which is kept below 10^{-5} torr ($1{,}33 \times 10^{-3}$ Pa).

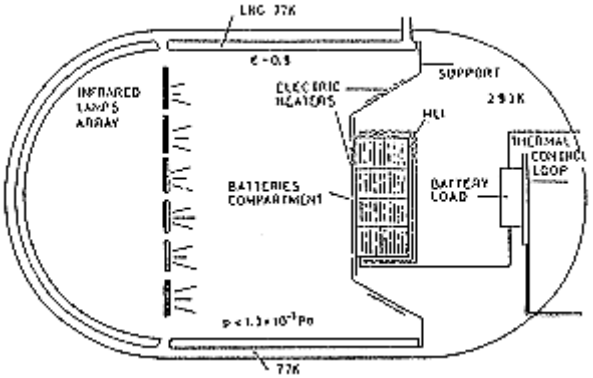

Note: non-si units are used in this figure

Figure 8-9: Test configuration of the batteries compartment of the SPOT multimission platform. From Fanoni (1983) [20].

The so-called MI model has been used for tests. The radiative surface, which in the satellite is placed in the +X wall, faces the cooled walls of the vacuum chamber whereas the part of the chamber simulating the platform tube is kept at 293 K.

Impinging radiations (Sun, albedo, Earth) are simulated by electric heaters bonded to the outer face of the radiative surface. Black paint is used in this face (instead of SSM) (see paragraph 3 in clause 8.7.2).

The emergency infrared lamps are used only if the electric heating fails.

Nearly one hundred chromel-alumel thermocouples are distributed throughout the batteries compartment.

The results agreed with the predictions as can be seen in Table 8-4.

Table 8-4: Estimated and Measured Performance of the SPOT Multimission Platform Batteries Compartment (*T* in K).

	Specified	Estimated	Measured
Mean Temperature of the Hottest Battery (Hot Case)	< 293	287	287
Mean Temperature of the Coldest Battery (Cold Case)	268	270	270,5
Top to Bottom Single Cell ΔT	≤ 2,5	1,1	1,1
Homologous Points, Two Cells in the Same Battery ΔT	≤ 2	1,8	1,3
Homologous Points, Two Cells from different Batteries ΔT	≤ 5	2,3	1,7

NOTE From Fagnoni (1983) [20].

8.8.3 High-resolution visible range instrument

The HRV system underwent four thermal tests before launching; three solar simulation tests and a thermoelastic test.

The first solar simulation test was made in the last quarter of 1980 on a dummy model of one HRV. The aim of this test was to refit the model and to assess the thermal control layout. The interfaces with the second HRV, the TMCU and the payload interface, as well as the equipment performance and electric heating were simulated. The test demonstrated the soundness of the thermal control layout. Values of several conductances were refined, and a correction of 30% was made to account for effects of joint in the MLIs (see ECSS-E-HB-31-01 Part 7, clause 6.13.1). As a consequence of this test the estimated effective thermal conductance of the +Z face had to be reduced.

A second solar simulation test was performed a year later with a modified) MLI; Kapton was used instead of Mylar in the outer shield, the number of shields was decreased and a lateral radiative window opened (see 6.3, in clause 8.7.3). This test, which was initially devised for the TMCU, also helped to evaluate the mentioned modifications, and to test operation modes such as calibration and refocalization of the optical system measuring its influence on the equipment involved.

The thermoelastic test performed on the dummy HRV during the CU-MSTH tests aimed at checking the predicted deformations and the model for calculating the line sight. The HRV was placed in horizontal position to cope with gravity action and furnished with the nominal heaters and thermocouples. The influence of temperature non-uniformities was the following:

A temperature increase of 10 K yielded an angular deviation of $2{,}2 \times 10^{-4}$ radians.

A temperature differential of 5 K on the pyramid in the +Z direction resulted in a pointing deviation of $2{,}5 \times 10^{-4}$ radians.

A temperature differential of 7 K in the tilted plate in the +Z direction yielded a pointing deviation of 10^{-4} radians.

The need for specifications of thermal uniformity (local and temporal) is clearly seen if one takes into account that the allowed angular deviation during the whole HRV lifetime is of the order 4×10^{-4} radians.

A last solar simulation test on the flight payload (2 HRV + TMCU) aimed at checking the thermal control loop, including the OBC software, and at fixing the threshold of the thermistors.

8.8.4 Payload telemetry system

Different thermal models were used for TMCU subsystems. The hyperfrequency plate was modelled with 13 nodes, the antenna with 35 nodes and the TMCU itself with 200 nodes. The first two models were incorporated (after reducing the number of nodes) into the third, giving rise to the overall model. The overall model, in its turn, furnished the inputs to the partial models which were dealt with independently.

Geometry definition models were also introduced to calculate external fluxes and radiosities (directly emitted plus reflected fluxes).

The whole payload underwent several thermal simulation tests. These tests aimed at:

1. Assessing the thermal control layout.
2. Refitting the thermal models.
3. Evaluating technical solutions.

The measurements indicated that the predictions were basically met. Temperature deviation from the predicted values were at most of the order of 3 K.

References: Alet & Foret (1983) [1]; Corai (1983) [15]; Fagnoni (1983) [20]; Mauduyt, Bonnet & Toulemont (1983) [34]; Racaud, d'Antin & Lelièvre (1983) [40]; Courtois & Weill (1985) [16]; Henry, Juvigny & Serradeil (1988) [25].

9
Olympus-1

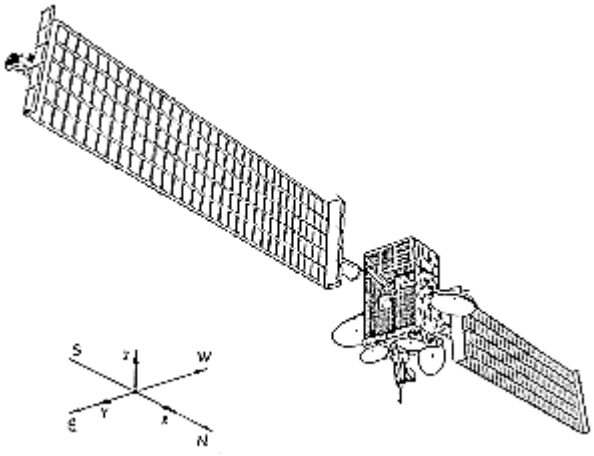

Figure 9-1: Olympus-1 in orbital flight. From Bonhomme & Steels (1984) [4], Steels & Baston (1986) [44].

9.1 Mission

Olympus-1 has been conceived, within the large-satellite, (L-Sat) programme, as a three axis stabilized demonstrator satellite with reduced power and mass (compatible with Ariane-3 launcher) to develop a series of telecommunications payloads and their in-orbit operation, to advance technological capabilities of the industry, to stimulate users and to promote new applications of space telecommunications.

Launching date: July 12, 1989

Mission life: 5 years. Olympus-Max standard satellite design life is 10 years.

Olympus-1 is a geostationary satellite. The following body-linked coordinate system will be used throughout this Part:

- x axis pointing towards North.
- y axis pointing towards East.
- z axis pointing away from the Earth.

9.2 Main subsystems

Olympus-1 satellite consists of three main modules (Figure 9-2).

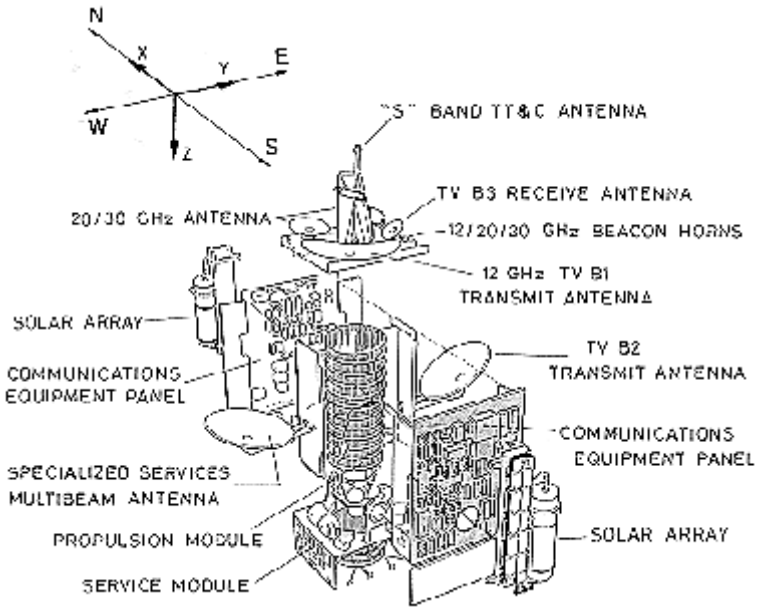

Figure 9-2: Exploded view of Olympus-1 satellite. From ESA (1984), Bowles (1987) [10], Paul (1989) [38].

Service Module, which contains most of the platform equipment.

Propulsion Module, containing the propellants (oxidizer and fuel), the pressurant tanks, associated piping and thrusters.

Communications Module, comprising the North and South radiating panels and the Earth-facing floor which provides most of the payload mounting area. The East and West faces of the spacecraft carry the European broadcast-beam and the specialized services antenna respectively. The main subsystems and components of the Olympus-1 satellite are listed in Table 9-1.

Table 9-1: Olympus-1 Main Subsystems

Subsystem	Components	Location in the satellite
Power	Solar Panel Assembly, AEG BSR silicon cells. For solar array deployment phases, see Figure 9-3. Radiator-mounted batteries. 32 cells-2 batteries Ni-Cd. 24 A.h. Saft. 31 cells-1battery Ni-H_2. 35 A.h. Eagle Picher. Charge and discharge regulators. Battery Management Unit.	+/- x sides. Radiator: +/-x sidewalls.
Combined Propulsion	ABM (490 N thrust). Marquardt. Eight (plus eight redundant) reaction control thrusters (22 N each). Marquardt. One oxidizer (nitrogen tetroxide) tank. 1,1. m dia. One fuel (mono-methyl hydrazine) tank. 1,1. m dia. Four helium pressurant tanks. Valves, filters, pipes. Support structure.	Propulsion Module: along the +/- z satellite axis. Thrust direction: -z
Attitude and Orbit Control	Three-axis stabilization which is active from transfer orbit on. Zero-momentum system. Sensors: IR earth sensor, sun acquisition. RF sensing (see TV Direct Broadcast, Table 9-2). Actuators: Reaction wheels (one for each axis) during quiescent phases. Thrusters during station keeping. Control Electronic Unit (CEU) based on Texas TI 9989microprocessor.	Service Module: + z side RF sensing: -z floor
Payload	Propagation Package, Specialized Services, TV Direct Broadcasting, Communications See Table 9-2.	Communications Module: - z floor, - y side, + y side, - z side. Service Module: + z side, inner faces of +/- x walls.

NOTE From Bonhomme & Steels (1984) [4], Paul (1989) [38].

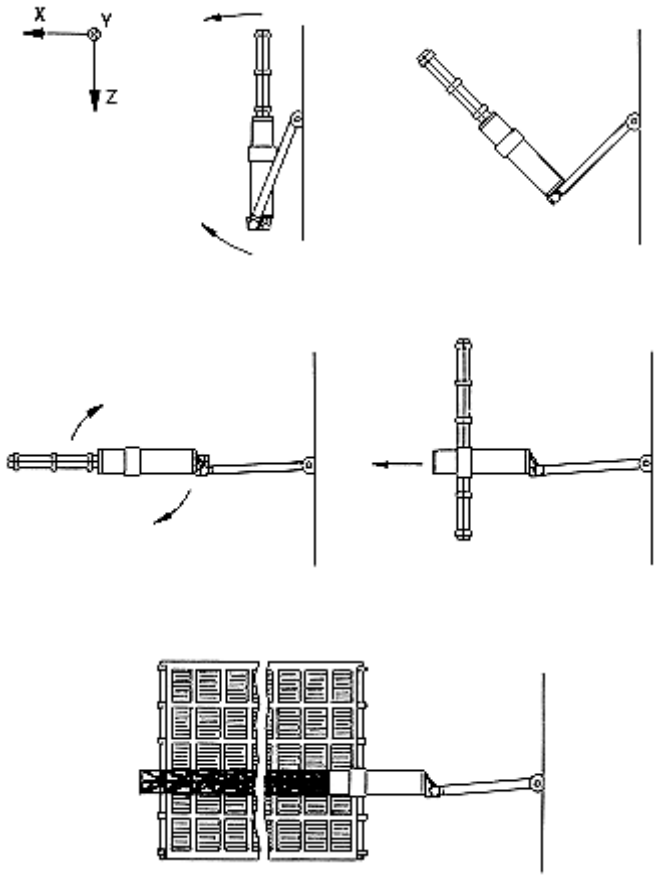

Figure 9-3: Schematic of the different phases of the Olympus-1 solar array deployment. Prepared by the compiler after Bonhome & Steels (1984) [4], Bowles (1987) [10].

Table 9-2: Olympus Payload

Type	Application	Component Characteristics	Responsible
12/20/30 GHz Propagation Package	Complementing and verifying propagation statistics in the higher frequency range.	Three beacons: One at 12,5 GHz to study frequency scaling of propagation characteristics. One each at 20 GHz and 30 GHz for direct signal measurement.	BTM (B) Overall coordination by Selenia Spazio (I)
12/14 GHz Specialized-Services	Experiments on advanced communications experiments between small Earth terminals	Five-beam antenna provides both receive and transmit bands. Repeater with four receive and four transmit chains. Four (plus one back up) 30 W TWTA 13,1-13,2 GHz and 14,1-14,5 GHz/12,52-12,57 GHz up/down Ku-band. Four channels provide two 18 MHz and two 30 MHz at 33,3 dBW with a 4 x 4 SS-TDMA	Marconi Space Systems (UK) Overall coordination by Selenia Spazio (I)

Type	Application	Component Characteristics	Responsible
		switching matrix.	
Television Direct-Broadcast	TV B1. One channel to establish a pre-operational Italian service. TV B2. Fully steerable channel to any European country.	Two DBS 230 W TWTA 17,6-17,8 GHz/12,1-12,2 GHz up/down Ku-band. TV B1. Channel allocated to Italy: 1,0 x 2,4 elliptic beam with an EIRP of 62,4 dBW. RF sensing and pointing loop. TV B2. Channel to any European country. 1,5 circular beam, 27 MHz bandwith, 63 dBW EIRT. TV B3. Dedicated receive antenna for common receiving.	Selenia Spazio (I)
20/30 GHz Communications	Point-to-point and multipoint teleconferencing and other experimental applications.	Two (plus one back up) 300 W TWTA 28-28,6 GHz/18,9-19,4 GHz up/down Ka-band providing fully steerable spot beams of 0,6 dia with 40 MHz and 700 MHz bandwith, 52,1 dBW EIRP.	Selenia Spazio (I).

NOTE From Bowles (1987) [10], Paul (1989) [38], INTERAVIA (1989) [28].

Olympus-1 was launched on July 12, 1989 from Kourou, French Guiana, by Ariane 3.

Total Mass of the satellite is 2595 kg at launch, 1450 kg in geostationary orbit. Payload mass 359 kg.

Deployed dimensions are: Solar array span 25,67 m, body 2,568 m high x 1,75 m x 2,10 m

Payload power: 2470 W RF in sunlight, 1500 W in eclipse

Platform reliability: 0,9 after 6 yr.

From INTERAVIA (1989) [28].

Olympus-1 has been developed under ESA by a team consisting of the following industrial groups:

British Aerospace (Space Systems) Ltd. (UK): Prime contractor.

Selenia Spazio (I): Coordination of the four communication payloads. Design and development of both TV Direct Broadcasting and 20/30 GHz Communications Payload.

BTM (B): Propagation Package Payload.

SPAR Aerospace Ltd. (Can.): Overall responsibility of the solar arrays, with major subcontracts to AEG (D) and Fokker (NL).

SNIA-BDP (I): Integration and testing of the Combined Propulsion System.

Fokker (NL): Spacecraft structure.

Aeritalia (I): North and south radiator panels. Thermal control.

David Florida Laboratories. (Can.): Environmental and final testing.

9.3 Orbit

Geostationary. Equatorial. Location: 19° W.

From INTERAVIA (1989) [28].

9.4 Thermal design requirements

Olympus-1 thermal-control subsystem will ensure that, in all mission modes, the satellite and its equipment are maintained within acceptable temperature limits.

9.5 Thermal control

Thermal requirements can be fulfilled with a passive thermal-control system consisting of:

1. SSM radiators in the +/-x faces. Total radiating area: 9 m^2.

   Area of each panel: 2,57 m x 2,10 m.

   Rejected heat transfer rate:

   $Qe \approx 3{,}5$ kW at 300 K inner temperature, $Qe \approx 5{,}3$ kW at 330 K inner temperature.

2. Mylar and Kapton electrically conductive MLI blankets for internal equipment, for all radiator areas not covered by SSMs and for the other four faces of the satellite.

3. Constant conductance heat pipes on the structural aluminium honeycomb payload walls (North and South radiators) in areas of high dissipation near the high power TWTAs and EPCs.

   Heat pipes are of extruded aluminium with 20 axial grooves and flanged. Working fluid is Ammonia. Outer square cross section side: 9,5 x 10^3 m or 10^{-2} m. Lengths between 0,682 m and 1,2 m. Maximum integral heat transport: 20 W.m. Manufactured by Dornier (G). (Chalmers, Burkle & Case (1988)). 38 heat pipes were mounted on the South radiator and 24 on the North radiator.

4. Conductive white paint (see ECSS-E-HB-31-01 Part 5, clause 5.9) coating the antennae.

5. Electric heaters controlled either automatically or by telecommand.

   From Bonhomme & Steels (1984) [4], Boggiatto, Colizzi, Perotto & Tavera (1985) [3], Bowles (1987) [10].

   The batteries are directly mounted on the radiator panels in the +/-x (North and South) faces.

   Thermal control layout of Olympus-1 satellite is shown in Figure 9-4. Inner equipment and outer SSM and MLI layouts of the North and South radiators are those used for thermal vacuum tests. See clause 9.6.1.

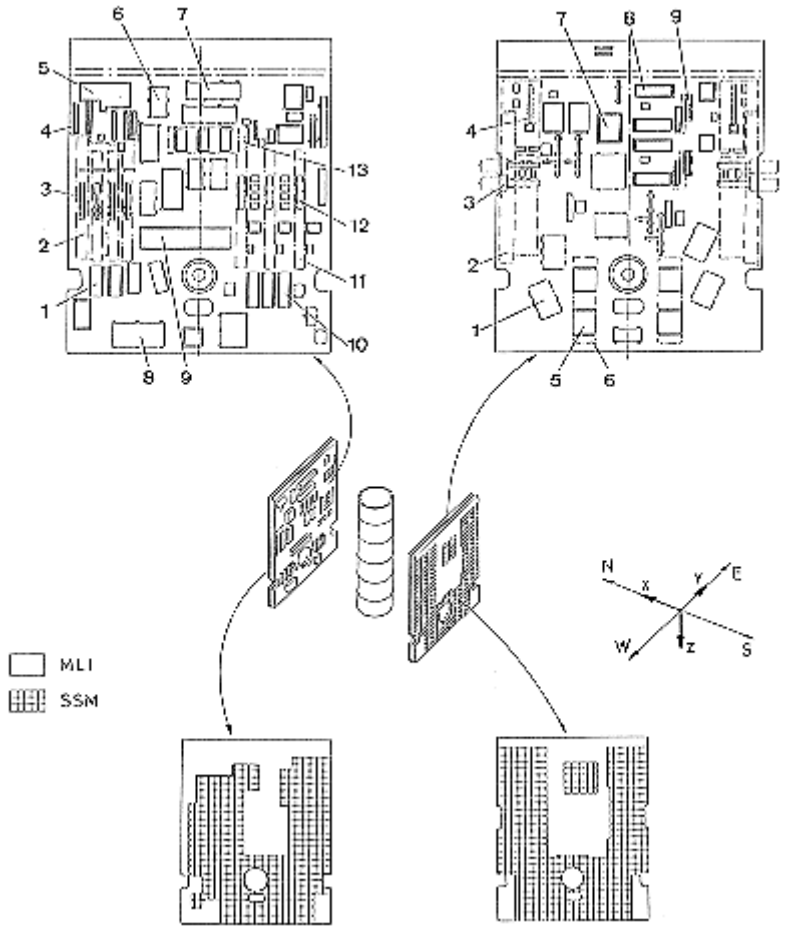

Figure 9-4: Olympus-1 satellite thermal control layout used for thermal vacuum tests. From Boggiatto, Colizzi, Perotto & Tavera (1985) [3]. Explanation is given in Table 9-3.

Table 9-3: Payload Subsystems Identification in Figure 9-4.

Key	North Panel		South Panel	
	Payload	**Subsystem**	**Payload**	**Subsystem**
1	Specialized Services Payload	EPC	Television Direct Broadcast	EPC HV
2		HP Assembly		TWT, HP Assembly
3		TWT		TWT
4		Output Filter		Output Filter
5		Output Switch Network		EPC LV
6		Input Switch Network		EPC, HP Assembly
7		Receiver	Propagation	Frequency Source

Key	North Panel		South Panel	
	Payload	Subsystem	Payload	Subsystem
8		Power Switch Drive Unit	Package	EPC
9		Local Oscillator		TWT
10	20/30 GHz Propagation Package	EPC		
11		HP Assembly		
12		TWT		
13		Output Filter		

The performance characteristics of Olympus-1 batteries are summarized in Table 9-4. The corresponding thermal design layouts are given in Figure 9-5.

Table 9-4: Olympus-1 Battery Performance Characteristics

Type	Ni-Cd	Ni-H_2
Electrical		
No. of Cells/Batteries	32/2	31/1
Capacity [A.h/Battery]	24	35
Max. d.o.d. (%)	60	70
Design Lifetime [yr]	7	7
Thermal		
Temperature Range [K]	268-288	268-288
Temperature Difference within Battery [K]	< 2	N.A.
Required Heating [W]	24	32
Thermal Capacity [J/K]	37400	40000
Máx. Dissipation Discharge Average [W]	42,9	121,4
Máx. Dissipation Trickle Charge Average [a] [W]	11,1	15,8
Geometrical		
Footprint [m x m]	0,62 x 0,21	0,67 x 0,44
Height [m]	0,224	0,340
Total Mass [kg]	37	36,5

[a] The trickle charge resistor limits the battery current when the battery temperature exceeds a safety limit.

NOTE From Konzok, Gutschmidt, Stümpel, Schlitt & Dunbar (1987) [33].

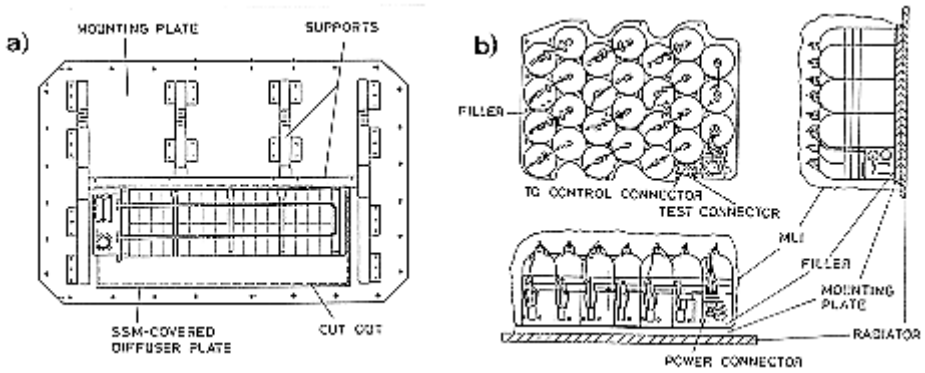

Figure 9-5: Olympus-1 satellite battery thermal control layout. a) Ni-Cd battery; b) Ni-H_2 battery. From Konzok, Gutschmidt, Stümpel, Schlitt & Dunbar (1987) [33].

9.6 Thermal test of olympus-1

Two different types of Olympus-1 thermal tests have been reported, namely: Thermal Vacuum Test and Infrared Test.

A calendar of Olympus thermal tests is given in Table 9-5.

Table 9-5: Olympus-1 Thermal Test

No.	Test	Date	Place	Comments
1	Thermal-vacuum	June-July 1984	ESTEC	Thermal Model. North and South Radiators. See clause 9.6.1.
2	Solar simulation, 1st series	Nov. 1984	Jet Propulsion	Thermal Model. Reconfigured.
3	Solar simulation, 2nd series	Dec. 1984	Jet Propulsion	Thermal Model.
4	Infrared Test	Jan. 1986	David Florida	Thermal Model. See clause 9.6.2.
5	Appendage Release under Thermal Vacuum	May 1986	David Florid	Thermal Model. Date not clearly established.
6	Solar simulation	June 1987	Jet Propulsion	Flight Model of Olympus-1
7	Thermal-Vacuum	July-Aug. 1988	David Florida	Flight Model of Olympus-1. Partial retrofitting after 6.

NOTE From ESA Bulletins.

9.6.1 Thermal vacuum test

The thermal vacuum test for the development of the Olympus-1 heat pipe radiator was performed during mid 1984 by use of the Thermal Vacuum Chamber HBF-3 at ESTEC.

The usable test volume of the chamber is a sphere 3 m in diameter. Cryogenic shrouds on the top and lateral walls of the chamber were kept at the appropriate temperature to simulate the space environment.

The two radiators were tested together. They formed two opposite vertical walls of a closed and insulated box. The radiators faced the cryogenic shrouds of the test chamber and the z-axis was horizontal so that the heat pipes were held in horizontal position. During the test the box was heated and its temperature controlled to simulate the thermal environment within the spacecraft.

The layouts of the internal faces of both radiators are shown in Figure 9-4. The subsystems were simulated by dummies reproducing the following actual thermal and thermooptical characteristics: thermal/mechanical interface with the radiator, power dissipation, thermal capacity, external shape, finish and dimensions.

The external radiator surfaces were covered by SSMs and by MLIs where required. MLIs were optimized by use of analytical predictions.

Tilt measurement sensors, three for each radiator, were used to keep horizontal the heat pipes during the test. The temperature at selected nodes of the thermal mathematical model on the radiator and on the test fixture was monitored by means of 400 thermocouples.

Three steady-state test cases were considered, as it is indicated in Table 9-6.

Table 9-6: Representative Cases Considered in the Thermal Test

Test Case	Intended Simulation	Main Features		Shroud Temp. [K]	Rejection Heat Transfer Rate [W]	
		External	Internal		North Radiator	South Radiator
1	Cold Equinox	No solar input	On-station sunlight operation	100	747	589
2	Long Duration Eclipse (Cold Case)	No solar input	Minimum allowable temperature of electronic units	200	546	108
3	Solstice (Hot case)	Solar input	Full power operation	240	702	626

NOTE From Boggiatto, Colizzi, Perotto &Tavera (1985) [3].

Two different thermal network computer models were used in order to complement and interact with the thermal vacuum tests. They consisted of 185 and 195 nodes respectively with 850 conductors in each model. At least one node was assigned to each electronic unit, with several to the critical units, as the TWTs. In several instances a preliminary multi-node model was introduced on items which were intended to be dealt with as a single node in the final model. The solution of that local network led to

the definition of linear conductors representing the same situation but with an equivalent reduced network.

The interaction of thermal test and thermal model consisted of four main steps.

1. Pre-test predictions were made, on the basis of the expected values of the boundary temperatures and dissipations, to provide a feeling of the test results and to verify that the temperature limits of the critical components are not overrun.
2. Thermal vacuum test itself, as indicated above.
3. Interaction. After test completion the thermal model is modified if required. To this aim, the actual test conditions are fed into the thermal model and the nodal temperatures calculated. This comparison with the test results suggests several adjustments: node-thermocouple correspondence, heat leaks to the supporting frame, addition of nodes to cope with temperature non-uniformities, improved values of the material properties, ...
4. Correlation Success and Closure. The interaction activity ends when the temperature difference $\Delta T = Tmeasured\text{-}Tcalculated$ meets the following criteria:

1. Average deviation less than 1,5 K.

2. Standard deviation less than 2,5 K.

3. $\Delta T < U_{TP}$ for every thermal sensor.

U_{TP} is the test uncertainty prediction, which is defined as follows:

$$U_{TP} = \sqrt{U_S^2 + U_{TE}^2} + U_I + U_M \qquad [9\text{-}1]$$

U_S is the RMS uncertainty due to specimen parameters.

U_{TE} is the RMS uncertainty due to test environment parameters.

U_I is the modellization error, assumed to be ± 3 K.

U_M is the overall measurement uncertainty at the test facility, assumed to be ± 1 K.

The following uncertainties in the specimen and test parameters were assumed:

U_S Outer radiation effective thermal conductance (see ECSS-E-HB-31-01 Part 7, clause 6.1.1) ±5 %

U_S Inner radiaton effective thermal conductance ±10%

U_S Inner thermal conductance ±20 %

U_{TE} Input power ±5 %

U_{TE} Boundary temperature ±3 K

Representative results are summarized in Table 9-7 and in Figure 9-6. Several thermocouples were excluded from the correlation for accidental reasons.

Table 9-7: Subsystem Temperature [K] after Different Steps in the Test-Mathematical Model Interaction.

Subsystem	Prediction			Test			Post Test					
	Case 1	Case 2	Case 3	Case 1	Case 2	Case 3	Case 1		Case 2		Case 3	
							ΔT [K]	U_{TP} [K]	ΔT [K]	U_{TP} [K]	ΔT [K]	U_{TP} [K]
Television Direct Broadcast, TWT	292,7	240,2	321,8	289,0	238,3	317,4	-0,8	8,3	-2,3	8,4	-0,6	8,1
Television Direct Broadcast, EPC, LV	291,2	244,6	317,6	296,3	236,9	323,1	-1,4	7,5	-1,2	7,7	-0,7	7,1
Television Direct Broadcast, TWT, HP Assembly	289,3	240,2	318,3	279,2	238,7	307,6	0,9	7,8	1,2	8,1	1,1	7,9
Television Direct Broadcast, EPC, LV, HP Assembly	287,3	244,5	313,8	275,2	236,4	304,0	-1,5	7,3	-0,3	8,2	0,1	7,7
Propagation Package, TWT 30 GHz	295,9	281,5	312,9	283,0	274,7	297,1	-0,4	7,7	-0,1	8,1	0,1	7,6
Propagation Package, Frequency Source	287,4	273,4	311,6	284,5	274,7	306,2	-0,6	7,6	-0,2	7,8	0,5	7,2
Specialized Services, TWT	303,0	291,4	325,0	298,4	282,5	321,0	-2,6	8,2	-1,9	8,5	-0,9	8,0
Specialized Services, EPC	288,1	279,0	325,8	281,7	269,8	319,7	-0,5	8,0	0,1	8,3	0,4	7,8
Specialized Services, TWT, HP Assembly	300,4	288,8	322,5	293,2	277,8	316,0	-1,4	7,9	-1,6	8,1	-1,0	8,0
Specialized Services, Local Oscillations	288,1	280,9	312,4	289,8	283,0	313,2						
Communications, 20/30 GHz TWT	318,5	314,5	342,9	303,5	298,5	325,4	-1,1	8,5	0,2	8,6	0,3	8,2
Communications, 20/30 GHz EPC	289,1	286,2	318,3	277,8	278,6	308,6						
Communications, 20/30 GHz RDU	277,6	267,4	304,3	266,2	261,9	295,1						
Communications, 20/30 GHz HP Assembly	313,1	308,6	337,1	295,2	290,2	317,0	-0,7	8,1	-0,3	8,4	0,5	8,2

NOTE From Boggiatto, Colizzi, Perotto & Tavera (1985) [3].

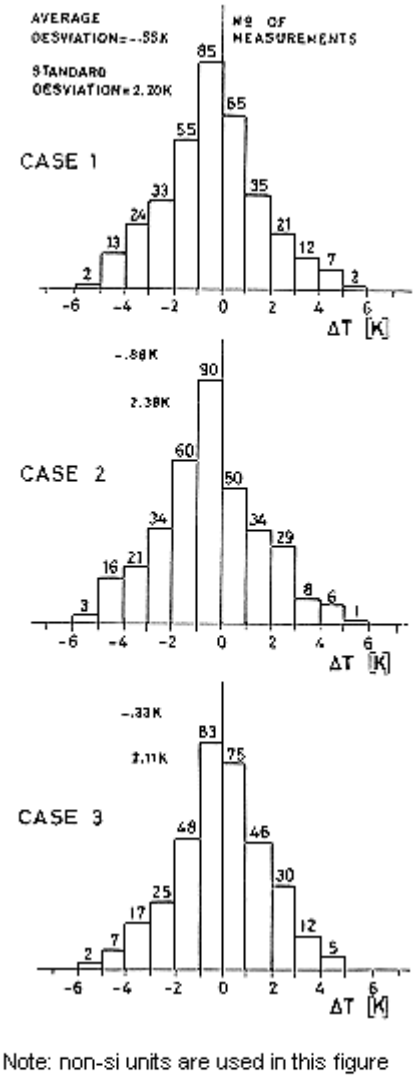

Note: non-si units are used in this figure

Figure 9-6: Temperature Difference Histograms for the three test cases considered in the Thermal Vacuum Tests of Olympus-1 satellite (see Table 9-6 above). From Boggiatto, Colizzi, Perotto & Tavera (1985) [3].

9.6.2 Infrared test

Solar simulation tests of large spacecraft present major sizing and cost problems with presently available solar simulation facilities.

In these facilities, critical orbital conditions are reproduced within a thermal-vacuum environment by use of cryogenic shrouds, to simulate the cold space, and a "solar" beam to simulate the required solar radiation flux on the spacecraft.

In addition to size difficulties, which in the case of the Olympus class spacecraft rendered unsuitable the available European facilities, the classic solar simulation test present other drawbacks.

1. A sophisticated motion system is required to orientate the spacecraft to the proper incidence with respect to the solar beam.
2. Infrared and albedo radiation data, which are required in the case of low orbits, can not be obtained.

An alternative method to perform a thermal balance test, within the usual thermal vacuum facility, consists in locally irradiating the spacecraft with closely placed, suitable infrared lamps.

The wide use of this alternative technique is based on the following premises:

1. Spectral reflectance data of the spacecraft outer faces are known (angular variations included).
2. A thermal mathematical model furnishes the local fluxes corresponding to direct and reflected incoming radiation.
3. A sufficiently large number of infrared lamps are available to irradiate the different zones where the flux is uniform, within a given level of tolerance and uniformity.

   In the case of Olympus-1 tests, a ±6 % level of non-uniformity was tolerated on radiator SSMs, a ±10 % on outer MLIs and even larger levels in zones were the reflections complicated the prediction of the radiation fluxes to be reproduced in the tests.
4. Special radiometers meeting the required level of accuracy are available.

The method should be validated, whenever possible, by comparison with the classic solar simulation tests.

The first attempts for the introduction of this technique have been reported by Messidoro, Boggiatto, Pataccia & Buratti (1983) [36] and by Tan & Walker (1983) [47].

The Olympus satellite infrared test was carried out at the David Florida Laboratories (Ottawa) during the second half of January 1986, following 3 months of preparation. These tests have been reported by Messidoro & Colizzi (1986) [37]. A block diagram showing the activities related to infrared tests is shown in Figure 9-7.

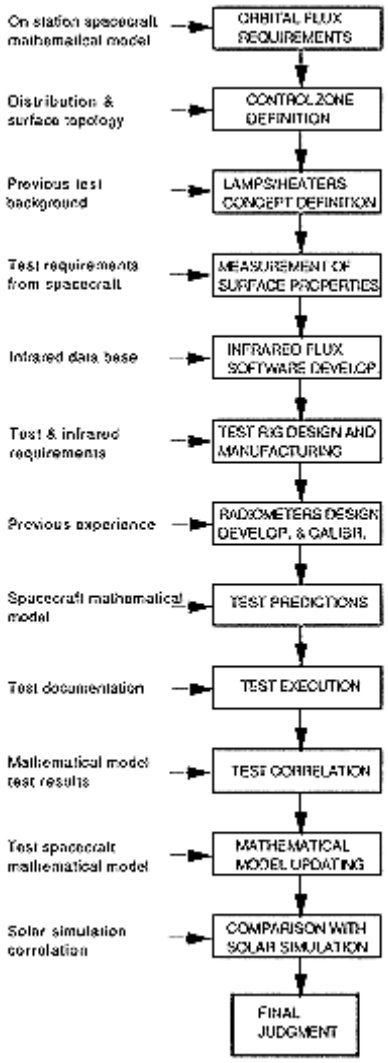

Figure 9-7: Infrared test related activities. From Messidoro & Colizzi (1986) [37].

The high vacuum infrared chamber is 6,7 m in diameter and 10,7 m high. The thermal environment was simulated by cryogenic shrouds and infrared heating. The vacuum was 3 x 10^{-3} Pa to 10^{-4} Pa.

The spacecraft was instrumented with about 600 thermocouples and special tilt sensors to control its attitude and the horizontality of heat pipes. A mounting fixture with stainless steel cables holds the spacecraft with its z axis horizontal within an accuracy of 5 x 10^{-5}. The heat transfer between the spacecraft and the chamber interfaces was minimized. The support structure included brackets to hold the infrared heaters rig, baffles and cables.

The infrared lamps (Research Inc. 5236-5) and other heating elements were attached to aluminium tubes in predetermined locations to obtain the required heat transfer rates. 80 body-and-disc radiometers were used to measure the actual fluxes.

The heating elements were connected to dedicated power supplies and the data were acquired via the data processing system.

The test results fairly compared with predictions and were in good agreement with similar data from the solar simulation test.

The power supply and control rack operation was not as effective as expected. This affected the eclipse transient phase modifying the foreseen switching ON/OFF sequence.

Other small faults and errors, detected during the test, were corrected on-line with minimal impact on the test.

As an example, a comparison of required vs. measured heat transfer rates for the winter solstice case is shown in Table 9-8.

Table 9-8: Winter Solstice Heat Transfer Rates, *Qe*[W.m^{-2}], Measured and Compared with the Requirements

Location a	Measured	Requirements	
		Max	Min
South Radiator	124,6	138,4	85,4
South Radiator	90,5	101,2	85,2
Upper Floor Antenna	580,4	768,0	562,0
Upper Floor Tower	159,0	165,4	124,4
North Radiator	45,0	48,5	29,5
North Radiator	33,6	34,6	28,6
+y MLI	1303,2	1429,0	1165,0
+y MLI	760,7	761,1	593,1
+y Antenna Dish	386,1	264,0	216,0

[a] Different control zones in the same location have been considered.

NOTE From Messidoro & Colizzi (1986) [37].

The resulting temperature-time profiles of relevant spacecraft zones are shown in Figure 9-8.

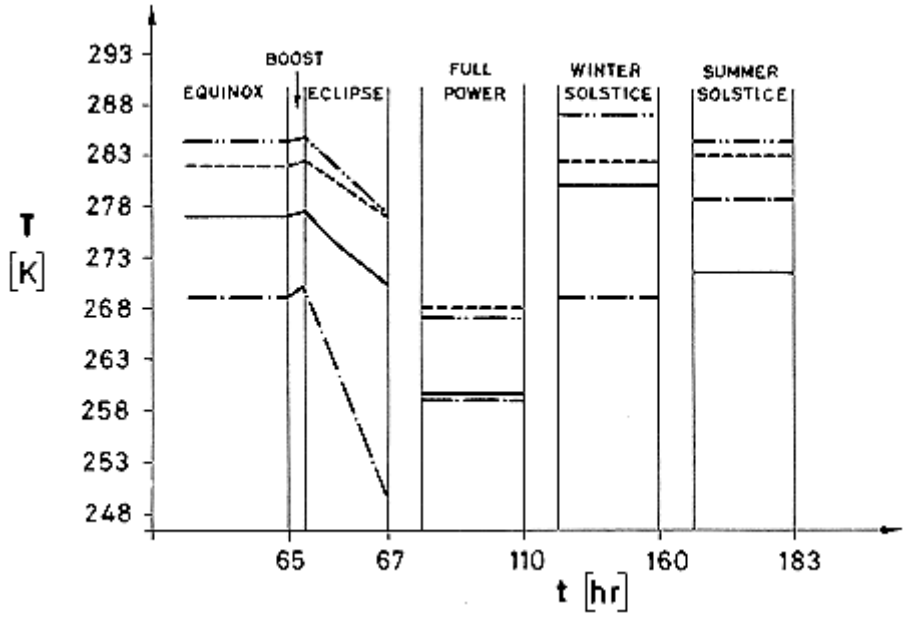

Figure 9-8: Temperature vs. time profiles of Olympus-1 satellite as obtained from the infrared test. ——— North radiator, inner face. —.— South radiator, outer face. — — Communications Module – Service Module, central cylinder. —..— Communications Module, upper floor. From Messidoro & Colizzi (1986) [37].

References: Messidoro, Boggiatto, Pataccia & Buratti (1983) [36]; Tan & Walker (1983) [47]; Bonhomme & Steels (1984) [4]; ESA (1984); Boggiatto, Colizzi, Perotto & Tavera (1985) [3]; Messidoro & Colizzi (1986) [37]; Steels & Baston (1986) [44]; Bowles (1987) [10]; Konzok, Gutschmidt, Stümpel, Schlit & Dunbar (1987) [33]; Chalmers, Burkle & Case (1988) [13]; INTERAVIA (1989) [28]; Paul (1989) [38].

10
ERS-1

10.1 Mission

The objectives of the ERS–1 mission are both of scientific and economic nature aiming to:

- Increase the scientific understanding of coastal zones and global ocean processes.
- Monitor the polar regions, sea ice and icebergs.
- Enable significant advances in physical oceanography glaciology, climatology and sea pollution.
- Develop and promote economic/commercial applications related to a better knowledge of ocean parameters and sea–state conditions.

Their results will be major contributions to the World Climate Programme.

ERS–1 uses microwave and radar techniques to perform global measurements and imaging independently of clouds and sunlight conditions.

ERS–1 performs measurements of parameters not included in previous satellite systems: sea state, sea–surface winds, ocean circulation and sea–ice levels.

Launcher: Ariane V44

Launching date: July 17, 1991

Launch site: Kourou

Mission life: 3 years

The nominal orbit is a sun–synchronous near circular near polar orbit. The following body–linked coordinate system will be used throughout this Part (see Figure 10-1):

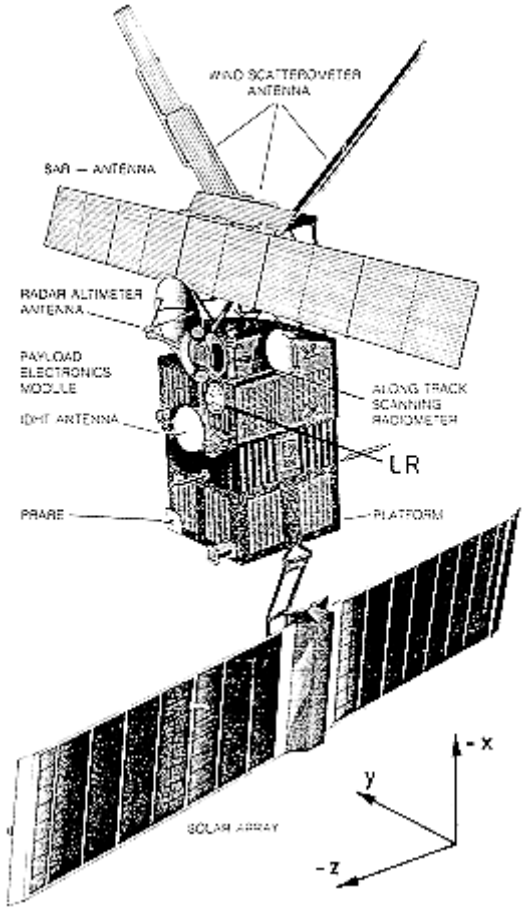

Figure 10-1: ERS-1 in flight configuration. From Francis et al. (1991) [21].

–Z axis Earth–pointed (nominal mode)

–Y axis pointing in flight direction (nominal mode)

–X axis forming a right–handed reference system

In safe mode the attitude changes to a sun–oriented (+Z) condition.

10.2 Main subsystems

The satellite (see Figure 10-2) consists of two major elements: the Payload and the Platform.

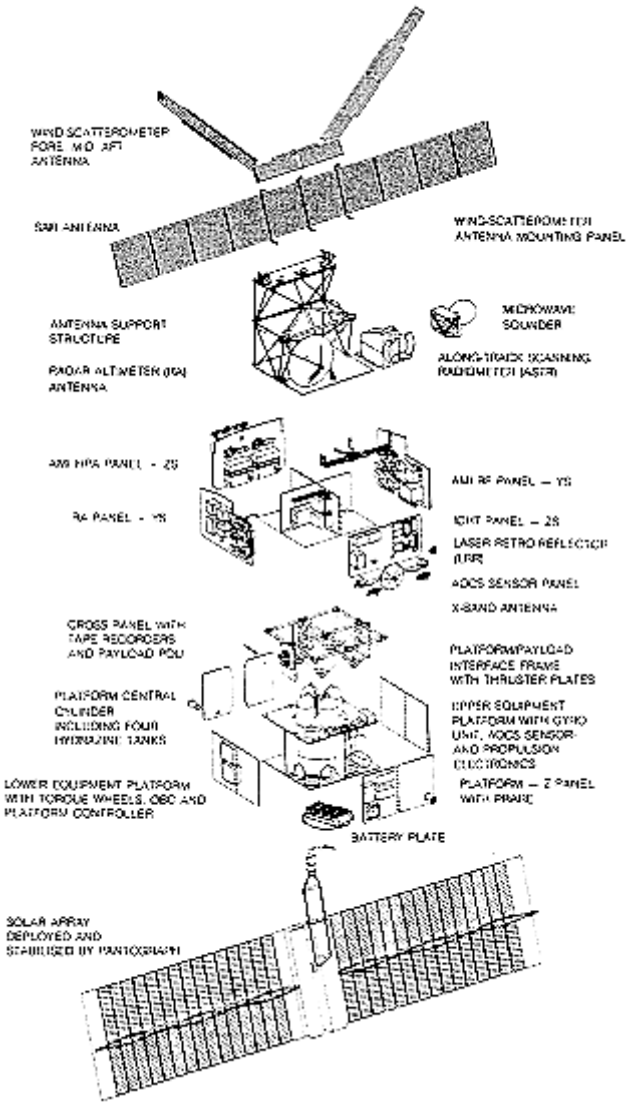

Figure 10-2: Exploded view of ERS-1 satellite. From Francis et al. (1991) [21].

The Platform is based on the "Plate Forme Multimission" PFM developed by Matra for CNES in the frame of the French SPOT programme, and is adapted to the specific ERS–1 requirements. Therefore, in the following main attention will be given to the Payload. Information covering the SPOT platform can be found in Clause 8.

The Platform composes three main assemblies: a Service Module, a Reaction Module and a Solar Array. The Platform provides functions as: power supply and distribution, telemetry, tracking and command, attitude and orbit control, control of on–board operations by the on–board computer (OBC), and structural interface.

The main subsystems and components of the ERS–1 payload are listed in Table 10-1.

Table 10-1: Payload Main Subsystems

Subsystem	Type	Application	Component Characteristics	Responsible
Earth Observation Instruments	AMI Active Microwave Instrument	- Synthetic aperture radar systems for high resolution imaging. - Wave spectra. - Wind scatterometry over ocean surface	Image mode: Bandwith, 15,55± 0,1 MHz; peak power, 4,8 kW; Antenna size, 10 m x 1 m; polarization, L-V; sampling rate, $19x10^6$ samples/s; spatial resolution, 30 m x 30 m; swath width, 100 km; frequency, 5,3 GHz (C-band); data-rate, <105 Mbit/s. Wave mode: Wave direction, 0-180° ± 20°; wave length, 100-1000 m ± 25%; spatial sampling, 5 km x 5 km every 200-300 km; frequency, 5,3 GHz; polarization, L-V. Wind mode: wind direction, 0-360° ± 20°; wind speed, 4-24 m/s ± 2 m/s or 10%; spatial resolution, 50 km; grid spacing, 25 km; swath width, 500 km; frequency, 5,3 GHz; polarization, L-V; peak power, 4,8 kW.	Marconi
	RA Radar Altimeter	Ku-band radat altimeter comprising nadir looking instrument for measurements over ocean and ice surface	Frequency, 13,8 GHz; transmit peak power, 55 kW; antenna diameter, 1,2 m; height noise, 3 cm at 8 m wave height; mass, 96 kg; DC power, 130 W.	Selenia
	LRR Laser Retroreflector	To support RA time delay calibration and satellite ranging	Wavelength, 350-800 nm; ,efficiency, ≥ 0,15 EOL; reflection coefficient, ≥ 0,80 EOL; Field of view, 60° elev. half-cone, 360° azimuth.	Aerospatiale
	ATSR Along Track Scanning Radiometer /Microwave Sounder	Measurement of sea surface temperature and atmospheric water vapour content. Consists of two instruments, Infrared Radiometer (IR) and Microwave Radiometer (MWR)	IR Radiometer: Swath width, 500 km; spectral channels, 1,6, 3,7, 11 and 12 μm; spatial resolution, 1 km x 1 km (at nadir); radiometric resolution, < 0,1 K; predicted accuracy, 0,5 K. MWR Radiometer: Channels, 23,8, 36,5 GHz; instantaneous field of view, 20 km.	ETCA

Subsystem	Type	Application	Component Characteristics	Responsible
	PRARE Precision Range and Range Rate Equipment	-Provides precise range and range rate data in X-band and support functions in S-band. (This element is accommodated within the service module of the platform)	Uplink, 7225 MHz PSK 10 Mbit/s; Ground transponder, 60 cm parabolic dish, 2 W transmit power; down link, 8489 MHz PSK 10 Mbit/s, 1 W transmit power; satellite antennae, crossed dipoles at X- and S-bands; ranging accuracy, 5-10 cm (predicted).	
Instrument Data Handling and Transmission System (IDHT)		Mission specific instrument data handling, due to the high data rates of the payload. Provides data collection, tape recorder storage, formatting and playback or real-time transmission for payload instruments.	2 x band links	LABEN
Payload support subsystems: structure	PEM Payload Electronics Module	Housing of the majority of the instrument electronics		
	Antennae Support Structure	Provides the mechanical interface for the payload appendages		Contraves
Power distribution				ETCA
Thermal control				Fokker

NOTE From Haimler, Overbosch and Pieper (1987) [24]; Francis et al. (1991) [21]; Ege (1991) [19].

Main characteristics of ERS-1 are:

Total mass: 2400 kg

Payload weight: 1000 kg

Overall height: 11,8 m

Solar array: 11,7 m x 2,4 m

Payload support structure: 2 m x 2 m x 3 m

SAR–antennae: 10,0 m x 1,0 m

Wind scatterometer antennae

Fore and aft antenna: 3,6 m x 0,25 m

Mid antenna: 2,3 m x 0,35 m

RA antenna: 1,2 m

Payload power: 1 kW (in sunlight)

Solar array power: 1,8 kW (in sunlight)

ERS–1 has been developed under ESA by an industrial consortium headed by Dornier System consisting of the following industrial groups:

MATRA	Platform, satellite AIT & GSE
FOKKER	Payload thermal control, Payload AIT & GSE
CONTRAVES	Payload structure
ETCA	Payload PDU, ATSR
LABEN	IDTH
MARCONI	AMI
SELENIA	RA
MDA	Ground support
DSF	Subcontracts with ORS, Aeroespatiale, Laben, CRISA, IGG, TRW.

10.3 Orbit

Sun–synchronous near circular and near polar, 777 km altitude, 100 minutes period. Repetitive ground track pattern. Sun period 66 minutes, eclipse period 34 minutes. Repetition period 3 days, with 14 1/3 nodal periods per day (43 in total). Nominal local solar time (15th June) at descending node 10 h 30 min.

From Haimler, Overbosch & Pieper (1987) [24].

10.4 Thermal design requirements

The primary requirement for the Thermal Control Subsystem (TCS) is to guarantee that specified temperature limits (see Table 10-2) are not exceeded during all mission phases throughout the lifetime.

Table 10-2: Typical Design Temperature Limits and PEM Dissipations

Sub-system/ Instrument	Unit	Typical design temperature limits [K]					PEM dissipation [W]				
		Operating		Non-operating		Switch-on	Equipment	Nominal attitude		Safe mode	Return from s.m.
		Min	Max	Min	Max	Min		Average	Peak		
AMI	Typically	263	313	228	343	263	Inside PEM	416	1056*	off	
	Electronic Power Conditioners	268	313	253	328	263	Outside PEM	25	85*		
RA	Typically	268	318	233	333	248	On +Y panel	148	174	off	
	Microwave Subsystem	273	318	233	343	248					
	High Power Amp.	268	318	233	333	248					
IDTH	Typically	263	313	233	323	248	- Z panel	57	226*	off	
	Modulators	280	310	233	323	248					
	Electronic power Conditioners	263	313	243	333	248					
	Tape recorders	268	305	233	323	248	Tape recorders	27	68		
ATSR							Inside PEM	35	35	off	
							Outside PEM	77	77		
							Sum inside	695	1572	15	25
							Sum outside	110	170		
							Sum total				

Sub-system/ Instrument	Unit	Typical design temperature limits [K]					PEM dissipation [W]				
		Operating		Non-operating		Switch-on	Equipment	Nominal attitude		Safe mode	Return from s.m.
		Min	Max	Min	Max	Min		Average	Peak		
								805	1742	15	25
PL Support	Power distribution unit	258	313	--	--	--	Power distribution unit	12	13	15	25
	Sun/earth sensors						Sun/earth sensor (outside)	8	8		
	Payload support structure	263	318	253	323	253					
		--	--	223	343	--					

NOTE * The duration of peak dissipation is limited to 10 minutes maximum per orbit.

The design has to employ mainly passive means for temperature control. When necessary this passive design may be assisted by active elements. Further requirements and constraints to the TCS are to minimize:

- electrical energy consumption
- temperature gradients in the structure (compatible with thermal distortions requirements)
- mass

The most important design constraints are:

- two different satellite orientations (nominal, safe mode)
- high heat dissipation within the electronics
- high number (43) of different operation timelines
- limited heater power available
- limited radiator area
- restricted heater operation during nominal mission phases (sun period only)
- heat flux between platform and payload are minimized
- limited area for heater mat application

For the purpose of the thermal design definition a limited number of artificial thermal timelines has been derived out of the large number of timelines possible. Characteristics of instrument dissipation are gathered in Table 10-2.

10.5 Thermal control

The Platform thermal subsystem is based on the design of SPOT–1 (see Clause 8 for more information).

The good radiative and conductive decoupling of PL and PF from each other allows for a modular design and testing. On the other hand, the large size of this kind of satellites requires modular testing.

Concerning the Payload, the TCS consists of:

1. Antennae and Antenna Support Structure posses a totally passive thermal design. MLI is covering the antenna rear–sides. Front sides are either white painted or taped (aluminium) and silver painted. Struts and nodal points of the Antenna Support are also wrapped in MLI.
2. ATSR thermal layout is complemented by thermostat controlled heaters.
3. PEM thermal control is based on passive thermal control supported by an active heater system; thermal blankets except for defined radiator areas: OSR in –Z, –Y faces. Black Paint radiator in –X faces.

Special attention has been given to the thermal problems of the SAR antenna deployment (see Figure 10-3).

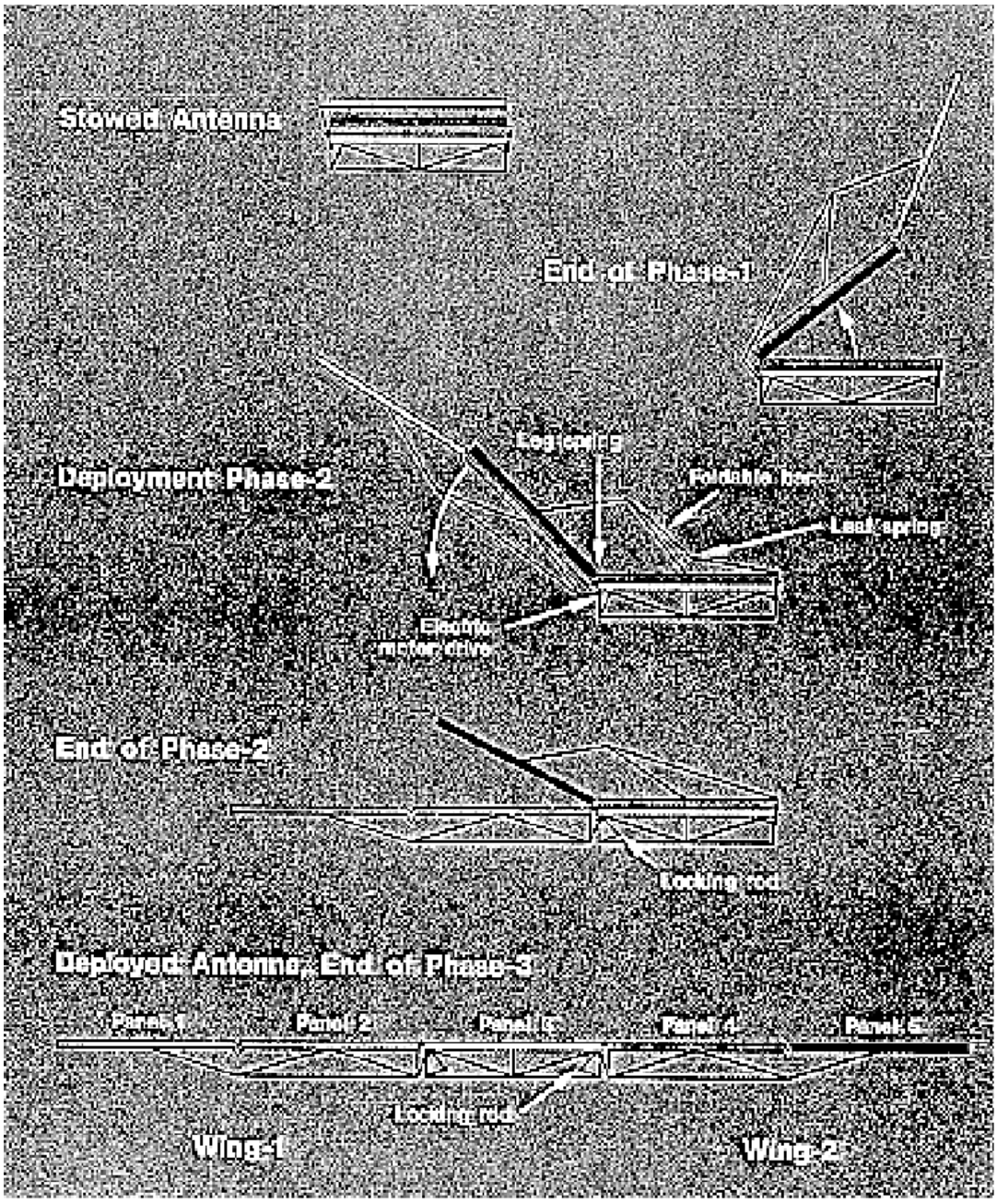

Figure 10-3: Schematic of the different phases of ERS-1 SAR Antenna deployment. From Francis et al. (1991) [21].

In the following attention is concentrated on the PEM.

The PEM is an aluminum sandwich box type structure supported by nine vertical titanium beams. Titanium has been chosen to take advantage of the low thermal conductivity and thermal expansion coefficient, to minimize both the conductive heat flux to and from the PF and thermal distortions.

Thermal requirements can be fulfilled with a passive thermal control system supported by active heater, consisting of:

1. SSM and OSR thermal radiators, located on the side panels of the PEM where the majority of the electronic units is mounted. A small radiator, dedicated for tape recorder cooling is placed on top of the PEM. For location of radiators see Figure 10-4

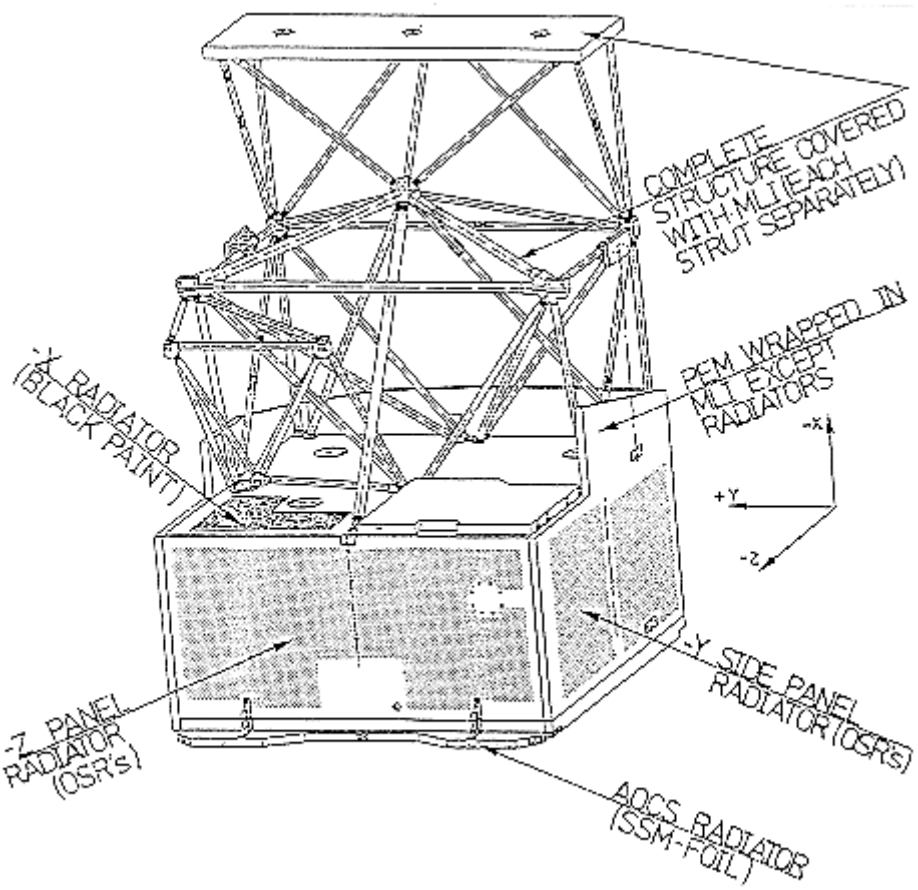

Figure 10-4: ERS-1 satellite. PEM external thermal design. From Haimler, Overbosch & Pieper (1987) [24]

Total radiation area: 4 m^2.

Rejected heat transfer rate: 700 W

2. Multilayer insulation blankets

   External blankets: an outer (space viewing) layer of 2 mil Kapton, aluminized on the inner side, covering a package of aluminized mylar sheets separated by Dacron net.

   Inside blankets: two sets of blankets are employed

   (a) Kapton only to withstand ~420 K of the TWT collector heads for: the High Power Amplifier (HPA) panel set, protecting the AMI Electronic Power Conditioning (EPC) from the AMI TWT'S and insulating the complete HPA panel from the rest of the PEM.

   (b) blanket insulating the PEM from the PF and that insulating the –X radiator internally.

3. Thermal doublers. Units with a moderately high ratio of thermal dissipation to footprint area are provided with a local thickening (up to 3 mm) of the panel facesheets.

4. Constant conductance heat pipes (CCHP). Axially grooved aluminium heat pipes, with Ammonia as working fluid, manufactured by Dornier System GmbH.

   The +Z panel is equipped with 11 CCHP's for the AMI–TWT'S and EPC's.

The –Y panel is equipped with 4 CCHP's.

The –X panel is equipped with 4 CCHP's for tape recorders mounted to a cross panel.

The +Z and –Y panel are provided with heat pipes which cover almost their whole length, imbedded inside the honeycomb.

5. Black paints are used to cover the surface inside the satellite coatings for antennae.

6. Heater system. Electric heaters controlled either automatically or by telecommand.

The layout of the PEM is shown in Figure 10-5

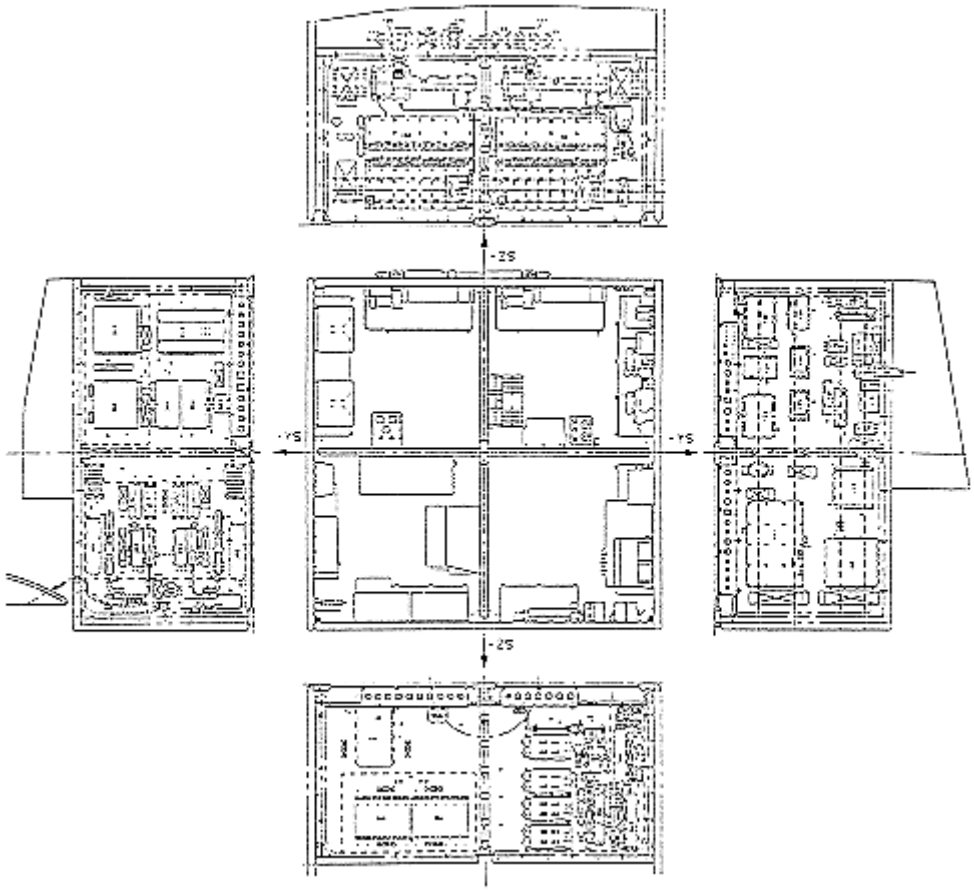

Figure 10-5: ERS-1 satellite. PEM internal thermal design. From Haimler, Overbosch & Pieper (1987) [24].

10.6 Thermal tests

A calendar of ERS-1 Thermal Tests is given in Table 10-3.

Table 10-3: ERS-1 Thermal Test

No.	Test	Date	Place	Comments
1	Thermal Balance	Summer 1989	LSS	EM
2	Thermal Vacuum	Summer 1989	LSS	EM

Two different types of thermal tests have been reported, namely Thermal Vacuum Test and Thermal Balance Test.

10.6.1 Thermal balance test of the engineering model

Objective

To qualify the thermal design and to verify the thermal mathematical model of the Payload.

Facilities

LSS (Largest Space Simulation) chamber at ESTEC, Noordwijk, The Netherlands. The chamber is a vertical cylinder 10 m in diameter and 15 m in height. The collimation mirror is 6 m in diameter.

INTESPACE in Toulouse, France, for the Platform flight model.

Equipment or subsystems tested

Due to the physical size of the satellite in deployed configuration, the space simulation test had to be performed on the Payload, the Platform and the large antenna systems separately.

With this split and the LSS a fully illuminated Payload was achieved.

The absence of the Platform and parts of the antenna systems did not influence the test objectives: a good thermal decoupling between these parts was considered in the design, and the absence of the items was accounted for in the mathematical model.

Besides, the absence of earthshine required compensation. This was achieved by means of electrical heaters attached to the bottom panels of the PEM and to the antenna rear sides. Although the heaters did not dissipate the heat on the radiator areas, where earthshine is observed in orbit, the temperature level could be boosted to the desired level.

Test setup

- LSS
- Test article with aprox. 600 thermocouples
- EGSE (Electrical Ground Support Equipment)
- PROPOS (PROgrammable POwer Supply)
- TDH (Test Data Handling system peripheries)

The most complex item was the EGSE composed of the:

- Platform simulator which gives:

— power supply

— onboard data handling interface

— heater control via the onboard computer

— OCOE (Overall Check-Out Equipment), master controller of the Payload, and coordinator of the all EGSE subsystems.

Computer models description

Each subsystem has established mathematical models to support the conceptual and detailed thermal design and the verification.

The interface heat flow between all subsystems are controlled with the Thermal Interface Mathematical Model (TIMM) of the complete satellite.

The thermal compatibility with the launcher environment is verified with a special ARIANE dedicated model of ERS-1.

To execute the calculations ESA standard programs are used:

— VWHEAT, to calculate radiation couplings and absorbed external fluxes.

— SINDA, for temperature calculations.

The basic thermal design of the PEM has been defined with a flexible 100 node model. In addition, detailed models of each side panel (≈ 100 nodes each) have been established to support and refine the global design.

For verification by Thermal Balance Tests and final flight predictions a thermal mathematical model (of 400 nodes for the PEM) has been established. This model also includes the Antenna Support Structure to have one consistent temperature prediction for thermal distortion calculations.

Test definition

Definition of proper steady state cases are essential to perform a good model correlation. Artificial cases, but close to reality had to be defined. Steady state conditions were achieved by operating the instruments in continuous mode, disabling the heater system, adjusting fast spin (4 rpm) and no day/night simulation. The steady state cases were to determine the level and temperature inside the PEM. The transient cases had to verify the temperature excursions of highly dissipating units.

The proper performance of the heat pipes under 1 g conditions require a precise horizontal levelling.

The Thermal Balance Test was composed of 10 test phases (see Table 10-4). These cases were derived from the design cases which represent the envelope of worst conditions. The objectives of these cases are also reported in Table 10-4.

Table 10-4: Thermal Balance Test Phases. From Haimler, Kamp and Pieper (1990)

Test Phase	Sun simulation		Duration [h]	Motion Simulator		Shroud Temp. [K]	Instruments Operation	Heaters	Test Phase Objectives
	Inten-sity [W/m²]	Day/ Night Simulation		Spin	Space-craft Axis				
Payload Hot A Steady state	1600	no	31	4 rpm	Vertical	100	Steady state	off	Temperature distribution (A-chain operating)
Payload Hot B Steady State	1600	no	27	4 rpm	Vertical	100	Steady state	off	Temperature distribution (B-chain operating)
Payload Hot B Transient	1600	no	10	4 rpm	Vertical	100	transient timeline	off	Temperature excursions (A-chain operating)
Payload Hot A Transient									Temperature excursions (B-chain operating)
GRM cold transient + contingency phase	1600	no	3,5	4 rpm	Vertical	100	transient timeline	off	Verification of software controlled heat system
Cool-down to safe mode	1600	yes	19+5	1 r.p. orbit[2]	Vertical	100	transient timeline	(LL1,LL2,HL)	Determination of average time constant
Safe mode steady state				4 rpm				on[1] (LL1,LL2,HL)	
Payload off steady state	0	no	1,5		Vertical	100	off		Verification of low

Test Phase	Sun simulation		Duration [h]	Motion Simulator		Shroud Temp. [K]	Instruments Operation	Heaters	Test Phase Objectives
	Inten-sity [W/m²]	Day/ Night Simulation		Spin	Space-craft Axis				
Orbital transient	1350	no	31,5	HPA-radiator sun oriented 4 rpm	Vertical	100	off	LL1,LL2: on HL: off	level heater system Verification of low+high level heater system
	1600	no	33,5		Vertical	100	off	on (LL1,LL2,HL)	Verification of thermal design with in-flight sun incidence
	1600	yes	20,5	1 r.p. orbit[2]	tilted 22,5 deg	100	AMI: "of"[3] all others on (transient)	on (LL1,LL2,HL)	

[1] Heaters switch-on precautionally (LL1/2 = low level 1/2 heater bus, HL = high level heater bus).

[2] 1 Orbit = 100 min.

[3] Heat-pipe not operating due to tilt.

GRM: Global Reference Mission.

In the "Global Reference Mission" (GRM) the in-flight scenario was reproduced as close as possible: the instruments were operated as in flight, the heater system was actively controlled, and a slow spin with eclipse simulation. In the Safe Mode and PL-Off phases the aim was to confirm that the installed power is enough to guarantee the required temperature levels.

In the orbital transient phase the aim was to verify the complex radiation exchange within the Antenna Support Structure and the efficiency of the small radiators on the PEM top panel.

Definition of steady state conditions: when about 800f selected thermocouples showed temperature variations of less than 0,5 K over a period of 5 hours.

Temperature Prediction Uncertainties

Passive uncertainties: uncertainties due to specimen and environment parameter tolerances, and modellization error. Do not apply in cases and areas where heaters are effective (to cope with uncertainties).

Active uncertainties: set point tolerances of thermostats and thermistors used for heater control and tolerances in the assumed temperature differentials between thermostats or thermistors and the units to be controlled.

Test correlation criteria

The criteria for correlation are the following:

1. Maximum deviation in overall temperature level in all equipment nodes equal or less than 1,5 K.
2. Maximum individual deviation of all electronic equipment equal or less than 5 K (10 K) for equipment mounted inside (outside) the PEM.

Test evaluation

Three steps were considered:

1. During the test comparison of the results against the pre–test predictions.
2. After the test a data base is created, containing all data test, and predictions are made considering the actual test conditions, to compare with test results.
3. Correlations between the updated mathematical model and the test results, to verify and validate for flight predictions.

This process showed a good temperature correlation. Three modifications of the model were considered to refine the model and correct both a level offset and some punctual discrepancies.

The aims of the corrections were:

1. To trim the radiator areas of the flight model to assure a minimum heater power consumption for cold operational phases.
2. To improve the behavior of those instrument units which possess a temperature dependent performance.
3. To compute accurate thermal distortion budgets.

The factors considered for these corrections were:

1. Incorporation of a temperature dependent linear conductivity for the honeycomb core material, not previously considered.
2. Refining of the thermo optical properties of the radiators.

3. Update of conductance and radiative couplings.

After the incorporation of all adjustments into the mathematical model most of all thermocouples on units inside the PEM fulfilled the correlation criterion of ±5 K. In transient phases temperature excursions deviated less than 4 K from observations.

Some results are shown in Figure 10-6 and Figure 10-7 and Table 10-5. In this way a reduction of 15% in the final radiator area was considered for the flight model, saving 100 W heater power during cold operation phases.

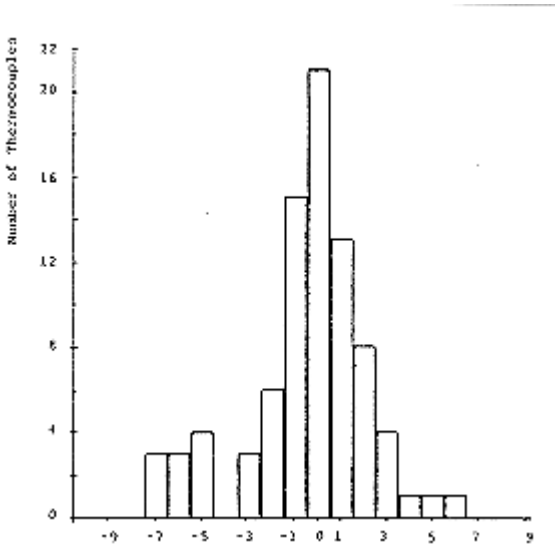

Figure 10-6: Temperature difference histograms for the PL-Off Phase. From Haimler, Kamp & Pieper (1990).

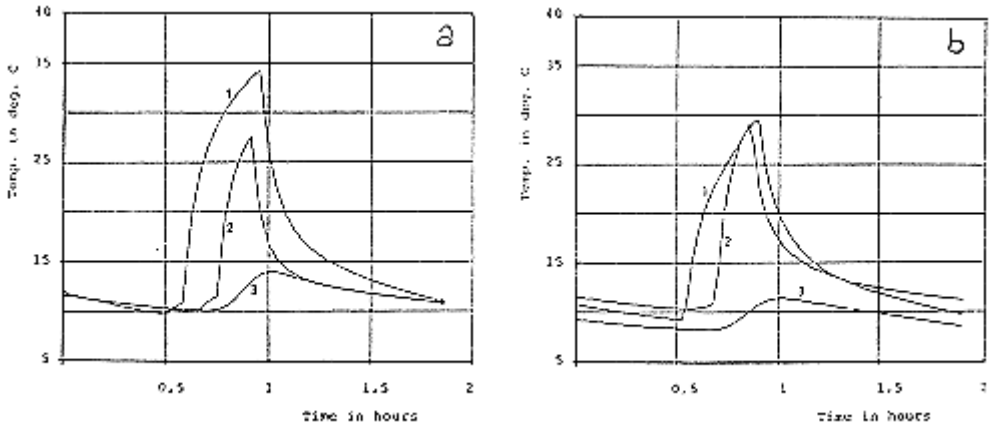

Note: non-si units are used in this figure

Figure 10-7: Transient temperature behaviour of IDHT TWT's: a) Predicted, b) measured. From Haimler, Kamp & Pieper (1990).

Table 10-5: Final Level Correlation Status. Average Measured Predicted Deviation for Steady State Case

Item	Hot A	Hot B	Safe Mode	PL-Off
AMI HPA	-2,6	-3,3	3,0	-1,9
RF Accesories	-5,4	-5,8	1,5	-3,0
AMI	-2,9	-4,3	3,2	-2,4
RA	0,3	-0,4	0,4	0,7
IDHT	-0,4	-1,0	-2,3	1,6
CROSS + TOP	-1,3	-2,6	2,2	1,8
AOCS	2,3	1,8	-4,4	1,0
LEVEL	-1,3	-2,1	0,3	0,1

10.6.2 Thermal vacuum test

Objective: verify the operational and functional performance of the payload at low and high qualification temperature levels in vacuum.

Schedule: 20 days

3,5 for pump–down, back–out and cooldown

9,5 for the Thermal Balance part

7,0 for the Thermal Vacuum part

No additional information on this subject was available at the time of compilation.

References: M. Haimler, E. Overbosch & E. Pieper, 1987 [24]; G. Jander, F. Zilly & R. Bisanz (1988) [29]; INTERAVIA (1989) [28]; M. Haimler, A. Kamp & B. Pieper (1990) [23]; M. Ege (1991) [19]; R. Francis et al. (1991) [21].

Bibliography

[1] Alet, I., Foret, J.L., "Le Controle Thermique de la Plate-Forme Spot", in "Environmental & Thermal Control Systems for Space Vehicles", ESA SP-200, Paris, Dec. 1983, pp. 119-125.

[2] Bachofer, B.T., "LANDSAT D - Case Study in Spacecraft Design", AIAA Professional Study Series, AIAA Educational Programs, New York, Aug. 1979.

[3] Boggiatto, D., Colizzi, E., Perotto, V., Tavera, S., "Thermal Vacuum Tests on Olympus Heat Pipe Radiators", Fifteenth Intersociety Conference on Environmental Systems, San Francisco, CA, July 15-17, 1985, SAE Technical Paper Series 851363.

[4] Bonhomme, R., Steels, R., "Development and Application of New Technologies in ESA's Olympus Programme", ESA Journal, Vol. 8, No. 4, 1984, pp. 357-379.

[5] Bouchez, J.P., Gülpen, J., "The European Geostationary Communication Satellite OTS - Two Years of Thermal Control Experience in Orbit". AIAA Paper No. 80-1500, AIAA 15th Thermophysics Conference, Snowmass, Colorado, July 14-16, 1980.

[6] Bouchez, J.P., Howle, D., "The Orbital Test Satellite OTS-2 - Two Years of Thermal Control Experience", ESA Bulletin No. 26, May 1981, pp. 54-61.

[7] Bouchez, J.P., Howle, D., "The Orbital Satellite (OTS) Thermal Experience after 3,5 Years in Orbit", AIAA Paper No. 82-0831, AIAA-ASME 3rd. Joint Thermophysics, Fluids, Plasma and Heat Transfer Conference, June 7-11, 1982, St Louis, Missouri, USA.

[8] Bouchez, J.P., Howle, D.H., "OTS-2: Results from Thermal Tests on a Satellite During Six Years in a Geostationary Orbit", AIAA Paper No. 84-1701, AIAA 19th Thermophysics Conference, Snowmass, Colorado, June 25-28, 1984.

[9] Bouchez, J.P., Howle, D.H., Stümpel, D., "Orbital Assessment of OTS Thermal Performance", Proceedings of Spacecraft Thermal and Environmental Control Systems Symposium, Munich, 1978, ESA SP-139, pp. 35-45.

[10] Bowles, O., "The New Olympian", Space, Vol. 2, No. 4, Dec. 1986-Feb. 1987, pp. 31, 32, 35, 36.

[11] Bulloch, C., "Los Esfuerzos Europeos en el Campo Espacial", Interavia, Vol. 33, No. 9, Sept. 1978, pp. 847-851.

[12] Caruso, P., Stipandic, E., "Thermal Design Concept for a High Resolution Ultraviolet Spectrometer", in "Heat Transfer, Thermal Control and Heat Pipes", Progress in Astronautics and Aeronautics, Vol. 70, W.B. Olstad, Ed., American Institute of Aeronautics and Astronautics, New York, 1980, pp. 251-266.

[13] Chalmers, D.R., Konzok, H.G., Bouchez, J.P., Howle, D., "OTS-2: Five Years of Thermal Testing on a Satellite in a Geostationary Orbit", Proceedings of the International Symposium on "Environmental and Thermal Systems for Space Vehicles", Toulouse, France, Oct. 4-7, 1983, pp. 425-436.

[14] Collette, R.C., Stockwell, B., "OTS Project: Basis of Future European Space Communication Systems", in "Communications Satellite Developments: Systems", Progress in Astronautics and Aeronautics, Vol. 41, G.E. La Vean & W.G. Schmidt, Eds., American Institute of Aeronautics and Astronautics, New York, 1976, pp. 285-308.

[15] Corai, J.C., "Ensemble Propulsif de la Plate-Forme SPOT", L'Aeronautique et L'Astronautique, No. 103, 1983-6, pp. 32-40.

[16] Courtois, M., Weill, G., "The SPOT Satellite System", in "Monitoring Earth's Ocean, Land, and Atmosphere from Space-Sensors, Systems, and Applications", Progress in Astronautics and Aeronautics, Vol. 97, A. Schnapf, Ed., American Institute of Aeronautics and Astronautics, Inc., New York, 1985, pp. 493-523.

[17] Cull, R., Stevenson, G., Mell, R., Harada, Y., "Requalification of S-13 G/LO", AIAA Paper No. 84-1755, AIAA 19th Thermophysics Conference, Snowmass, Colorado, June 25-28, 1984.

[18] Dyson, S.T., "French-English Glossary on Spot Remote Sensing and Their Applications", 1st ed., S. Dyson, "Bouygues", Miramont-de-Quercy, 82190 Bourg-de-Visa, France, Sept. 1986.

[19] Ege, M., "Industrial Cooperation on ERS-1", ESA Bulletin No. 5, pp. 88-93.

[20] Fagnoni, H., "Controle Thermique du "Compartment Batteries" Spot Multimission", in "Environmental & Thermal Control Systems for Space Vehicles", ESA SP-200, Paris, Dec. 1983, pp. 371-379.

[21] Francis, R., et al., "The ERS-1 Spacecraft and Its Payload", ESA Bulletin No. 65, pp. 26-48.

[22] Freeman, H.R., Longanecker, C.W.,"The International Ultraviolat Explorer (IUE) - Case Study in Spacecraft Design" , AIAA Professional Study Series, AIAA Educational Programs, New York, Aug. 1979.

[23] Haimler, M., Kamp, A., Pieper, B., "Features of the ERS-1 EM Payload TB/TV Test", SAE Technical Paper Series 901339, 20th Intersociety Conference on Environmental Systems, Virginia, July 9-12, 1990.

[24] Haimler, M., Overbosch, E., Pieper, E., "Thermal Control and Design of the ERS-1 Payload", Presented at the 17th ICES, 13-15 July 1987, Seattle, Washington.

[25] Henry, C., Juvigny, A., Serradeil, R., "High Resolution Detection Sub-Assembly of the SPOT Camera: On Orbit Results and Future Developments", Acta Astronautica, Vol. 17, No. 5, 1988, pp. 545-551.

[26] Hopkins, R.A., Brooks, W.F., "Orbital Performance of a One-Year Lifetime Superfluid Helium Dewar Based on Ground Testing and Computer Modelling", in "Advances in Cryogenic Engineering", Vol. 27, R.W. Fast, Ed., Plenum Press, New York and London, 1982, pp. 1087-1097.

[27] Hwangbo, H., Kelly, W.H., "Transfer Response of Thermal Louvers with Bimetallic Actuators", AIAA Paper No. 80-1539, AIAA 15th Thermophysics Conference, Snowmass, Colorado, July 14-16, 1980. Also published in "Heat Transfer and Thermal Control", Progress in Astronautics and Aeronautics, Vol. 78, A.L. Crosbie, Ed., American Institute of Aeronautics and Astronautics, New York, 1981, pp. 452-466.

[28] INTERAVIA, "Space Directory 1989-1990", Andrew Wilson, Ed., Interavia, S.A., Geneve, Switzerland.

[29] Jander, G., Zilly, F., Bisanz, R., "Thermal Aspects of the ERS-1 SAR Antenna Deployment", ESA SP-288, ESA, Paris, 1988, pp. 345-350.

[30] Karam, R.D., "Temperature Distribution in Louvered Panels", J. Spacecraft, Vol. 16, No. 2, March-April 1979, pp. 92-97.

[31] Karsten, L., Teule, F., "IRAS Thermal Misaligment - A Lesson for the Future", ESA Journal, Vol. 8, No. 3, 1984, pp. 245-259.

[32] Kirckpatrick, J.P., Brennan, P.J., "ATS-6 Flight Performance of the Advanced Thermal Control Flight Experiment", IEEE Transaction on Aerospace and Electronic Systems, Vol. AES-11, No. 6, Nov. 1975, pp. 1187-1195.

[33] Konzok, H.G., Gutschmidt, K., Stümpel, D., Schlitt, R., Dunbar, N., "Battery Thermal Design and Performance in European Geo-Satellite Programs", SAE Paper 871484, SAE Intersociety Conference on Environmental Systems, 17th Seattle, WA, July 13-15, 1987, 14 p.

[34] Mauduyt, J., Bonnet, G., Toulemont, Y., "Controle Thermique de L'Instrument HRV", in "Environmental & Thermal Control Systems for Space Vehicles", ESA SP-200, Paris, Dec. 1983, pp. 381-389.

[35] McLaurin, D.E., Gregory, D.N., "General Description of the Orbital Test Satellite", IEE-IOP Conference, London, April 1981.

[36] Messidoro, P., Boggiatto, D., Pataccia, M., Buratti, P., "Development of a S/C Infrared Test Technique as an Alternative to Solar Simulation - First Steps on L-Sat Thermal Model", in "Environmental & Thermal Control Systems for Space Vehicles", International Symposium, Toulouse, France, 4-7 Oct. 1983, ESA SP-200, ESA, Paris, 1983, pp. 11-17.

[37] Messidoro, P., Colozzi, E., "Infrared Test Technique Validation on the Olympus Satellite", Sixteenth Intersociety Conference on Environmental Systems, San Diego, CA, July 14-16, 1986, SAE Technical Paper Series 860939.

[38] Paul, J.H., "The Large Telecommunications Satellite 'Olympus'", ESA Bulletin, No. 58, May 1989, pp. 63-71.

[39] Petrac, D., Mason, P.V., "Infrared Astronomical Satellite (IRAS) Superfluid Helium Tank Tempertaure Control", in "Advances in Cryogenic Engineering", Vol. 29, R.W. Fast, Ed. Plenum Press, New York and London, 1984, pp. 661-667.

[40] Racaud, G., D'Antin, B., Lelièvre, P., "Le Controle Thermique de la TMCU du Spot", in "Environmental & Thermal Control Systems for Space Vehicles", ESA SP-200, Paris, Dec. 1983, pp. 487-493.

[41] Sherman, A., "History, Status and Future Applications of Spaceborne Cryogenic Systems", in "Advances in Cryogenic Engineering", Vol. 27, R.W. Fast, Ed., Plenum Press, New York and London, 1982, pp. 1007-1029.

[42] Skladany, J.T., Seivold, A.I., "Thermal Control of the International Ultraviolet Explorer", ASME Paper 76-ENAs-38, Intersociety Conference on Environmental Systems, San Diego, Calif., July 12-15, 1976.

[43] Smith, R.E., West, G.S., "Space and Planetary Environment Criteria Guidelines for Use in Space Vehicle Development, 1982 Revision (Volume 1)", NASA TM 82478, Jan. 1983, pp. 1-11.

[44] Steels, R., Baston, D., "Modal-Survey Testing of the Olympus Spacecraft", ESA Journal, Vol. 10, No. 4, 1986, pp. 363-371.

[45] Stümpel, D., "OTS Thermal Design and in-Orbit Performance", Proceedings of Spacecraft Thermal and Environmental Control Systems Symposium, Munich, 1978, ESA SP-139, pp. 27-34.

[46] Stümpel, D., "The OTS Hydrazine Reaction Control System Thermal Conditioning Technique", Proceedings of Spacecraft Thermal and Environmental Control Systems Symposium, Munich, 1978, ESA SP-139, pp. 375-382.

[47] Tan, G.B.T., Walker, J.B., "Spacecraft Thermal Balance Testing Using Infrared Lamps on a Dummy Spacecraft", in "Environmental & Thermal Control Systems for Space Vehicles", International Symposium, Toulouse, France, 4-7 Oct. 1983, ESA SP-200, ESA, Paris, 1983, pp. 19-25.

[48] Tward, E., Mason, P.V., "Damping of Thermoacoustic Oscillations", in "Advances in Cryogenic Engineering", Vol. 27, R.W. Fast, Ed., Plenum Press, New York and London, 1982, pp. 807-815.

[49] Urbach, A.R., Private communication, Boulder, Colorado, 7 March 1986.

[50] Urbach, A.R., Hopkins, R.A., Mason, P.V., "One Year of Stars, Provided by the IRAS Cryogenic System", in "Environmental and Thermal Control Systems for Space Vehicles", T.D. Guyenne & J.J. Hunt, Eds., ESA SP-200, Paris, 1983, pp. 171-177.

[51] Urbach, A.R., Mason, P.V., "IRAS Cryogenic System Flight Performance Report", in "Advances in Cryogenic Engineering", Vol. 29, R.W. Fast, Ed. Plenum Press, New York and London, 1984, pp. 651-659.

[52] Urbach, A.R., Mason, P.V., Brooks, W.F., "Progress Report on the Infrared Astronomical Satellite Cryogenic System", in "Advances in Cryogenic Engineering", Vol. 27, R.W. Fast, Ed., Plenum Press, New York and London, 1982, pp. 1039-1047.

[53] Van Leeuwen, P.L., "Thermal Design and Performance of the IRAS S/C System", in "Environmental and Thermal Control Systems for Space Vehicles", T.D. Guyenne & J.J. Hunt, Eds., ESA SP-200, Paris, 1983, pp. 163-170.

[54] Van Leeuwen, P.L., Private communication to Mr. Ch. Stroom, Amsterdam, The Netherlands, 7 July 1985.

[55] Waldrop, M.M., "Landsat, Space Telescope Suffer Setbacks", Science, Vol. 219, No. 4589, 11 March, 1983, pp. 1200-1201.

[56] Waldrop, M.M., "The Satellite Sale: Another Dose of Reality", Science, Vol. 221, No. 4611, 12 Aug., 1983, pp. 632-633.

[57] Wearmouth, C., McLaurin, D.E., "Development of the Orbital Test Satellite", in "Satellite Communications: Future Systems", Progress in Astronautics and Aeronautics, Vol. 54, D. Jaret, Ed., American Institute of Aeronautics and Astronautics, New York, 1977, pp. 201-221.